Nanostructured Dielectric Elastomer Transducers for Smart Implants

Inauguraldissertation
zur
Erlangung der Würde eines Doktors der Philosophie
vorgelegt der

Philosophisch-Naturwissenschaftlichen Fakultät
der Universität Basel

von

Bekim Osmani

aus Kumanovo, Mazedonien

Basel, 2017

Genehmigt von der Philosophisch-Naturwissenschaftlichen Fakultät

auf Antrag von:

Prof. Dr. Bert Müller, Fakultätsverantwortlicher
Prof. Dr. Roderick Lim, Korreferent

Basel, den 20. Juni 2017

Prof. Dr. Martin Spiess, Dekan

Contents

Summary

Nanotechnology based dielectric elastomer transducers (DETs) are used for a growing number of applications, including tunable optics, microfluidics, soft robotics, and haptic devices. DETs consist of non-conductive soft membranes sandwiched between compliant electrodes. They show unique performance characteristics, i.e. actuation strains similar to human skeletal muscles and millisecond response times which make them promising for applications as artificial muscles. Their main drawback, however, are the high driving voltages of several kilovolts. For medical applications their operation voltage is limited to a few tens of volts. Within the SmartSphincter project of the nano-tera.ch initiative, we have developed techniques to fabricate and characterize DET structures to be used as implants to treat fecal incontinence. Polydimethylsiloxane (PDMS) was selected as the material of choice for the membranes due to its biocompatibility and excellent elastic properties. The low adhesion of Au to PDMS has been reported in the literature and leads to the formation of Au-nanoclusters. The diameter of these nanoclusters was found to be (25 ± 10) nm and can be explained by the low surface energy of PDMS resulting in a Volmer-Weber growth mode. Therefore, we show that (3-mercaptopropyl)trimethoxysilane (MPTMS) can be used as a molecular glue to promote the adhesion between the plasma treated PDMS and Au electrode.

In order to reach actuation forces of several newtons as required for artificial fecal sphincters, multi-layer DETs have to be built. As a first step, a compact apparatus was designed and brought into operation to measure the exerted forces of planar DETs. DETs with an active area of 4 mm $\times$ 12 mm were fabricated on polyethylene naphthalate (PEN) cantilevers. The bending of the asymmetric cantilever was detected using a optical beam-deflection readout. The actuation force of such a single-layer DET was found to be below 1 mN. Therefore, thousands of DET layers have to be stacked to generate the required forces. Real-time measurements of the PEN cantilever curvature allow to extract the expected millisecond response time as well as to detect self-clearing effects of the electrode.

The electrostatic pressure in DETs drives the incompressible PDMS elastomer to expand laterally by tens of percent. A major goal is the development of nanometer-thin flexible and stretchable electrodes. The two main paths employed to increase an electrode's compliance involve either the manipulation of its intrinsic material properties or its structural features, such as the introduction of wrinkles, which arise above the critical stress of metal films on elastomer substrates. We have demonstrated that DETs with wrinkled Cr/Au electrodes show a drift of only 2 % compared to 15 % for the ones with planar electrodes. The effective elastic modulus of DETs was measured using state of the art nanoindenting techniques and atomic force microscopy (AFM) based nanoindentations. The elastic modulus of the PDMS film for single-layer DETs was found to increase by a factor of 2.3 after depositing a

10 nm-thin Au electrode.

We demonstrate that the interplay between functionalized, oxygen plasma-treated PDMS films and sputter-deposited Au electrodes allows to conserve the compressive stress within the electrode. Insulator-metal transition occurs at only 10 nm-thin Au electrodes and below this electrode thickness, AFM nanoindentations reveal no stiffening of the Au/PDMS heterostructure. Probing a DC-powered thin-film DET with an AFM spherical tip leads to increased indentation depths by several ten percent, as verified by dynamic FE models. Charge accumulation is found to be responsible for a softening effect of the DET structure. In conclusion, electrodes with a controlled topology can be prepared to trigger a preferred direction of the actuation. We show that wrinkle patterns formed on the elastomeric membrane depend on the plasma treatment parameters as well as on the elastic modulus of the bulk PDMS film. Nanomechanical mapping with sub-micrometer resolution reveals topology dependent elastic properties of plasma treated PDMS membranes. The material on the nano-hills is significantly stiffer with respect to the one located in the nano-valleys.

Operation voltages of DETs at a few volts require PDMS membranes with some hundred nanometers in thickness. Thin PDMS films were fabricated using in-house built electro-spray (ESD) or organic molecular beam deposition (OMBD) techniques. Although the homogeneity of thermally evaporated PDMS films using OMBD is superior with respect to spin-coating or electro-spraying, its applicability for DETs is restricted. The evaporation of PDMS prepolymers is limited to oligomers at low deposition rates, due to the thermal degradation of the used polymer. We show that by using SH-functionalized PDMS with a low molecular weight of 3'600 g/mol, one can electro-spray smooth PDMS membranes at growth rates 10-times higher compared to OMBD. An adhesive layer between the electrode and the elastomer is not required, as the Au clusters form strong covalent bonds to the SH-groups within the elastomer network. We also show that PDMS films can be cured in air using a high-power Xe-Hg ultraviolet light (UV) lamp, and tune the elastic modulus between 165 and 1'300 kPa in less than a minute. This production speed makes ESD and in-situ UV curing promising for fabricating of multi-layer DETs that can be operated at low voltages.

Zusammenfassung

Nanotechnologie basierte dielektrische Elastomerwandler (DETs) werden für eine wachsende Anzahl von Anwendungen eingesetzt, darunter elektrisch fokussierbare Linsen, Mikrofluidik, Softrobotik und Geräte mit haptischem Feedback. DETs bestehen aus nichtleitenden und weichen Elastomermembranen, eingeklemmt zwischen nachgiebigen Elektroden. Sie zeigen einzigartige Leistungsmerkmale, wie z.B. Dehnungen ähnlich wie bei menschlichen Skelettmuskeln und Reaktionszeiten im Millisekundenbereich, die sie für Anwendungen als künstliche Muskeln vielversprechend machen. Ihr Hauptnachteil sind jedoch die hohen Betriebsspannungen von mehreren tausend Volt. Für medizinische Anwendungen ist ihr Betrieb auf wenige Dutzend Volt begrenzt. Innerhalb des SmartSphincter Projekts haben wir Techniken entwickelt, um DET-Strukturen zu fabrizieren und zu charakterisieren und diese als Implantate zur Behandlung von Fäkalinkontinenz einzusetzen. Für die Elastomermembran wurde Polydimethylsiloxan (PDMS) aufgrund seiner Biokompatibilität und exzellenten elastischen Eigenschaften gewählt. Die geringe Adhäsion von Gold Elektroden zu PDMS ist bekannt und führt zur Bildung von Gold Nanoclustern. Der Durchmesser dieser Nanocluster beträgt ca. (25 ± 10) nm und kann durch die niedrige Oberflächenenergie von PDMS erklärt werden, was zu einem Volmer-Weber-Wachstum führt. Wir zeigen, dass (3-Mercaptopropyl) trimethoxysilan (MPTMS) als molekularer Leim verwendet werden kann und somit die Adhäsion Au-Elektrode auf plasmabehandeltem PDMS undbegünstigt.

Um Kräfte von mehreren Newton zu erzeugen, wie es für künstliche Fäkalsphinkter erforderlich ist, müssen mehrschichtige DETs fabriziert werden. Als erster Schritt wurde eine kompakte Vorrichtung entworfen und in Betrieb genommen, um die erzeugten Kräfte von planaren DETs zu messen. DETs mit einer aktiven Fläche von $4\,\text{mm} \times 12\,\text{mm}$ wurden auf dünnen Polyethylennaphthalat (PEN) Folien hergestellt. Die Biegung der asymmetrischen Folien/Cantilever wurde mittels einer Laserstrahlablenkung detektiert. Die erzeugte Kraft einer einschichtigen DET Struktur beträgt weniger als 1 mN. Demzufolge müssten tausende von DET-Schichten gestapelt werden, um Kräfte von einigen Newton zu erzeugen. Echtzeit-Messungen erlauben es, die Reaktionszeit zu extrahieren sowie Selbst-Clearing-Effekte von Elektroden nachzuweisen.

Der elektrostatische Druck in DETs zwingt die weiche aber inkompressible PDMS Membran seitlich zu expandieren. Ein wichtiges Ziel dabei ist die Entwicklung von dehnbaren, Nanometer dünnen Elektroden. Zwei Lösungsansätze, die zur Erhöhung der Nachgiebigkeit einer Elektrode dienen, beinhalten entweder die Manipulation ihrer intrinsischen Materialeigenschaften oder ihrer strukturellen Merkmale, wie die Einführung von Faltenstrukturen. Diese entstehen bei kritischen Spannungen von steifen Filmen auf weichen Elastomermembranen. Wir haben gezeigt, dass DETs mit gefalteten Cr/Au-Elektroden eine Drift von nur 2 % haben - gegenüber 15 % für

diejenigen mit planaren Elektroden. Der effektive Elastizitätsmodul von DETs wurde mitels neuesten Nanoindenter Technologien sowie Atomkraftmikroskopie (AFM) bestimmt. Der Elastizitätsmodul von PDMS Membranen bei einschichtigen DETs ist nach dem Sputtern einer 10 nm dünnen Au-Elektrode um einen Faktor von 2.3 gestiegen.

Wir zeigen, dass das Zusammenspiel von funktionalisierten und plasmabehandelten PDMS-Filmen und gesputterten Metallelektroden eine Druckspannung innerhalb der Elektrode erzeugt. Der Isolator-Metall-Übergang tritt bereits bei 10 nm-dünnen Au-Elektroden auf und unterhalb dieses Werts zeigen AFM Nanoindentationen keine Erhöhung der Steifigkeit von Au/PDMS Heterostrukturen.

Nanoindentationen mit einer sphärischen AFM-Spitze auf DETs bei angelegter Spannung führen zu erhöhten Eindringtiefen von mehreren zehn Prozent, wie auch dynamische FE-Modelle gezeigt haben. Die Ladungsakkumulation scheint für diesen Erweichungseffekt der DET-Struktur verantwortlich zu sein. Abschliessend wurden Elektroden mit einer kontrollierten Topologie fabriziert werden, um eine bevorzugte Richtung der Aktuation auszulösen. Wir zeigen, dass Faltenmuster von PDMS Membranen durch Plasmaparameter, Dicke der PDMS Membran sowie deren Elastizitätsmodul bestimmt werden. Die nanomechanische Kartierung mit Submikrometerauflösung zeigt topologisch abhängige elastische Eigenschaften von plasmabehandelten PDMS-Membranen. Das Material auf den Nanohügeln ist deutlich steifer als das in den Nanotälern.

DETs mit Betriebsspannungen von wenigen Volt erfordern PDMS-Membrane von einigen hundert Nanometer in Dicke. Für die Herstellung dieser Filme wurden zwei System hausintern entwickelt: das Elektrospray Depositionssystem (ESD) sowie die organische Molekularstrahldeposition (OMBD). Obwohl die Homogenität von thermisch verdampften PDMS Filmen mittels OMBD gegenüber Spincoating oder ESD bedeutend besser ist, so bleibt dessen Potential für DETs dennoch eingeschränkt. Die Verdampfung von PDMS Prepolymeren ist aufgrund der thermischen Stabilität auf Oligomere und bei niedrigen Evaporationsraten beschränkt. Wir zeigen, dass durch die Verwendung von ESD und thiol-funktionalisiertem PDMS, Membrane mit zehnfach höheren Wachstumsraten gegenüber OMBD fabriziert werden können. Eine Adhäsionsschicht zwischen der Elektrode und dem Elastomer ist nicht erforderlich, da Au-Cluster kovalente Bindungen zu SH-Gruppen innerhalb des Elastomernetzes eingehen. Wir zeigen auch, dass thiol-funktionalisierte PDMS-Filme mittels ultraviolettem Licht (UV) vernetzt werden können. Der Elastizitätsmodul kann in weniger als einer Minute zwischen 165 und 1'300 kPa eingestellt werden. Diese Fabrikationsgeschwindigkeit macht ESD und in-situ UV Härtung vielversprechend für die Herstellung von mehrschichtigen DETs, die bei kleinen Spannungen betrieben werden können.

List of Publications

Journal Articles

B. Osmani, H. Deyhle, T. Töpper, T. Pfohl, B. Müller, "Gold layers on elastomers near the critical stress regime," *Advanced Materials Technologies*, 1700105 (2017). http://dx.doi.org/10.1002/admt.201700105

B. Osmani, S. Seifi, H.S. Park, V. Leung, T. Töpper, B. Müller, "Nanomechanical probing of thin-film dielectric elastomer transducers," *Applied Physics Letters* **111**(9), 093104 (2017). http://dx.doi.org/10.1063/1.5000736

B. Osmani, G. Gerganova, B. Müller, "Biomimetic nanostructures for the silicone-biosystem interface: tuning oxygen-plasma treatments of polydimethylsiloxane," *European Journal of Nanomedicine* **9**(2), 69-77 (2017). http://dx.doi.org/10.1515/ejnm-2017-0002

T. Töpper, S. Lörcher, H. Deyhle, **B. Osmani**, V. Leung, T. Pfohl, B. Müller, "Time resolved plasmonics on self-assembled hetero-nanostructures for soft nanophotonic and electronic devices," *Advanced Electronic Materials*, **3**, 1700073 (2017). http://dx.doi.org/10.1002/aelm.201700073

B. Osmani, E.A. Aeby, B. Müller, "Stress measurements of planar dielectric elastomer actuators," *Review of Scientific Instruments* **87**, 053901 (2016). http://dx.doi.org/10.1063/1.4949519

F. Weiss, F.B. Madsen, **B. Osmani**, V. Leung, T. Töpper, B. Müller, "Molecular beam deposition of high-permittivity polydimethylsiloxane for nanometer-thin elastomer films in dielectric actuators," *Materials and Design* **105**, 106-113 (2016). http://dx.doi.org/10.1016/j.matdes.2016.05.049

F. Weiss, T. Töpper, **B. Osmani**, S. Peters, G. Kovacs, B. Müller, "Electrospraying nanometer-thin elastomer films for low-voltage dielectric actuators," *Advanced Electronic Materials* **2**(5), 1500476 (2016). http://dx.doi.org/10.1002/aelm.201500476

F. Weiss, T. Töpper, **B. Osmani**, H. Deyhle, G. Kovacs, B. Müller, "Thin film formation and morphology of electro-sprayed polydimethylsiloxane," *Langmuir* **32**(13), 3276-3283 (2016). http://dx.doi.org/10.1021/acs.langmuir.6b00476

E. Fattorini, T. Brusa, C. Gingert, S.E. Hieber, V. Leung, **B. Osmani**, M.D. Dominietto, F. Hetzer, B. Müller, "Artificial muscle devices: Innovations and prospects for fecal incontinence treatment," *Annals of Biomedical Engineering* **44**(5), 1355-69 (2016). http://dx.doi.org/10.1007/s10439-016-1572-z

T. Töpper, F. Weiss, **B. Osmani**, C. Bippes, V. Leung, B. Müller, "Siloxane-based thin films for biomimetic low-voltage dielectric actuators," *Sensors and Actuators A* **233**, 32-41 (2015). http://dx.doi.org/10.1016/j.sna.2015.06.014

Conference Proceedings

B. Osmani, T. Töpper, M. Siketanc, G. Kovacs, B. Müller, "Electrospraying and ultraviolet light curing of nanometerthin polydimethylsiloxane membranes for low-voltage dielectric elastomer transducers," *Proceedings of SPIE* **10163**, 101631E-1 (2017). http://dx.doi.org/10.1117/12.2258214

T. Töpper, **B. Osmani**, S. Lörcher, B. Müller, "Leakage current, self-clearing and actuation efficiency of nanometer-thin, low-voltage dielectric elastomer transducers tailored by thermal evaporation," *Proceedings of SPIE* **10163**, 101631F (2017). http://dx.doi.org/10.1117/12.2259897

B. Osmani, V. Leung, F. Weiss, T. Töpper, H. Deyhle, B. Müller, "Electrospraying of sub-micrometer SH-PDMS membranes on functionalized Au electrodes for low-voltage DEA," *Proceedings of EuroEAP*, (2016).

B. Osmani, H. Deyhle, F. Weiss, T. Töpper, M. Karapetkova, V. Leung, B. Müller, "Morphology and conductivity of Au electrodes on polydimethylsiloxane using (3-mercaptopropyl)trimethoxysilane (MPTMS) as an adhesion promoter," *Proceedings of SPIE* **9798**, 979822 (2016). http://dx.doi.org/10.1117/12.2219199

T. Töpper, F. Wohlfender, F. Weiss, **B. Osmani**, B. Müller, "Characterization of ultraviolet light cured polydimethylsiloxane films for low-voltage, dielectric elastomer actuators," *Proceedings of SPIE* **9798**, 979821 (2016). http://dx.doi.org/10.1117/12.2218608

V. Leung, E. Fattorini, M. Karapetkova, **B. Osmani**, F. Weiss, T. Töpper, B. Müller, "Biomimetic artificial sphincter muscles: status and challenges," *Proceedings of SPIE* **9797**, 97970M (2016). http://dx.doi.org/10.1117/12.2219090

T. Töpper, **B. Osmani**, F. Weiss, B. Müller, "Viscoelastic properties of polydimethylsiloxane studied by cantilever bending," *European Cells and Materials* **30**(1), 68 (2015).

B. Osmani, T. Töpper, C. Deschenaux, J. Nohava, F. Weiss, V. Leung, B. Müller, "Micro- and nanostructured electro-active polymer actuators as smart muscles for incontinence treatment," *AIP Conference Proceedings* **1646**, 91-100 (2015). http://dx.doi.org/10.1063/1.4908588

T. Töpper, **B. Osmani**, F. Weiss, C. Winterhalter, F. Wohlfender, V. Leung, B. Müller, "Strain-dependent characterization of electrode and polymer network of electrically activated polymer actuators," *Proceedings of SPIE* **9430**, 94300B (2015). http://dx.doi.org/10.1117/12.2084595

B. Osmani, T. Töpper, F. Weiss, F. Wohlfender, V. Leung, C. Bippes, B. Müller, "Nanomechanical characterization of polydimethylsiloxane films," *European Cells and Materials* **30**(1), 56 (2015).

F. Weiss, T. Töpper, **B. Osmani**, C. Winterhalter, B. Müller, "Impact of electrode preparation on the bending of asymmetric planar electro-active polymer microstructures," *Proceedings of SPIE* **9056**, 905607 (2014). http://dx.doi.org/10.1117/12.2045152

1 Introduction

The treatment of urinary and severe fecal incontinence (FI) is one of the largest growing markets in developed countries. The overall prevalence of FI in adults is reported to be between 11 and 15 % and is likely increasing due to demographic changes of our ageing society.[1] FI describes the loss of control of the defecation process and is one of the most devastating physical disabilities. It leads usually to a reduced quality of life and social isolation. It is reported that approximately one third of people living in retirement homes or institutions alike, are affected by FI.[2] Due to the underreported nature of FI, it is likely that its true prevalence is even higher.

For patients encountering FI for the first time, conservative therapies such as dietetics or specific pelvic floor trainings are advised. In a second step, surgical therapies aim the support of the natural sphincter muscle including the stimulation of the sacral nerves, insertion of absorption materials between the internal and external sphincter or implanting devices with a liquid-filled inflating cuff.[2] Current artificial sphincter systems consist of a hand-crafted balloon pump. They are slow, difficult to operate, and show considerable complication and revision rates.[2]

Smart designs based on dielectric elastomer transducers (DET) seem to be a promising approach. DETs are often referred to artificial muscles and have attracted broad interest due to their versatile applicability as actuators, sensors, and electric generators.[3–5] They are essential building blocks for applications in medicine, soft robotics, tunable optics, microfluidics and flexible optoelectronics. These structures show millisecond response times and mechanical strains of several 10 %.[6] Its specific continuous power is up to ten times higher than values obtained for human skeletal muscles.[3] However, their main drawback is the high operating voltages in the kV range.[7] Within the nano-tera.ch initiative we targeted the fabrication of a smart DET based artificial anal sphincter implant which can be operated at a few volts. This project was conducted together with clinicians from the Inselspital in Bern, Kantonsspital Schaffhausen and Winterthur as well as partners from the Swiss Federal Laboratories for Materials Science and Technologies (EMPA) in Dübendorf.

1.1 Dielectric elastomer transducers

The two main DET configurations can be divided into surface expansion and thickness compression transducers.[8] In their most primitive version, they are composed of an elastomer film, sandwiched between two compliant electrodes.[2,6] The elastomer film, often polydimethylsiloxane (PDMS), undergoes an expansion perpendicular to the applied electric field as a result of the Coulomb attraction of the oppositely charged electrodes. The generated Maxwell pressure, also called electrostatic pres-

sure p_{el}, is a physical quantity describing the amount of force acting on a defined area of a DET and is related to a certain applied driving voltage U:[9]

$$p_{el} = \epsilon_0 \epsilon_r \left(\frac{U}{d}\right)^2 \tag{1.1}$$

The electrostatic pressure p_{el} is proportional to the dielectric constant ϵ_r and to the square of the applied voltage and is inversely proportional to the square of the layer thickness d. The vacuum permittivity is given by ϵ_0. Therefore, the maximal compressive strain s_z in z direction is related to its elastic modulus E:

$$s_z = -\frac{p_{el}}{E} = -\frac{1}{E}\frac{\epsilon_0 \epsilon_r U^2}{d^2} \tag{1.2}$$

The elastomer layer is assumed to be incompressible with a bulk compressibility much higher than its elastic modulus. As its volume will remain constant, the compressive strain s_z is equally translated into strains in x- and y- directions. Typical electric fields of 100 V/µm are required which result in several kilovolts for DETs with commercially available membranes of 50 µm in thickness.[5]

In medical applications the operating voltage of DETs has to be reduced down to a very few tens of volts.[10] Therefore, one should either increase the dielectric constant or reduce the elastomer thickness. Many research groups report on increasing the dielectric constant using fillers such as TiO_2 and $BaTiO_3$ or by adding functional side groups to the PDMS chains.[11] According to Eq. (1.2), the reduction of the thickness of the elastomer layer has a great impact on the actuation strain. By using nanometer thin elastomer membranes with an elastic modulus of some hundreds of kilopascals, the calculated compressive strain s_z corresponds to several ten percents. Inherently by decreasing the layer thickness we reduce the exerted forces per layer. Thus, stacked multi-layer DETs have to be built to obtain the required forces.[12]

In this work, first we show how to measure forces of low-voltage single-layer DETs, present how to manipulate with nanostructures on elastomer films and fabricate soft electrodes.[13,14] Furthermore, we show how the interface between the elastomer membrane and the Au electrode can be enhanced by using a molecular glue or thiol-functionalized polymers.[15] Finally we show that functionalized PDMS films can be electro-sprayed and tuned in stiffness for applications as low-voltage DETs.[16]

1.2 Elastomer membranes

DETs are usually made of acrylic and silicone elastomers. In this work, we focus on silicone elastomers due to their biocompatibility and superior performance characteristics such as high applicable electric fields, tunable permittivity and tunable elastic modulus.[4] Silicone elastomers show millisecond response times due to the flexible Si-O bonds and there is no need for prestretching due to their low viscous losses .[4] Liquid precursors enable different thin-film fabrication techniques such as blade casting, spincoating, organic molecular beam (OMBD) or electro-spray deposition (ESD). Within this work, nanometer-thin PDMS films were fabricated using spincoating, OMBD and ESD techniques.[17–19] OMBD was conducted in ultra-high

vacuum (UHV) at a base pressure of ($\leq 10^{-7}$ mbar). PDMS prepolymers were evaporated using low-temperature effusion cells. The evaporated molecules are directed towards the substrate in such a way that there is no interaction between each other nor with other molecules inside the UHV chamber until they reach the substrate. Their mean free path, defined as the average distance atoms or molecules travel before interacting with another species, is in the range of some tens of meters. Therefore, to obtain nanometer thin films with a homogeneity of > 95 % OMBD is the method of choice.

In comparison, ESD has been shown to be very effective for fast deposition of elastomer films.[16] It can be operated in direct current (DC) or alternating current (AC) mode. A solution of PDMS/ethyl-acetate is sprayed using a nozzle with an inner diameter of 260 µm. The nozzle itself is attached to a voltage source whereas the substrate is grounded. Micrometer size droplets of the solution are accelerated within the electric field. The droplets, consisting mainly of solvents, will decrease in size due to evaporation of the solvent until the volume-to-charge ratio reaches a critical value. At this point, the droplet system exceeds the Rayleigh instability limit which leads to a 'Coulomb explosion'. The droplets split into finer droplets and repulsion forces cause the fine droplets to self-disperse. To manufacture nanometer-thin elastomer films for multi-stack DETs by ESD, the AC mode prevents charge accumulation on the substrate. Confluent PDMS layers were obtained even at thicknesses as thin as (220 ± 70) nm.[16] The elastic modulus could be set to (165 ± 35) kPa using a Hg-Xe lamp. In addition, the adhesive layer between the electrode and functionalized PDMS was not required, as Au nanoclusters form covalent bonds to the SH-groups of the elastomeric network.[16] The topology of the films was investigated using 3D-laser microscope and atomic force microcopy.

1.3 Compliant metal electrodes

Another key element for DETs are compliant electrodes. As reported by McCoul at al. they should be mechanically compliant and electrically conductive.[20] Mechanical compliance includes thin and soft electrodes with a good adhesion to the elastomer membrane. Electrical conductivity implies low sheet resistance R at 0 % strain and small changes in R during the actuation. One approach is based on the intrinsically stretchable composite materials, such as elastomers filled with conductive nanoparticles.[20] Here we focus on structural features, such as the introduction of wrinkles, which arise above the critical stress of metal films on elastomer substrates.[14] Many materials and related fabrication and characterization methods have been proposed for the compliant electrodes, including carbon powder, metallic thin films or the implantation of metal nanoclusters.[21] In comparison to other techniques, ion implantation doesn't form confluent metal films, but rather to PDMS/metal composite and is thus not further discussed. In addition, the diffusion depth of the ion-implanted Au particles into the elastomer membrane of nanometer-thin DETs is difficult to control.

Metal electrodes with a thickness of ∼20 nm , such as Au, can be easily deposited on elastomer substrates using cathodic sputtering, electron beam or thermal evapo-

ration techniques. A big drawback of metallic electrodes is the relatively high elastic modulus, i.e. 79 GPa for bulk Au compared to the soft sandwiched elastomer having an elastic modulus of ∼1 MPa. A second hindrance is the limited elasticity of about 3 % comparably and the low adhesion of Au to PDMS, which has to be overcome by the deposition of an additional adhesive layer of Cr or Ti.[22] For nanometer-thin DETs, however, it is inappropriate as it leads to a rise of several orders of magnitudes for the overall DET stiffness. An approach for improving the adhesion of Au to PDMS are bifuncunctional molecules such as (3-mercaptopropyl) trimethoxysilane (MPTMS) which can serve as molecular adhesives. MPTMS has two kinds of functional groups that can form bonds to the metal and elastomer.[15] The thiol head (-SH) binds to Au, whereas the three methoxy (-OCH3) functional groups bind to th silanized PDMS (-OH) surface. Therefore, the introduction of silanol functional groups on the PDMS surface is required and can be realized via oxygen plasma treatments.

Plasma treatments of elastomer films do not alter only its chemistry but also the topography of the surface. Wavy patterns arise due to the mismatch of the thermal expansion coefficient of the formed silica-like layer and the bulk PDMS. The heating originates from the plasma itself and causes the PDMS layer to expand. Upon cooling, the bulk PDMS shrinks much more than the stiff silica-like film and exerts a compressive stress on the stiff film on top. We demonstrate that wrinkles can be tailored in amplitude and periodicity.[23] Furthermore, we show that by depositing Au on MPTMS-functionalized and oxygen-plasma-treated PDMS membranes, we can conserve the compressive stress and fabricate soft Au electrodes.[14]

The nanomechanical properties were extracted using AFM nanoindentation techniques. Micrometer-sized spots were partitioned into hundreds or thousands of subdomains, each serving as a nanoindentation site. The elastic modulus for each subdomain was calculated out of force distance curves using the Hertz contact model. For samples showing high adhesion forces, the Johnson-Kendall-Roberts (JKR) contact model was used. Furthermore, we have varied the Au electrode thickness and measured the mechanical impact on the overall DET structure.[15]

2 Results

2.1 Stress measurements of planar dielectric elastomer actuators

Fabrication of planar thin-film DETs on polymeric substrates.

Quantification of exerted forces of single-layer DETs.

System can be calibrated by by rotating the apparatus around its perpendicular axis and measuring the gravity induced displacement on the PSD for selected angles.

The curvature for small deflections is modeled using differential equations for the deflection of an elastic beam.

Measurements with a sampling rate of 50 Hz allow to extract the response time of DETs.

Actuation data on double-logarithmic plots show that curvature of polymeric substrate is proportional to the square of the applied voltage.

Structural changes are detected as well as breakdown voltages.

The apparatus is capable of measuring forces of multi-layer DETs.

Published in Review of Scientific Instruments

Stress measurements of planar dielectric elastomer actuators

Bekim Osmani, Elise A. Aeby, and Bert Müller

Citation: Review of Scientific Instruments **87**, 053901 (2016); doi: 10.1063/1.4949519
View online: http://dx.doi.org/10.1063/1.4949519
View Table of Contents: http://aip.scitation.org/toc/rsi/87/5
Published by the American Institute of Physics

REVIEW OF SCIENTIFIC INSTRUMENTS **87**, 053901 (2016)

Stress measurements of planar dielectric elastomer actuators

Bekim Osmani, Elise A. Aeby, and Bert Müller
Biomaterials Science Center, University of Basel, Gewerbestrasse 14, 4123 Allschwil, Switzerland

(Received 6 December 2015; accepted 2 May 2016; published online 17 May 2016)

Dielectric elastomer actuator (DEA) micro- and nano-structures are referred to artificial muscles because of their specific continuous power and adequate time response. The bending measurement of an asymmetric, planar DEA is described. The asymmetric cantilevers consist of 1 or 5 μm-thin DEAs deposited on polyethylene naphthalate (PEN) substrates 16, 25, 38, or 50 μm thick. The application of a voltage to the DEA electrodes generates an electrostatic pressure in the sandwiched silicone elastomer layer, which causes the underlying PEN substrate to bend. Optical beam deflection enables the detection of the bending angle vs. applied voltage. Bending radii as large as 850 m were reproducibly detected. DEA tests with electric fields of up to 80 V/μm showed limitations in electrode's conductivity and structure failures. The actuation measurement is essential for the quantitative characterization of nanometer-thin, low-voltage, single- and multi-layer DEAs, as foreseen for artificial sphincters to efficiently treat severe urinary and fecal incontinence. *Published by AIP Publishing.* [http://dx.doi.org/10.1063/1.4949519]

I. INTRODUCTION

Dielectric elastomer actuators (DEAs) consist of electrically insulating membranes sandwiched between compliant electrodes. Their performance characteristics, i.e., lateral strains similar to mammalian skeletal muscles[1] and millisecond response times,[2] offer a wide variety of applications including artificial muscles.[3] Using polydimethylsiloxane (PDMS) as an elastomer membrane, electrical fields of 100 V/μm are required to generate strains comparable to human skeletal muscles.[4] Current research activities for medical applications[5] focus on the reduction of the operation voltage to a few 10 V, which implies the fabrication of sub-micrometer-thin elastomer layers. In order to reach the necessary actuation forces[6] multilayer devices have to be built. A proper characterization of the accessible strain levels as the function of the applied voltage is, therefore, crucial to improving future DEA devices. Recently, the critical need for standardization of dielectric elastomer transducers has been addressed.[7] The present communication presents a compact cantilever-based setup to reproducibly and precisely measure the actuation forces and the related strains of DEAs. DEAs are especially interesting since they can also operate in sensor mode.[8]

Cantilever bending is well known, e.g., from atomic force microscopy and heteroepitaxy studies.[9] In static mode, they can act as mechanical sensors to measure surface stress.[10–12] Force sensing via cantilevers was also shown for a zinc oxide film sandwiched between two electrodes.[13] Disposable polymer micromechanical cantilever arrays were fabricated by means of vario-thermal micro-injection molding techniques[14] and were used to detect single-stranded DNA sequences and metal ions. In cell biology and for the characterization of biomaterials cantilevers serve for the determination of contractile cell forces. For example, an ensemble of fibroblasts seeded to a single-crystalline silicon cantilever can be detached by means of trypsin and the related cantilever relaxation monitored.[15] Elastic and shear moduli were measured using cantilevers with a piezoelectric layer on a stainless steel plate. The electric field causes the cantilever to bend compressing the softer substrate.[16] Bending is usually detected using (i) piezoresistive or piezoelectric readout techniques or (ii) optical methods including the interferometry-based and the beam-deflection readout, which is most common because of simplicity and lateral resolution.[17]

II. EXPERIMENT

A. Fabrication of DEA on polyethylene naphthalate (PEN) cantilever

Biaxially oriented polyethylene naphthalate (PEN) sheets (Teonex® Q51, Synflex, Germany) 16, 25, 38, or 50 μm thick in A4-format were weighted with an electronic laboratory balance (Shimadzu Corporation, Type UW620HV, readability of 0.001 g) to verify their average thicknesses, cf., Table I. The PEN sheets were cut to the size of 3 in. wafers and cleaned by ethanol. In order to keep the substrates planar, we have deployed single-crystalline 3 in. Si wafers as a mechanical support.

The backside of the PEN substrate was coated with a 20 nm thin Au film using a DC magnetron sputter coater (SCD040, Balzers Union, Liechtenstein) at a discharge current of 15 mA in a 0.05 mbar Ar-atmosphere and served as a reflective layer. A quartz crystal microbalance (QSG 301, Balzers Union, Liechtenstein) monitored the deposition.

On the front size of the PEN substrate, the DEA films were fabricated. The 20 nm-thin Au electrodes were sputtered through Mo masks under the same conditions as the reflective layer. The seven windows in the Mo masks, each 4 mm × 22 mm, were cut using a pulsed Nd:YAG solid-state laser. Subsequent to the sputtering of the first Au electrodes the elastomer layers were spin-coated (WS-400B-6NPP/LITE/AS, Laurell Technologies Corporation, North

TABLE I. Geometrical parameters of the PEN cantilevers with DEA on top.

	PEN cantilever			DEA layer thickness		
Sample	Thickness (μm)	Width (mm)	Length (mm)	Elastomer (μm)	Electrodes (nm)	Reflective layer (nm)
#1	16 ± 0.3	4 ± 0.5	12 ± 1	1.0 ± 0.2	20 ± 2	20 ± 2
#2	25 ± 0.5	4 ± 0.5	12 ± 1	1.3 ± 0.3	20 ± 2	20 ± 2
#3	38 ± 0.6	4 ± 0.5	12 ± 1	5.0 ± 1	20 ± 2	20 ± 2
#4	50 ± 0.8	4 ± 0.5	12 ± 1	5.0 ± 1	20 ± 2	20 ± 2

Wales, PA, USA) with a rotation speed of 6000 rpm for the duration of 2 min. For this purpose, the two liquid components of the silicone elastomer kit, Dow Corning® 184 Silicone Elastomer Kit, Dow Corning Europe S.A, Belgium, were mixed and degassed for a 30 min period. For the preparation of the films marked #1 and #2, the methylsiloxane-based solvent, Dow Corning® OS-20 Fluid, Dow Corning Europe S.A, Belgium, was added to 10 ml containers at a ratio of 1:5 to reduce the obtained film thickness. Seven PEN cantilevers with the DEA on top, see scheme in Figure 1(a), were cut off with a standard roller cutter from each 3 in. PEN substrate.

The 3D Laser Microscope Keyence VK-X200, Keyence International, Belgium, was used to measure the film thickness with a spatial resolution of 0.5 nm. Table I lists the results of the thickness measurements.

In order to contact the bottom Au electrode, a 3 mm broad stripe of the PDMS-layer was removed through washing in ethyl acetate immediately after spin coating. In a next step, the PDMS was thermally cured at a temperature of 75 °C for a period of 24 h. Finally, the film for the other electrodes was sputtered on the cured PDMS layer.

DEA/PEN cantilevers 22 mm long and 4 mm wide were cut out of the processed PEN substrate and mounted on a polytetrafluoroethylene (PTFE) holder so that the free-standing area of 12 mm × 4 mm could contribute to the actuation. Figure 1 displays (a) the DEA design on the PEN cantilever, (b) the mounting on the PTFE holder with the organization of the electrical contacts, and (c) the scheme of the bending mechanism for the anisotropic microstructure.

The DEA was powered with either the source Stanford Research System PS310, GMP SA, Lausanne, Switzerland or the Amplifier Nanobox USB, Piezosystem Jena GmbH, Germany. The applied voltage was monitored using the portable high-voltage USB oscilloscope Handyprobe HP3-5, TiePie Engineering, Holland.

The mechanical properties of the DEA structure were assessed by the atomic force microscope FlexAFM C3000, Nanosurf AG, Switzerland. To this end, 400 indentation measurements on 60 μm × 60 μm arrays at a load of 100 nN using a spherical tip with a radius of 500 nm (B500_FMR, Nanotools GmbH, Germany) were acquired. The mean Young's modulus of DEA microstructures was calculated using the FLEX-ANA® (Automated Nanomechanical Analysis) software from Nanosurf. Potential effects of the PEN substrate were neglected since the indentation depths were well below 500 nm.

B. Bending radius measurements of the DEA/PEN cantilever

The apparatus consists of two compartments, labeled (A) and (B), as shown in Figure 2(a). In the temperature-controlled chamber with the label (A), the DEA/PEN cantilever is mounted on a PTFE holder and connected to the power source. This compartment has three DN 50 mm openings that allow for the visual inspection and keeping records with a camera. The opening on the back gives direct access

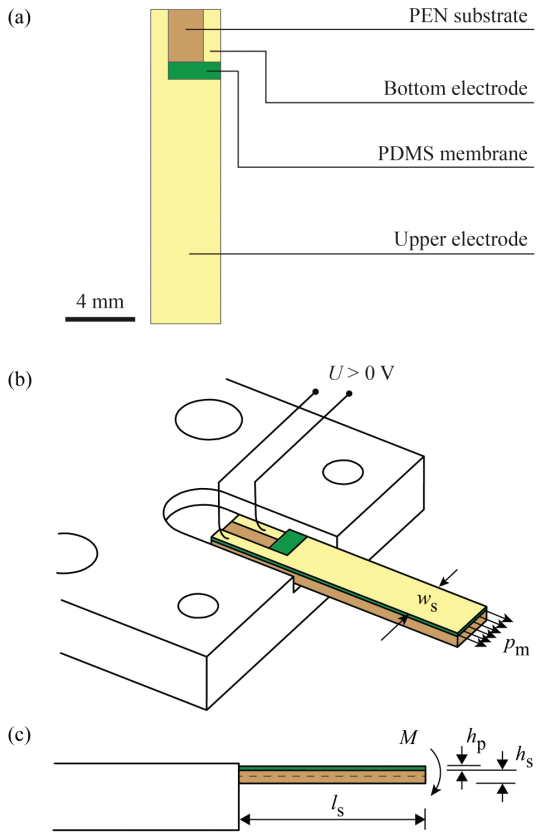

FIG. 1. Completion of the DEA/PEN cantilever. (a) Top view of the cantilever showing the sandwiched PDMS layer on the PEN substrate. (b) DEA/PEN cantilever mounted on a grooved PTFE holder and with an illustration of the electrical contacts. The Maxwell pressure p_m in the elastomer film induces the torque M. (c) Side view of the cantilever including the main geometrical parameters.

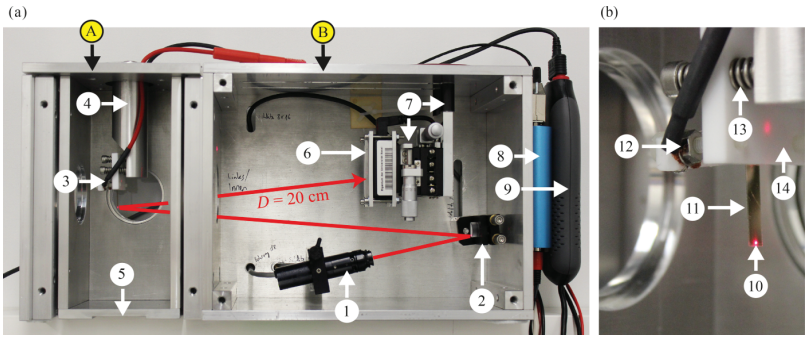

FIG. 2. Apparatus for bending measurements of the DEA/PEN cantilever. The voltage-induced bending of the DEA cantilever is detected by the optical beam-deflection method. The vertical arrangement of the cantilever prevents a gravity-induced bending. The rotation of the apparatus around its axis can be used for calibration purposes as described below. (a) The photograph shows the compartment for the cantilever, labeled (A) and the one for the optical detection, labeled (B). The path of the laser beam is drawn in red color. (b) The detailed view displays the positioning of the cantilever. The main components of the apparatus are (1) the diode laser L2S-WEB-SL, Laser 2000 GmbH, Germany, (2) the broadband mirror, Thorlabs GmbH, Germany, (3) the cantilever holder made from PTFE, (4) the rotatable support for the cantilever holder, (5) two Peltier elements 6.3 A/65 W/16.7 V/74 K, Deltron AG, Switzerland, (6) the PSD SPOTCOM-L09, Duma Optronics Ltd., Israel, (7) the two-dimensional linear translation stage, Newport, Taiwan, (8) the amplifier Nanobox USB, Piezosystem Jena GmbH, Germany, (9) the oscilloscope Handyprobe HP3-5, TiePie Engineering, Holland, (10) the reflected laser beam on the backside of the Au-coated cantilever, (11) the DEA/PEN cantilever, (12) the support for the electrical contacts, (13) the screws for adjusting the beam direction, and (14) the PTFE cantilever holder.

to the cantilever. The PTFE cantilever holder is mounted on a rotatable solid aluminum arm with three screw/spring joints to adjust the direction of the reflected laser beam, as shown in Figure 2(b). Note that the actuators will be integrated into medical implants intended to operate at body temperature, and the DEA is sensitive to ambient air conditions. Flooding the compartment with rare gases or nitrogen at well-defined temperature is therefore a key feature of the apparatus.

The compartment (B) contains the elements for the optical detection of the cantilever bending, i.e., the laser, a mirror, and the position-sensitive detector (PSD). The size of the PSD is 9 mm × 9 mm and has a position accuracy of ±12.5 μm. It can be translated in two directions by means of a linear translation stage and in the third direction using rails on top of the apparatus.

An input of electrical energy by applying a voltage U to the DEA with the related electrostatic pressure p_m acting on the elastomer film leads to a torque that bends the asymmetric cantilever. The laser beam is reflected on the back side of the Au-coated cantilever and is positioned close to its free end. The sensitivity of the system depends on the cantilever length l_s and the distance D between cantilever and PSD. The choice of these two parameters allows measuring of actuation forces as small as 0.1 N. The curvature of the cantilever k_s, i.e., the inverse bending, is derived from the displacement d of the laser beam on the PSD,

$$k_s = \frac{1}{2Dl_s}d = 208\frac{1}{m^2}d. \tag{1}$$

The displacement d is directly provided by the optical beam position and power measurement system (SpotON, Version 5.30.1, Duma Optronics Ltd., Israel) that controls the 24 bit A/D electronics box via the USB 2.0 port at an update rate of 50 Hz.

III. RESULTS AND DISCUSSION

A. Calibration

Equation (2) describes the gravity-driven deflection of the neutral axis $\delta(x)$ for a one-sided fixed horizontal cantilever determined by its free length l_s, the elastic modulus E_s, and the area moment of inertia I_s,[18]

$$\delta(x) = \frac{q}{24E_sI_s}(x^4 - 4l_sx^3 + 6l_s^2x^2). \tag{2}$$

The deflection at the apex δ_t for $x = l_s$ yields to

$$\delta_t = \delta_{x=l_s} = \frac{ql_s^4}{8E_sI_s}. \tag{3}$$

The curvature k_s can be approximated using the deflection at apex and cantilever length,[10]

$$k_s \approx \frac{2\delta_t}{l_s^2}. \tag{4}$$

Thus, assuming the uniform load $q = mg/l_s$, the curvature k_s depends on the cantilever orientation φ,

$$k_s = \frac{mgl_s}{4E_sI_s}\sin\varphi, \tag{5}$$

where m is the total mass, here the one of the PEN substrate including the DEA structure. Because of the area momentum of inertia I_s, the value of the average cantilever thickness h_s has to be precisely known. The data of the manufacturer should be verified. Here, the rotation of the apparatus, which is displayed in Figure 2(a), around the perpendicular axis is useful. One can easily measure the curvature k_s, for example, in angular steps of 30° along 720°. Figure 3(a) shows such experimental data with the plotted Equation (5) for the substrate only and for the substrate with a fabricated DEA on top. The error indicates reasonable reliability and reproducibility. Using Equation (5), the curvature is converted into the thickness

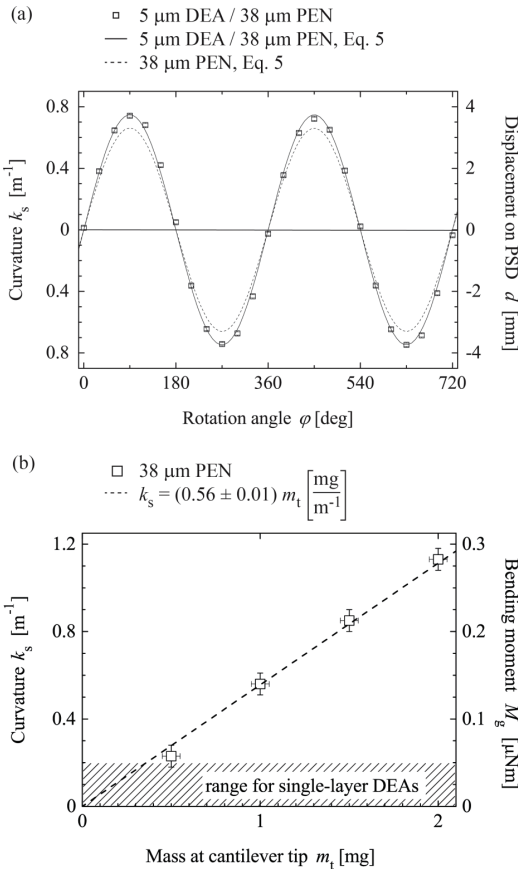

FIG. 3. Calibration of the PEN cantilever. (a) The system is calibrated, rotating the apparatus around its perpendicular axis and measuring the gravity-induced displacement on the PSD for the selected angles. The amplitude of the fitted sine is compared with the prediction for a one-sided fixed horizontal beam under a uniformly distributed load. (b) The curvature k_s was measured for selected amounts of water placed near the tip of the cantilever in Al container. The system shows a linear behavior for bending radii larger than 1 m.

$h_s = (37.7 \pm 0.6)\ \mu$m, a value that corresponds to the information of the manufacturer.

To verify the linear behavior of the cantilever deflection in the stress interval of interest, an increasing amount of water was put in an Al container near the free end of the horizontally oriented cantilever. To this end, a single-channel micropipette with 2 μl water (Finnpipette, Labsystems 4500, Finland) was applied. Figure 3(b) summarizes a selected series of experiments, which demonstrate the linearity for curvatures of up to 1 m^{-1}. Therefore, the method allows testing multilayer DEAs, if a single-layer DEA produces curvatures of up to 0.2 m^{-1} as for the present experiment.

An alternative to determine the geometrical and mechanical parameters of the cantilever is the measurement of the flexural bending frequencies. Utilizing the presented experimental setup, however, a reliable analysis was only possible with single-crystalline Si cantilevers and not with the much softer PEN.

B. Background

The dependence between the curvature k_s of the cantilever and the voltage U applied to the DEA microstructure on top should be predicted. The DEA with an elastomer thickness h_p and a relative permittivity ε can transduce the applied voltage U into mechanical work according to the Maxwell stress,[19] generally termed as the actuation pressure p_m,

$$p_m = \varepsilon_0 \varepsilon \frac{U^2}{{h_p}^2}. \tag{6}$$

The generated force F for a single-layer DEA is length independent. It is determined by the cross-sectional area A, given by the width w and height h_p,

$$F = p_m A = p_m h_p w = \varepsilon_0 \varepsilon \frac{U^2}{h_p} w. \tag{7}$$

Since the Young's modulus of the substrate is about three orders of magnitude higher than the one of the deposited DEA, the induced bending moment M on the asymmetric cantilever with the thickness h_s can be written as

$$M = F\left(\frac{h_s}{2} + \frac{h_p}{2}\right). \tag{8}$$

Using the differential equation for the deflection of an elastic beam,[10] the curvature k_s for small deflections is known as

$$k_s = \frac{1}{R} \cong \frac{\partial^2 z}{\partial x^2} \cong \frac{M}{E^* I} = \frac{M(1-\nu_s)}{E_s I_s}, \tag{9}$$

with E^* as the biaxial modulus[20] that relates to the Young's modulus E_s and the Poisson's ratio ν_s as $E^* = E_s/(1-\nu_s)$. Replacing the area moment of inertia of the cantilever using $I_s = (w h_s^3)/12$, the curvature k_s can be expressed as a function

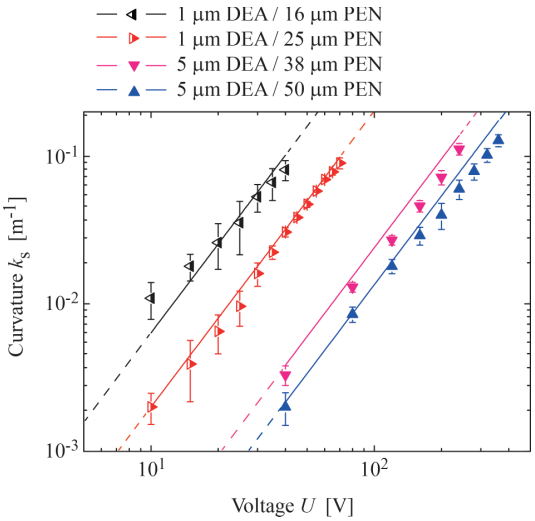

FIG. 4. Actuation of DEA on PEN-cantilevers as a function of the applied voltage U. The error bars correspond to the standard deviation obtained from multiple measurements. The lines originate from the predictions according to Equation (10).

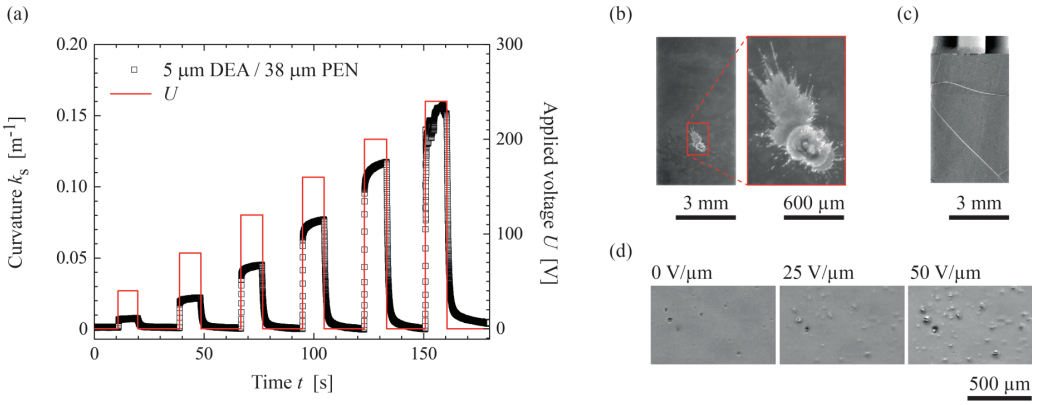

FIG. 5. (a) The curvature measurements with a 50 Hz sampling rate demonstrate the time response of the DEA/PEN actuator to voltages applied for a duration of 10 s. The application of 240 V resulted in a discontinuous behavior, which indicates the formation of changes within the Au electrodes. (b) The optical micrograph of the DEA electrode acquired with two magnifications shows the morphology after dielectric breakdown. (c) Optical micrograph to demonstrate the formation of characteristic cracks. (d) The series of optical micrographs indicates morphological changes as the function of the applied electric field. The values are given above each image.

of U^2 and a constant term

$$k_s = \frac{F(h_p + h_s)(1 - \nu_s)}{2E_s I_s} = U^2 \frac{6\varepsilon_o \varepsilon (h_p + h_s)(1 - \nu_s)}{E_s h_p h_s^3}. \quad (10)$$

C. Actuation curves for single-layer DEA on PEN cantilever

Figure 4 shows the actuation behavior of DEA/PEN cantilevers applying voltages U between 10 and 370 V. The 5 μm-thick elastomer films were deposited on the 38 and 50 μm-thick PEN-substrates. As the DEA structures with a thickness of 1 μm evolve smaller bending moments than the 5 μm-thick microstructures, they were prepared on 16 and 25 μm-thin PEN-substrates. For these thinner DEA-microstructures, the voltage was limited to 72 V to prevent the electrical breakdown. The precise value depends on humidity, temperature, film thickness, elastomer pre-stretching, and the stiffness of the electrodes.[7,21,22] The maximal curvatures were below 0.1 m^{-1}. Therefore, the experiments only cover the linear regime. Figure 4 represents the obtained actuation data on a double-logarithmic plot and demonstrates the quadratic dependence of the curvature k_s from the applied voltage U. The system allows detecting bending radii R up to 850 m, which corresponds to $k_s = 0.0012$ m^{-1}. The experimental data reasonably agree with the ones predicted from Equation (10), cf., Figure 4.

D. Real-time measurement of actuation curves

Figure 5(a) displays experimental data on the temporal response of a DEA/PEN cantilever to rectangular voltage pulses with a duration of 10 s. The actuator reacts with the expected millisecond response.[2] Especially for the higher voltages, however, one clearly observes a creep. This creep may originate from the viscoelastic deformation of the PDMS membrane and the morphology changes of the relatively stiff electrodes with forming cracks owing to the areal strain.[23–25] The integration of an adhesive layer can prevent the crack formation and allows for significantly larger electric fields.[26] The areal strain in the top electrode depends on the Young's modulus of the DEA and the applied voltage U. Assuming a uniform electric field at a voltage of 240 V and a Young's modulus of (411 ± 38) kPa, as experimentally derived, the areal strain of a free standing membrane corresponds to 6.7%. As the DEA/PEN cantilevers are one-side constrained, the electro-creasing to cratering instability has to be considered. This phenomenon can be suppressed or delayed by stiffening or pre-stretching the elastomers. The electrical energy density u_{max} is a critical performance parameter for DEA and expressed as[27]

$$u_{max} = Z\mu = \varepsilon \frac{E_b^2}{2}. \quad (11)$$

Assuming the parameters $Z = 0.53$, $\varepsilon = 2.7\varepsilon_0$, and $\mu = 137$ kPa for the PDMS used, the derived value for the breakdown voltage $E_b = 78$ V/μm corresponds well to the experimental results of the present study. Gatti *et al.* have shown recently that the dielectric breakdown limit depends on its thickness and the pre-stretch ratio.[28] They have identified a value of about 70 V/μm for a 20 μm-thin PDMS membrane. Figure 5(b) shows selected optical micrographs of a DEA/PEN cantilever after electrical breakdown.

As displayed in Figure 5(a), the discontinuous curvature changes during the application of a constant voltage as high as 240 V implying local structural failures and the significant formation of cracks, as shown in Figure 5(c). Structural changes can even be recognized well below the breakdown voltage, cf., the series of optical micrographs in Figure 5(d). The magnitudes of the applied electrical fields are displayed above the micrographs.

IV. CONCLUSIONS

A compact, portable apparatus to measure the actuation of DEA on micrometer-thin polymer cantilevers was designed, built, and brought into operation. The detected actuation values

correspond reasonably well to the predictions. The actuation force F of a single-layer DEA calculated from Equation (10) is below 1 mN. The apparatus is therefore well suited also for the characterization of multi-layer actuators. The electrical breakdown is observed at 80 V/μm that is smaller than the dielectric strength of 140 V/μm reported for the used silicon elastomer[8] (Dow Corning® Sylgard 184). We presume that impurities and thickness variations within the elastomer layer caused the reduction. The presented apparatus for measuring the voltage-dependent curvature will allow improving the actuator performance that includes the long-term behavior.

ACKNOWLEDGMENTS

The financial support of the nano-tera.ch initiative, project SmartSphincter, is gratefully acknowledged. The authors thank Sascha Martin from the machine shop at the Physics Department of the University Basel for the manufacturing of the mechanical components. Synflex GmbH, Germany kindly provided the PEN Teonex® Q51 substrates. The authors also thank Monica Schönenberger from the Nanotech Service Lab for her assistance at the 3D Laser microscope as well as Tino Töpper, Vanessa Leung, and Florian Weiss for their support in component selection and discussion of technical details.

[1]J. D. W. Madden, N. A. Vandesteeg, P. A. Anquetil, P. G. A. Madden, A. Takshi, R. Z. Pytel, S. R. Lafontaine, P. A. Wieringa, and I. W. Hunter, IEEE J. Oceanic Eng. **29**(3), 706–728 (2004).
[2]R. Pelrine, Science **287**(5454), 836–839 (2000).
[3]Y. Bar-Cohen, *Electroactive Polymer (EAP) Actuators as Artificial Muscles: Reality, Potential, and Challenges* (SPIE Press, 2004).
[4]B. Müller, H. Deyhle, S. Mushkolaj, and M. Wieland, Swiss Med. Wkly **139**(41-42), 591–595 (2009).
[5]T. Töpper, F. M. Weiss, B. Osmani, C. Bippes, V. Leung, and B. Müller, Sens. Actuators, A **233**, 32–41 (2015).
[6]A. O'Halloran, F. O'Malley, and P. McHugh, J. Appl. Phys. **104**(7), 071101 (2008).
[7]F. Carpi, I. Anderson, S. Bauer, G. Frediani, G. Gallone, M. Gei, C. Graaf, C. Jean-Mistral, W. Kaal, and G. Kofod, Smart Mater. Struct. **24**(10), 105025 (2015).
[8]P. Brochu and Q. Pei, Macromol. Rapid Commun. **31**(1), 10–36 (2010).
[9]D. Sander, A. Enders, and J. Kirschner, Rev. Sci. Instrum. **66**(9), 4734–4735 (1995).
[10]M. Godin, V. Tabard-Cossa, P. Grütter, and P. Williams, Appl. Phys. Lett. **79**(4), 551–553 (2001).
[11]C. A. Klein, J. Appl. Phys. **88**(9), 5487–5489 (2000).
[12]M. Liangruksa, Master thesis, Virginia Polytechnic Institute and State University, Virginia, 2008.
[13]T. Itoh and T. Suga, Appl. Phys. Lett. **64**(1), 37–39 (1994).
[14]P. Urwyler, O. Häfeli, H. Schift, J. Gobrecht, F. Battiston, and B. Müller, Procedia Eng. **5**, 347–350 (2010).
[15]J. Köser, S. Gaiser, and B. Müller, Eur. Cells Mater. **21**, 479–487 (2011), http://www.ncbi.nlm.nih.gov/pubmed/21623572.
[16]A. Markidou, W. Y. Shih, and W. H. Shih, Rev. Sci. Instrum. **76**(6), 064302 (2005).
[17]M. Bicker, U. Von Hülsen, U. Laudahn, A. Pundt, and U. Geyer, Rev. Sci. Instrum. **69**, 460–462 (1998).
[18]W. Flügge, *Handbook of Engineering Mechanics* (McGraw-Hill, New York, 1962).
[19]R. Pelrine, R. Kornbluh, J. Joseph, R. Heydt, Q. Pei, and S. Chiba, Mater. Sci. Eng. C **11**(2), 89–100 (2000).
[20]T. Miyatani and M. Fujihira, J. Appl. Phys. **81**(11), 7099–7115 (1997).
[21]B. Osmani, T. Töpper, C. Deschenaux, J. Nohava, F. M. Weiss, V. Leung, and B. Müller, AIP Conf. Proc. **1646**(1), 91–100 (2015).
[22]S. Rosset and H. Shea, Appl. Phys. A **110**(2), 281–307 (2013).
[23]I. M. Graz, D. P. Cotton, and S. P. Lacour, Appl. Phys. Lett. **94**(7), 071902 (2009).
[24]T. Töpper, B. Osmani, F. M. Weiss, C. Winterhalter, F. Wohlfender, V. Leung, and B. Müller, Proc. SPIE **9430**, 94300B (2015).
[25]K. Jia, T. Lu, and T. J. Wang, Sens. Actuators, A **239**, 8–17 (2016).
[26]B. Osmani, H. Deyhle, F. M. Weiss, T. Töpper, M. Karapetkova, V. Leung, and B. Müller, Proc. SPIE **9798**, 979822 (2016).
[27]X. Zhao and Q. Wang, Appl. Phys. Rev. **1**(2), 021304 (2014).
[28]D. Gatti, H. Haus, M. Matysek, B. Frohnapfel, C. Tropea, and H. F. Schlaak, Appl. Phys. Lett. **104**(5), 052905 (2014).

2.2 Morphology and conductivity of Au films on polydimethylsiloxane using (3-mercaptopropyl)-trimethoxysilane as adhesion promoter

Functionalization of plasma treated PDMS surface using (3-mercaptopropyl)trimethoxysilane (MPTMS) serves as soft interface between Au electrode and PDMS film.

Elastic modulus of DETs increases with the square of the Au electrode thickness.

Four-point resistance measurements show improved conductivity for Au electrodes with MPTMS interface.

Published in Proceedings of SPIE

Morphology and conductivity of Au films on polydimethylsiloxane using (3-mercaptopropyl)trimethoxysilane (MPTMS) as an adhesion promoter

Bekim Osmani
Hans Deyhle
Florian M. Weiss
Tino Töpper
Maria Karapetkova
Vanessa Leung
Bert Müller

Morphology and conductivity of Au films on polydimethylsiloxane using (3-mercaptopropyl)trimethoxysilane as adhesion promoter

Bekim Osmani, Hans Deyhle, Florian M. Weiss, Tino Töpper, Maria Karapetkova, Vanessa Leung, and Bert Müller*
Biomaterials Science Center, Department of Biomedical Engineering, Medical Faculty, University of Basel, 4123 Allschwil, Switzerland.

ABSTRACT

Dielectric elastomer actuators (DEA) are often referred to as artificial muscles due to their high specific continuous power, which is comparable to that of human skeletal muscles, and because of their millisecond response time. We intend to use nanometer-thin DEA as medical implant actuators and sensors to be operated at voltages as low as a few tens of volts. The conductivity of the electrode and the impact of its stiffness on the stacked structure are key to the design and operation of future devices. The stiffness of sputtered Au electrodes on polydimethylsiloxane (PDMS) was characterized using AFM nanoindentation techniques. 2500 nanoindentations were performed on 10 x 10 μm^2 regions at loads of 100 to 400 nN using a spherical tip with a radius of (522 ± 2) nm. Stiffness maps based on the Hertz model were calculated using the Nanosurf Flex-ANA system. The low adhesion of Au to PDMS has been reported in the literature and leads to the formation of Au-nanoclusters. The size of the nanoclusters was (25 ± 10) nm and can be explained by the low surface energy of PDMS leading to a Volmer-Weber growth mode. Therefore, we propose (3-mercaptopropyl)trimethoxysilane (MPTMS) as a molecular adhesive to promote the adhesion between the PDMS and Au electrode. A beneficial side effect of these self-assembling monolayers is the significant improvement of the electrode's conductivity as determined by four-point probe measurements. Therefore, the application of a soft adhesive layer for building a dielectric elastomer actuator appears promising.

Keywords: Molecular adhesive, soft adhesive, nanoclusters, nanoindentation, nanometer-thin films, atomic force microscopy, four-point probe resistivity, MPTMS

1. INTRODUCTION

Dielectric elastomer actuators (DEAs) have received increased attention in recent years due to their versatile applicability as actuators, sensors, and electric generators [1-4]. Rolled actuators are often compared to human skeletal muscles because of their millisecond response time and large strains of several ten percent [5]. Recent works show a promising step toward biomedical applications for implant devices to be operated at voltages below 24 V and are proposed as the method of choice for future implants to treat fecal incontinence [6-8]. For planar DEAs, polydimethylsiloxane (PDMS) elastomer films are sandwiched between two compliant electrodes and transduce the electrical energy into mechanical work [9]. As the PDMS film can be regarded as incompressible, the electrostatic pressure leads to lateral strains of typically 5 to 15 %. Therefore, a key factor is the development of compliant electrodes showing suitable conductivity and the necessary adhesion to the elastomer layer. Many materials and related fabrication and characterization methods have been proposed for the compliant electrodes, including carbon powder, metallic thin films or the implantation of metal nanoclusters in the first tens of nanometers of the elastomer layer [10]. Metal electrodes with a thickness of up to about 20 nm, such as Au, can be easily deposited on elastomeric substrates using cathodic sputtering, electron beam or thermal evaporation techniques [11]. A first hindrance for the metallic electrodes is the relatively high elastic modulus of 79 GPa for Au and the limited elasticity of about 3 % compared to the soft sandwiched elastomer of about 1 MPa [12]. A second hindrance is the comparably low adhesion of Au to PDMS, which has to be overcome by the deposition of an additional adhesive layer of Cr or Ti [13]. For submicrometer thin DEAs, however, it is a suboptimal method as it leads to a rise of several orders of magnitudes in overall DEA stiffness [14].

An approach for improving the adhesion between Au and PDMS significantly is the transfer of Au films deposited on rigid substrates to PDMS using (3-mercaptopropyl)trimethoxysilane (MPTMS) as a molecular adhesive [15].

*bert.mueller@unibas.ch; phone +41 61 207 54 445; fax +41 61 265 9699; www.bmc.unibas.ch

Electroactive Polymer Actuators and Devices (EAPAD) 2016, edited by Yoseph Bar-Cohen, Proc. of SPIE
Vol. 9798, 979822 · © 2016 SPIE · CCC code: 0277-786X/16/$18 · doi: 10.1117/12.2219199

A similar procedure to transfer atomically flat gold films onto the elastomer is presented [16]. MPTMS has two kinds of functional groups that can form bonds between metal and elastomer. The thiol head (-SH) binds to Au, whereas the three methoxy (-OCH_3) functional end groups can bind to a silanized PDMS (-OH) surface in the presence of water as catalyst. Therefore, the introduction of silanol functional groups on the PDMS surface is needed and can be realized via oxygen plasma or ultraviolet/ozone treatments [17, 18]. The plasma treatment evokes a silica like surface layer, which increases with treatment time and power. I was found to be between 5 and 35 nm thick [19]. The native PDMS and the plasma treated region are distinguished by monitoring the phase shift during an atomic force microscopy (AFM) scan in tapping mode [20]. The modified SiO_x surface increases not only the hydrophilic properties but also alters the nanostructured morphology of the film [21]. The gained hydrophilicity is temporary and decays with time due to the migration of the smaller polymer chains from the bulk to the surface, reorientation of the polar groups and the condensation of hydroxyl groups [21-23]. The plasma treatment also alters the surface topography. Wrinkles arise due to the mismatch of the elastic modulus of the silica-like layer and the bulk PDMS layer and can be tailored in amplitude and periodicity [24, 25]. One observes an enormous variance of the estimated elastic modulus for the silica-like surface layer. The quantitatively investigated values vary with the treatment time, plasma power, and oxygen concentrations and were found to be between 4 MPa and 1.5 GPa [19, 20].

In the present work, we have evaluated the applicability of MPTMS as a molecular adhesive between the DC-sputtered Au electrode and the PDMS for DEA applications. The nanomechanical properties were extracted using a spherical amorphous high–density diamond–like carbon (HDC/DLC) AFM tip. The average stiffness was extracted from 2,500 force-distance curves (FDC) for native and functionalized PDMS (fPDMS). Furthermore, we have varied the Au electrode thickness and measured the mechanical impact on the overall DEA structure. The conductivity on PDMS and fPDMS surfaces for electrode thicknesses of 5 to 15 nm was assessed using a four-point probe setup.

2. MATERIALS AND METHODS

2.1 Preparation and functionalization of PDMS

PDMS (Dow Corning® 184 Silicone Elastomer Kit, Dow Corning Europe S.A, Belgium) was prepared by mixing the prepolymer (component A) and the crosslinker (component B) at a volume ratio of 10:1. The mixture was degassed for a period of 30 minutes and spin-coated on 2-inch Si(100) at rotation speed of 6,000 rpm for a period of 120 s. The films were cured at a temperature of 75 °C for a period of 24 hours, *cf.* scheme in Figure 1(a).

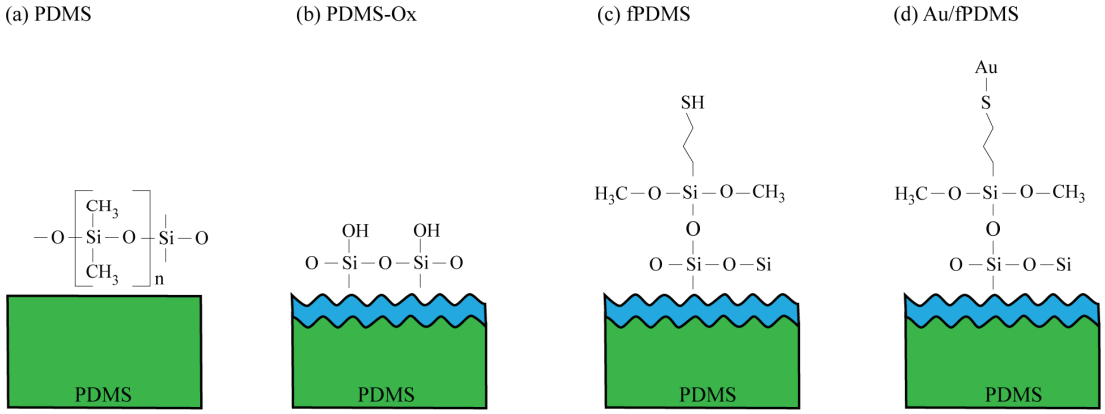

Figure 1. Schematic illustrations of PDMS surface modification using oxygen plasma and functionalization with MPTMS, which acts as a molecular adhesive between the sputtered Au and the underlying PDMS-Ox layer. (a) A native PDMS layer (green color) is spin-coated on a rigid silicon wafer and is thermally cured. (b) Processing with oxygen plasma applying a power of 200 W for a period of 24 s leads to a silica like layer (blue color) and formation of Si-OH polar groups on the surface (PDMS-Ox). (c) Functionalizing of the PDMS-Ox surface by vapor deposition of (3-mercaptopropyl)trimethoxysilane in vacuum and subsequent washing in ethyl acetate to remove the excessive MPTMS layers. (fPDMS). (d) DC sputtering of Au on the functionalized surface leads to covalent bonds between Au the thiol (-SH) functional group (Au/fPDMS).

The specimens were oxygen plasma treated using the RF power of 200 W at a frequency of 40 kHz for a period of 24 s (PICO System, Diener Electronics, Ebhausen, Germany). The oxygen partial pressure was kept constant at 0.3 mbar with a flow rate of 20 sccm. The plasma treatment altered the surface topography and increased the SiO_x concentration on the surface (PDMS-Ox) as indicated in the scheme of Figure 1(b).

MPTMS was deposited on the activated PDMS-Ox surface in a vacuum. A 5 mL glass container filled with MPTMS of a purity ≥ 94.5 % (Sigma-Aldrich, Switzerland, CAS Number: 4420-74-0, formula: $C_6H_{16}O_3SSi$, formula weight: 196.34 g/mol) was kept in a vacuum chamber at 0.1 mbar for a period of 60 minutes. The low pressure enabled the evaporation and, therefore, the coating of the whole chamber with MPTMS. Finally, the vacuum chamber was vented with air and one of the three methoxy ($-OCH_3$) functional end groups was enabled to bind to the silanized PDMS (-OH) surface in the presence of water as catalyst. The excess MPTMS was washed out in an ethyl acetate (Merck KGaA, Darmstadt, Germany) bath. The functionalized surface is schematically shown in Figure 1(c).

In a final step, *cf.* the scheme in Figure 1(d), Au electrodes (Lesker, East Sussex, UK) were sputtered using a DC magnetron sputter coater (SCD040, Balzers Union, Liechtenstein) at a discharge current of 15 mA in a pressure of 0.05 mbar Ar atmosphere (Carbagas AG, Gümligen, Switzerland). The thickness of the 5, 7, 10, and 15 nm Au electrodes was monitored with a quartz crystal microbalance (QSG 301, Balzers Union, Liechtenstein).

2.2 Calculation of elastic modulus

The elastic moduli for native PDMS and functionalized PDMS (fPDMS) films were assessed by atomic force microscopy (FlexAFM C3000, Nanosurf AG, Switzerland). A series 2,500 force-distance curves (FDC) was calculated for 10 µm × 10 µm regions at loads using a spherical tip with a radius of (522 ± 2) nm (B500_FMR, Nanotools GmbH, Germany). The spring constant of the cantilever was determined using the thermal tune method and was found to be (1.9 ±0.1) Nm. During a single nanoindentation (NI) measurement, the sample was moved toward the AFM tip until the pre-defined force P of 100, 200, 300, or 400 nN was reached. The additional information of the z-piezo allowed the exact calculation of the NI depth h. The mean elastic modulus E was calculated using the HERTZ contact model implemented in the FLEX-ANA® software (Automated Nanomechanical Analysis, Nanosurf AG, Switzerland). Potential substrate effects were neglected, since the indentation depths were below 300 nm, whereas the spin-coated films were (8 ± 1) µm thick.

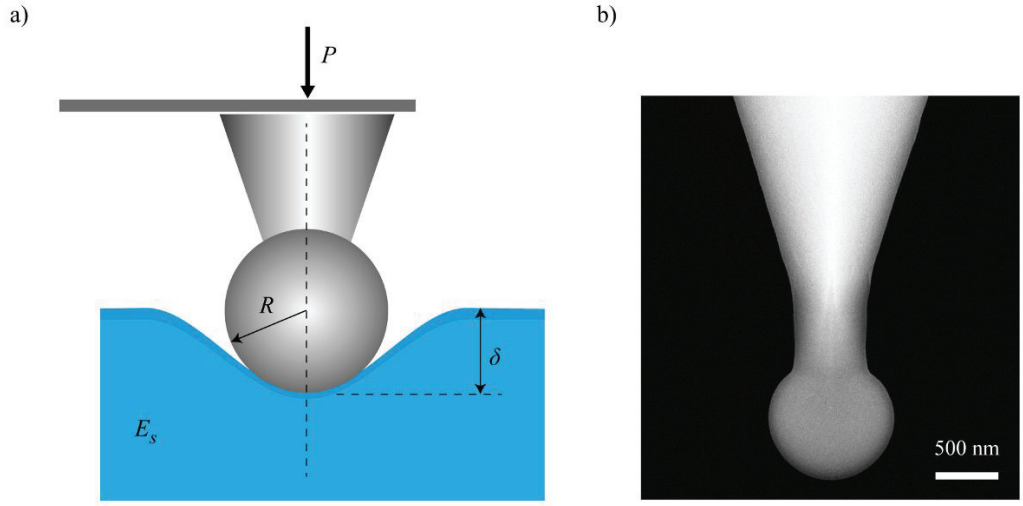

Figure 2. (a) Hertz contact model used for nanoindentation measurements (b) SEM image of a B500 tip.

2.3 AFM Imaging

AFM images were acquired by raster scanning a soft AFM probe (Tap190Al-G probe, NanoAndMore GmbH, Wetzlar, Germany) in tapping mode (vibration amplitude 2.0 V, set point 20 %) using a FlexAFM System (Nanosurf AG, Liestal, Switzerland). 512 lines at a speed of 1 s per line were acquired for each image. The raw data were leveled by subtracting a mean plane and removing a polynomial background of the second degree. Root-mean-square (RMS) roughness values were calculated using the open source software for SPM data analysis Gwyddion, Version 2.41.

2.4 Four-point conductivity measurements

The sheet resistance of the Au films was quantified using the four-point probes setup as schematically shown below (see Figure 8 (a) and (b)). The advantage of four-terminal sensing is that the resistances of wires, contacts and the internal resistance of the two-terminal sensing are eliminated. First, four liquid metal drops (Coollaboratory Liquid Pro, Coollaboratory, Magdeburg, Germany) were placed on the Au electrode at equal distances. The semi-spherical probe tips (SPA-3J, Everett Charles Technologies, Distrilect) were mounted on micropositioners (Signatone, APS Solutions GmbH, Munich, Germany) and were lowered contacting the liquid metal drops. A constant current of 1 to 15 mA was applied to the outer tips using a commercially available source meter (Keithley 2401). The voltage drop between the inner tips was measured using a multimeter (Agilent 34461A Truevolt).

Depending on the geometry of the electrode, the resistance calculations differ [26]. In this work, the measurements have been performed on round- and cantilever-shaped electrodes. For the round-shaped electrodes, the voltage drop U can be expressed as a function of applied current I and the sheet resistance R_S:

$$U = \frac{IR_S}{\pi}\left[\ln(2) + \ln\left(\frac{\left(\frac{d}{s}\right)^2 + 3}{\left(\frac{d}{s}\right)^2 - 3}\right)\right]. \tag{1}$$

The sample diameter was d = 50.8 mm and the tips were equally spaced at a distance *of* s = 6 mm.

For cantilever-shaped electrodes, the sheet resistance of a Hall bar was calculated according to the formula:

$$U = IR_S\left(\frac{l}{w}\right), \tag{2}$$

where the width of the cantilever was w = 4 mm, and the length was l = 16 mm.

3. RESULTS AND DISCUSSION

3.1 Morphology of native PDMS and sputtered Au electrodes

The surface morphology of the spin-coated and thermally cured PDMS, *cf.* AFM images in Figure 3(a), was flat and showed a root-mean-square roughness of 0.23 nm for the 1 μm^2 AFM scan. Subsequent sputtering of a 15 nm-thin Au electrode significantly increased the roughness, in the particular case to 1.69 nm. The electrode was sputtered at a rate of 15 nm per minute and led to the formation of Au-nanoclusters, as shown in the AFM images of Figure 3(b) and (c). The diameter of the nanoclusters was found to be from 20 nm to 40 nm and can be explained by the low surface energy of PDMS leading to a Volmer-Weber growth mode [27].

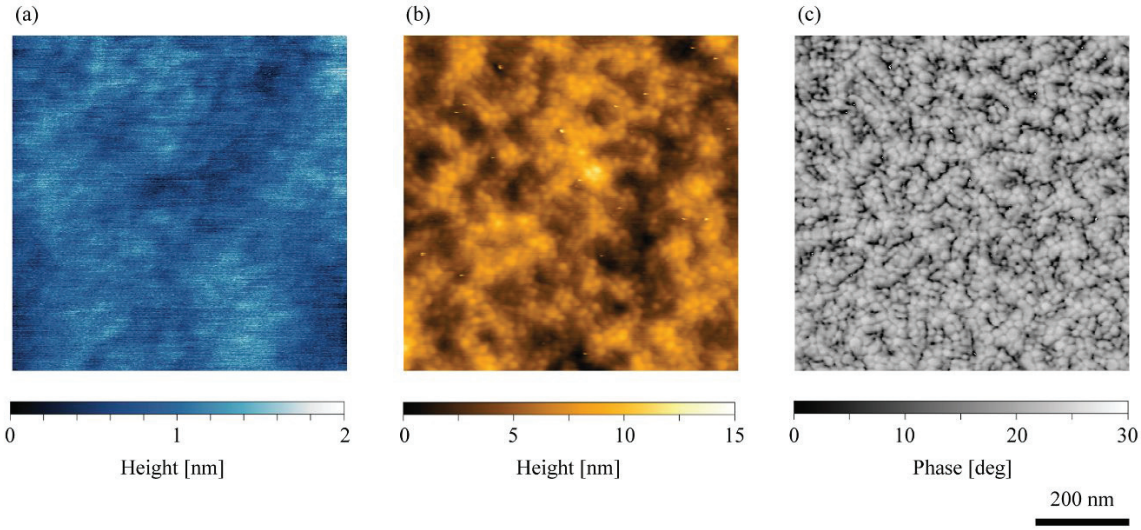

Figure 3. (a) AFM scan of a spin-coated native PDMS layer reveals a flat surface with RMS of 0.23 nm. (b) AFM scan of a sputtered 15 nm Au electrode on a PDMS layer shows RMS of 1.69 nm. The low adhesion of Au to PDMS leads to the formation of Au-nanoclusters with an average diameter of (25 ± 10) nm. (c) Phase signal of the AFM scan on the sputtered 15 nm Au/PDMS. The dark areas in the height scan on the left contain nanoclusters of similar size as seen in the phase image.

3.2 PDMS activation: PDMS-Ox

The activation of PDMS with oxygen plasma led to a spontaneous formation of wrinkles as shown by the scheme and the AFM image in Figure 4. During the plasma treatment, a bilayer structure forms. The structure undergoes a buckling instability due to the thermal expansion differences of the stiffer silica film and the softer PDMS.

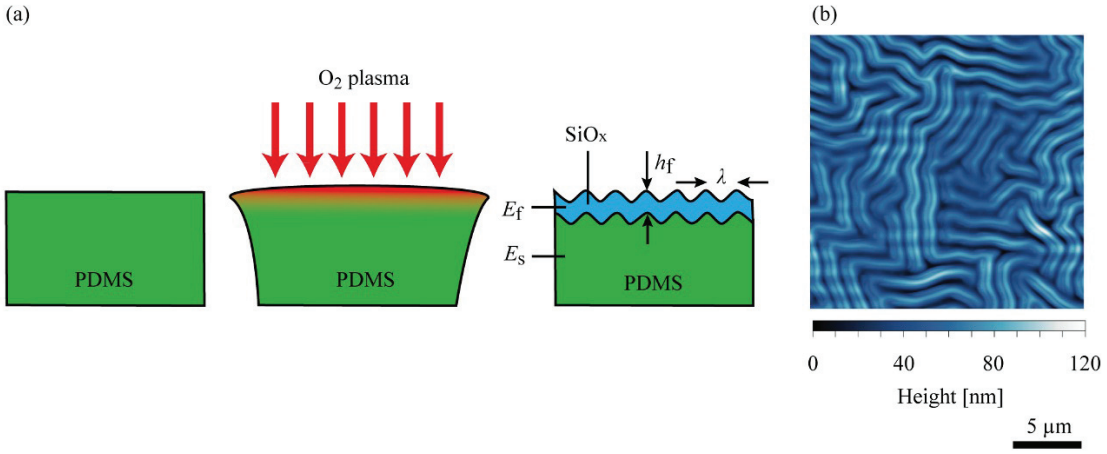

Figure 4. Schematic representation of PDMS surface modifications using oxygen plasma treatment. The plasma treatment changes the surface chemistry and surface morphology. Wrinkles arise due to the mismatch of the elastic moduli of the silica-like layer E_f and the bulk PDMS E_s. (b) AFM scan of a 20 µm × 20 µm region after plasma treatment. The characteristic wrinkles are the prominent features.

It wrinkles at an equilibrium wavelength and amplitude that minimizes the elastic energy of the entire system. The wavelength of the wrinkles is linearly proportional to the thickness of the film and the ratio between the elastic moduli of

film and underlying substrate [19]. The morphology of the wrinkled, silanized surface is exemplarily represented by the AFM image in Figure 4(b).

3.3 Functionalization of PDMS-Ox with MPTMS

The vacuum deposition of MPTMS on the PDMS-Ox surface was validated by comparing the phase shift of the oscillating AFM tip in tapping mode. For this purpose, we used a square mesh mask with and area of $7.5 \times 7.5\ \mu m^2$ openings to selectively plasma treat and functionalize the native PDMS surface. The average phase shift was found to be $15° \pm 5°$ for the plasma treated surface. After the subsequent vacuum deposition of the MPTMS on the silanized PDMS surface, the phase shift was $35° \pm 5°$ indicating a significant change in the treated areas, *cf.* Figure 5.

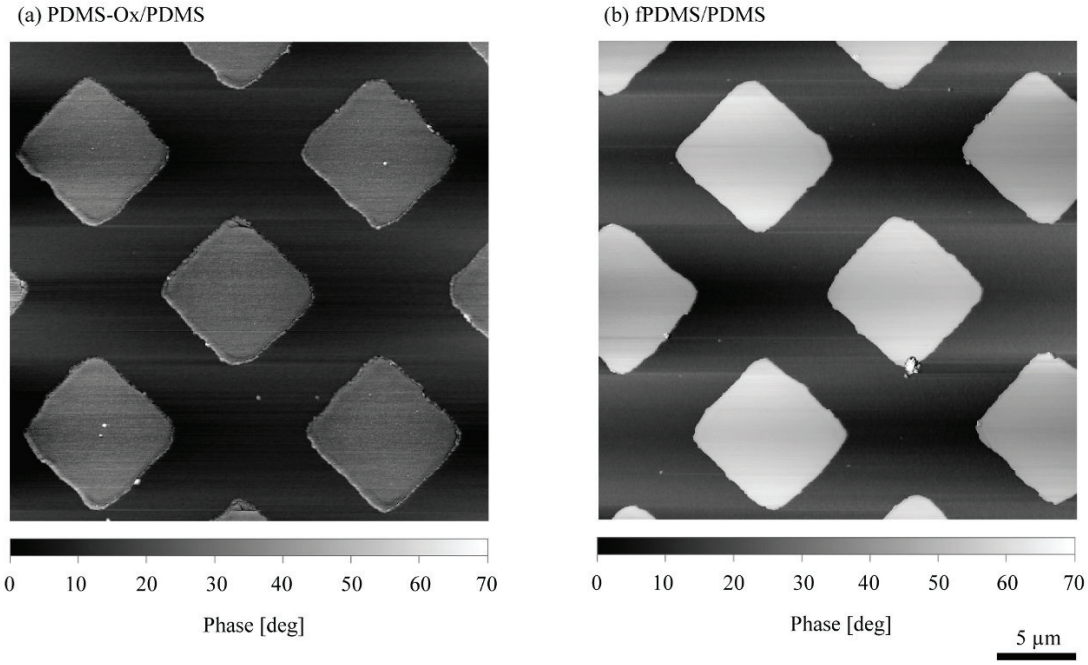

Figure 5. (a) AFM scan of PDMS-Ox squares on a PDMS substrate layer. The phase image indicates the changed surface functionality (b) AFM scan of fPDMS squares on a PDMS substrate. The functionalization of the PDMS-Ox with MPTMS increased the phase shift by about 20°.

3.4 Morphology of Au on fPDMS

Wrinkles on the PDMS-Ox surface were maintained after functionalization with MPTMS. The wavelength of the wrinkles λ on the fPDMS surface was found to be (2.0 ± 0.1) µm. It was determined by the two-dimensional Fast Fourier Transform (FFT) implemented in Gwyddion. To calculate the amplitude of the wrinkles, a height histogram was generated from the *z*-data. The histogram exhibits two peaks that correspond to the valleys and hills positions, respectively. The peaks were fitted with Gaussians. The distance between the peaks corresponded to the amplitude and was found to be (61 ± 3) nm. No preferential orientation of the wrinkles could be observed. After the subsequent deposition of 15 nm Au, the wrinkles were not detected anymore, see Figure 6(b).

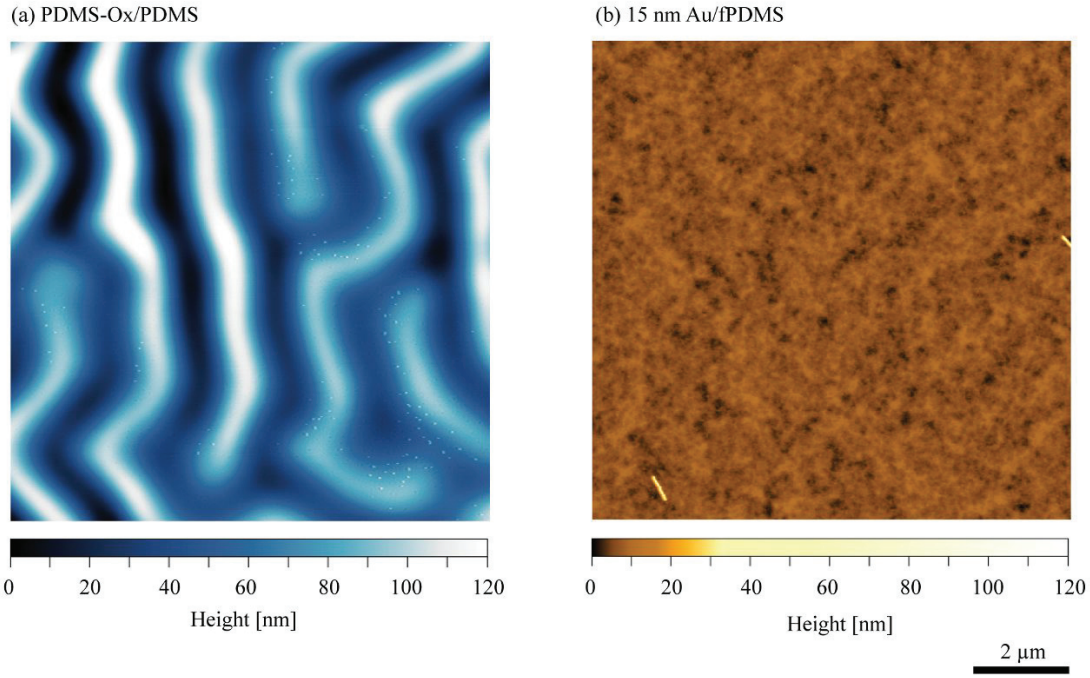

Figure 6. (a) AFM scan of fPDMS. The wrinkles do not show any preferential orientation. (b) AFM scan obtained after deposition of 15 nm Au.

3.5 Stiffness of fPDMS and modification due to Au layer

The elastic modulus of the sample E_s was computed using the linear HERTZ contact theory, where the indentation depth δ is related to the contact radius a and the indenter radius R:

$$\delta = \frac{a^2}{R} = \left(\frac{9P^2}{16RE_r^2} \right)^{1/3}, \tag{3}$$

where P is the applied force and E_r the reduced elastic modulus, which is defined as

$$\frac{1}{E_r} = \frac{1-\nu_s^2}{E_s} - \frac{1-\nu_i^2}{E_i}. \tag{4}$$

The second term contains the elastic modulus E_i and Poisson ratio ν_i of the indenter and can be neglected for rigid tips on soft samples. The Poisson ratio ν_s for PDMS is 0.5, and, therefore, the elastic modulus of the sample E_s can be approximated to:

$$E_s = E \approx 0.56 \sqrt{\frac{P^2}{R\delta^3}}. \tag{5}$$

Figure 7 shows the elastic modulus E as a function of the Au thickness t. The plotted values represent the average elastic modulus out of 2,500 nanoindentation (NI) measurements performed. For bare PDMS (t = 0 nm), the measured value corresponds well to values obtained by other research teams [28]. The elastic modulus seems to follow a parabolic fit: $E = A + Bt + Ct^2$ with A = (1.00 ± 0.03), B = (0.09 ± 0.02), and C = (0.01 ± 0.001).

The elastic modulus E as a function of the Au thickness t for fPDMS is shown in Figure 7(b). It is not significantly increasing in the region, where wrinkles were observed. In this region it can be approximated by E = (2.1 ± 0.1) MPa.

Geometrical artefacts between the tip sphere and the valleys inside a single wrinkle can be neglected since the bending radius of the wrinkle was found to be three times higher than the radius of the indenter sphere itself. The values for 10 nm Au and 15 nm Au electrodes are around 2 MPa higher than on bare PDMS.

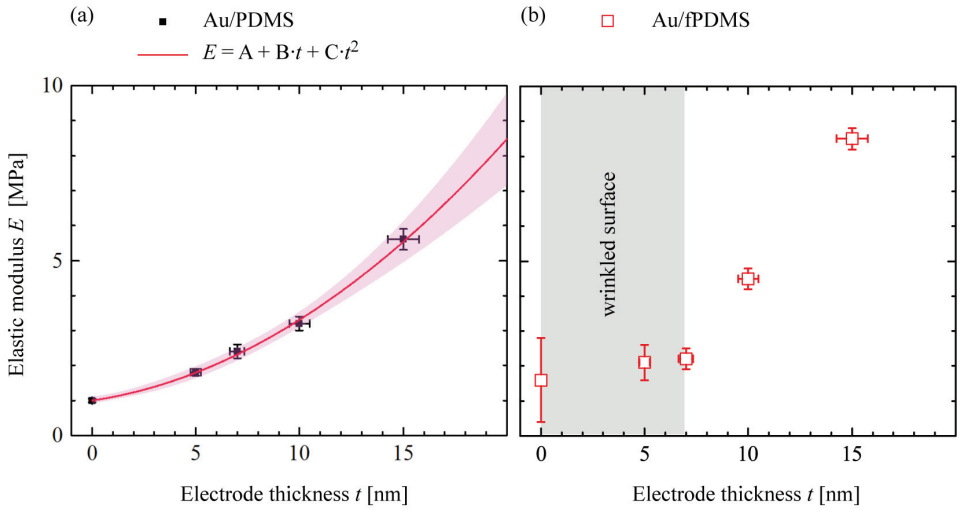

Figure 7. Mechanical properties of sputtered Au on (a) PDMS and (b) fPDMS as a function of the Au layer thickness t. (a) The fitted elastic modulus shows a quadratic behavior. (b) The stiffness seems to remain constant for the region, where wrinkles observed.

3.6 Four-point conductivity measurements

The sheet resistance R_s is defined as a function of the applied current I and the voltage drop U on a four probe setup.

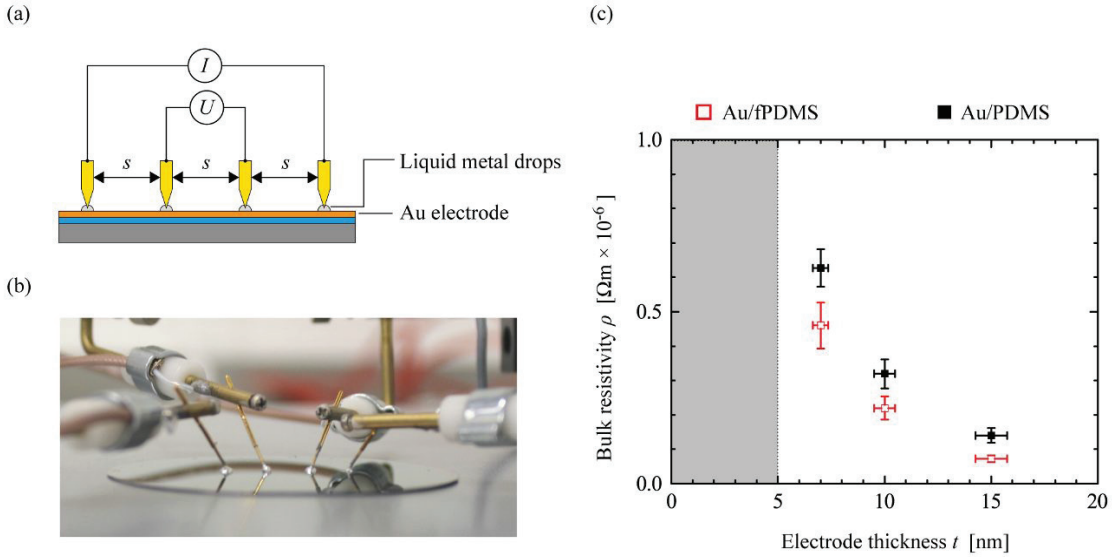

Figure 8. The four-point resistance measurements of sputtered Au electrodes, schematically shown in panel (a) and by a photograph in panel (b), show a better conductivity for Au electrodes with an underlying MPTMS/PDMS-Ox surface, see diagram. The Au electrode is contacted using eGaIn drops.

Furthermore, the bulk resistivity ρ is the product of the sheet resistivity R_s and the electrode thickness t:

$$\rho = R_s t \ . \tag{6}$$

In Figure 8(a), the bulk resistivity ρ on bare PDMS and fPDMS is compared for three selected electrode thicknesses. The bulk resistivity increases for both systems as the thickness of Au electrode decreases. It is known that the increase is particularly noticeable when the thickness of the Au electrode drops below 15 nm [29]. The resistivity values for the Au electrodes on the fPDMS surface are lower compared to the untreated samples.

3.7 Exposure of Au-layer to strain

The Au/fPDMS structure was fabricated on a stretchable substrate, *cf.* Figure 9(a,b).

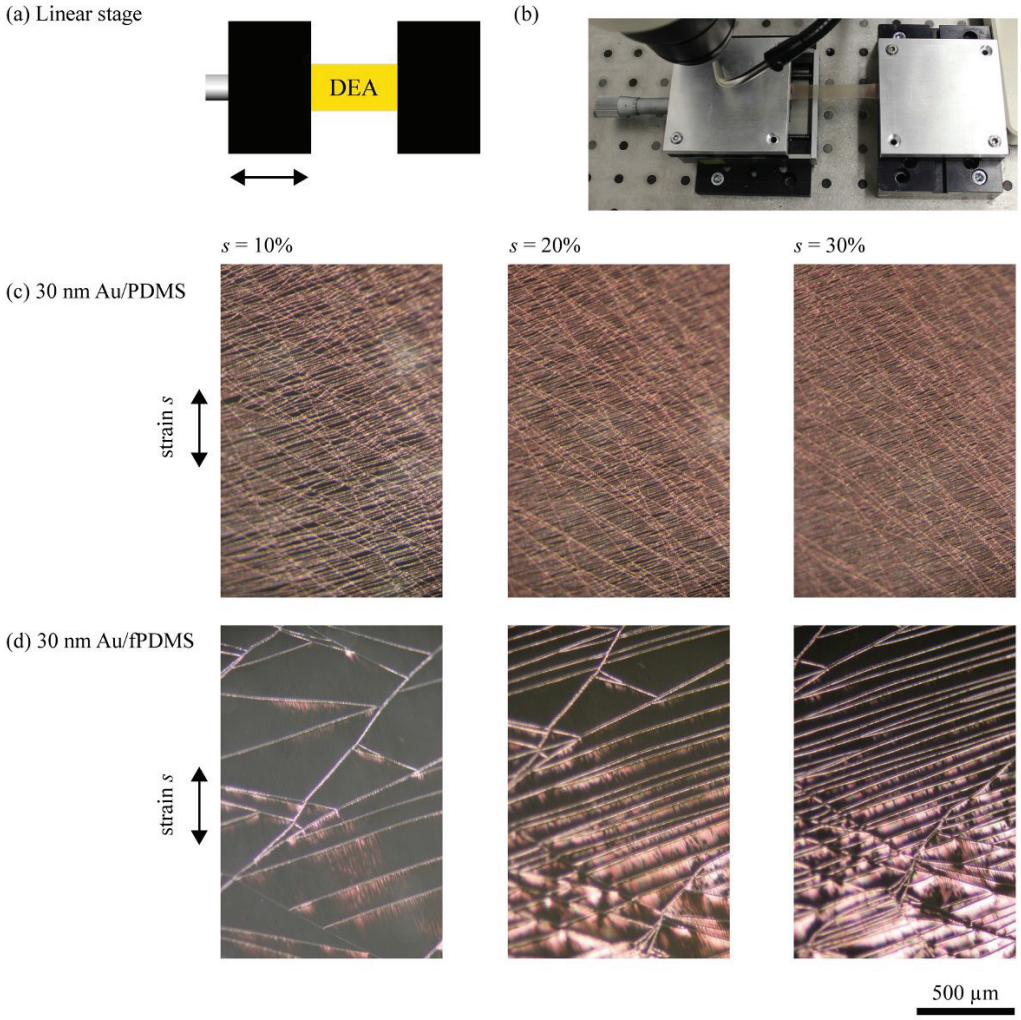

Figure 9. (a) Schematic design of the setup. (b) Photograph of the experimental setup. (c) Optical micrographs of a stretched Au layer on PDMS. (d) Optical micrographs of stretched Au layer on fPDMS.

The effect of the applied unidirectional strains using a linear stage was monitored with an optical microscope. The cracks on the electrode were studied for strains up to 30%. The crack density for Au/PDMS is significantly higher than for Au/fPDMS indicating a better adhesion of the Au electrode to the PDMS.

4. CONCLUSIONS

We have successfully applied MPTMS as a molecular adhesive between the sputtered Au electrode and the oxygen plasma activated PDMS surface. Nanoindentation measurements showed a moderate stiffness increase from 1 MPa to 2 MPa. As expected, the adhesion of Au to PDMS was significantly improved as seen in reduced crack formation under mechanical strain. Furthermore, the conductivity of the Au electrodes was improved making this a promising method for the fabrication of planar DEA structures.

ACKNOWLEDGEMENT

The financial support of the nano-tera.ch initiative, project SmartSphincter, as well as the Swiss Nanoscience Institute (SNI) for the financial contribution to the AFM is gratefully acknowledged. The authors also thank Nanotools GmbH, Germany, for kindly providing us with two extra B500 AFM cantilevers and Frederikke Bahrt Madsen at the Technical University of Denmark for the discussion of the results.

REFERENCES

[1] Y. Bar-Cohen, [Electroactive polymer (EAP) actuators as artificial muscles: Reality, potential, and challenges] SPIE Press, (2004).

[2] P. Brochu, and Q. Pei, "Advances in dielectric elastomers for actuators and artificial muscles," Macromolecular rapid communications, 31(1), 10-36 (2010).

[3] I. A. Anderson, T. A. Gisby, T. G. McKay *et al.*, "Multi-functional dielectric elastomer artificial muscles for soft and smart machines," Journal of Applied Physics, 112(4), 041101 (2012).

[4] F. Carpi, I. Anderson, S. Bauer *et al.*, "Standards for dielectric elastomer transducers," Smart Materials and Structures, 24(10), 105025 (2015).

[5] G. Kovacs, P. Lochmatter, and M. Wissler, "An arm wrestling robot driven by dielectric elastomer actuators," Smart Materials and Structures, 16(2), S306 (2007).

[6] T. Töpper, F. Weiss, B. Osmani *et al.*, "Siloxane-based thin films for biomimetic low-voltage dielectric actuators," Sensors and Actuators A: Physical, 233, 32-41 (2015).

[7] E. Fattorini, T. Brusa, C. Gingert *et al.*, "Artificial muscle devices: Innovations and prospects for fecal incontinence treatment," Annals of Biomedical Engineering, 1-15 (2016).

[8] F. M. Weiss, T. Töpper, B. Osmani *et al.*, "Electrospraying nanometer-thin elastomer films for low-voltage dielectric actuators," Advanced Electronic Materials, (2016).

[9] R. E. Pelrine, R. D. Kornbluh, and J. P. Joseph, "Electrostriction of polymer dielectrics with compliant electrodes as a means of actuation," Sensors and Actuators A: Physical, 64(1), 77-85 (1998).

[10] S. Rosset, and H. Shea, "Flexible and stretchable electrodes for dielectric elastomer actuators," Applied Physics A, 110(2), 281-307 (2013).

[11] H. Schmid, H. Wolf, R. Allenspach *et al.*, "Preparation of metallic films on elastomeric stamps and their application for contact processing and contact printing," Advanced Functional Materials, 13(2), 145-153 (2003).

[12] T. Li, Z. Huang, Z. Suo *et al.*, "Stretchability of thin metal films on elastomer substrates," Applied Physics Letters, 85(16), 3435-3437 (2004).

[13] Y.-L. Loo, R. L. Willett, K. W. Baldwin *et al.*, "Additive, nanoscale patterning of metal films with a stamp and a surface chemistry mediated transfer process: Applications in plastic electronics," Applied Physics Letters, 81(3), 562-564 (2002).

[14] B. Osmani, T. Töpper, C. Deschenaux *et al.*, "Micro- and nanostructured electro-active polymer actuators as smart muscles for incontinence treatment," AIP Conference Proceedings, 1646(1), 91-100 (2015).

[15] I. Byun, A. W. Coleman, and B. Kim, "Transfer of thin Au films to polydimethylsiloxane (PDMS) with reliable bonding using (3-mercaptopropyl) trimethoxysilane (MPTMS) as a molecular adhesive," Journal of Micromechanics and Microengineering, 23(8), 085016 (2013).

[16] B. Atmaja, J. Frommer, and J. C. Scott, "Atomically flat gold on elastomeric substrate," Langmuir, 22(10), 4734-4740 (2006).

[17] K. Efimenko, and J. Genzer, "Tuning the surface properties of elastomers using hydrocarbon-based mechanically assembled monolayers," MRS Proceedings 710, (2001).
[18] W. Kaczorowski, W. Szymanski, D. Batory *et al.*, "Effect of plasma treatment on the surface properties of polydimethylsiloxane," Journal of Applied Polymer Science, 132(11), (2015).
[19] S. Béfahy, P. Lipnik, T. Pardoen *et al.*, "Thickness and elastic modulus of plasma treated PDMS silica-like surface layer," Langmuir, 26(5), 3372-3375 (2009).
[20] K. Mills, X. Zhu, S. Takayama *et al.*, "The mechanical properties of a surface-modified layer on polydimethylsiloxane," Journal of materials research, 23(01), 37-48 (2008).
[21] D. Bodas, and C. Khan-Malek, "Hydrophilization and hydrophobic recovery of PDMS by oxygen plasma and chemical treatment - An SEM investigation," Sensors and Actuators B: Chemical, 123(1), 368-373 (2007).
[22] J.-H. Kim, "Hydrophobicity loss and recovery of silicone HV insulation," Dielectrics and Electrical Insulation, IEEE Transactions on, 6(5), 695-702 (1999).
[23] N. Maheshwari, A. Kottantharayil, M. Kumar *et al.*, "Long term hydrophilic coating on poly (dimethylsiloxane) substrates for microfluidic applications," Applied Surface Science, 257(2), 451-457 (2010).
[24] D. B. Chua, H. Ng, and S. F. Li, "Spontaneous formation of complex and ordered structures on oxygen-plasma-treated elastomeric polydimethylsiloxane," Applied Physics Letters, 76(6), 721-723 (2000).
[25] A. Tserepi, E. Gogolides, K. Tsougeni *et al.*, "Tailoring the surface topography and wetting properties of oxygen-plasma treated polydimethylsiloxane," Journal of Applied Physics, 98(11), 113502 (2005).
[26] F. Smits, "Measurement of sheet resistivities with the four-point probe," Bell System Technical Journal, 37(3), 711-718 (1958).
[27] O. Graudejus, P. Görrn, and S. Wagner, "Controlling the morphology of gold films on poly (dimethylsiloxane)," ACS applied materials & interfaces, 2(7), 1927-1933 (2010).
[28] A. Sharfeddin, A. A. Volinsky, G. Mohan *et al.*, "Comparison of the macroscale and microscale tests for measuring elastic properties of polydimethylsiloxane," Journal of Applied Polymer Science, 132(42), (2015).
[29] T. Töpper, B. Osmani, F. M. Weiss *et al.*, "Strain-dependent characterization of electrode and polymer network of electrically activated polymer actuators," SPIE Smart Structures and Materials + Nondestructive Evaluation and Health Monitoring 94300B, 1-11.

2.3 Micro- and nanostructured electro-active polymer actuators as smart muscles for incontinence treatment

Fabrication of DETs with nanostructured Cr/Au electrodes.

DETs with oriented wrinkled Cr/Au electrodes exhibit on average a 65 % larger actuation.

The impact of a several nm thin Au electrode on the overall elastic modulus is quantified using a state of the art nanoindentation tester with an included integrated reference system. A 10 nm Au electrode increased its elastic modulus from 1.7 to 4.0 MPa.

Mechanical modeling of bilayer structures using the Voigt-Reuss-Hill model show that the elastic modulus of nanometer-thin Au electrodes is by several order of magnitudes lower than that for bulk Au.

Published in AIP Conference Proceedings

Micro- and nanostructured electro-active polymer actuators as smart muscles for incontinence treatment

Bekim Osmani, Tino Töpper, Christian Deschenaux, Jiri Nohava, Florian M. Weiss, Vanessa Leung, and Bert Müller

Citation: AIP Conference Proceedings **1646**, 91 (2015); doi: 10.1063/1.4908588
View online: http://dx.doi.org/10.1063/1.4908588
View Table of Contents: http://aip.scitation.org/toc/apc/1646/1
Published by the American Institute of Physics

Micro- and Nanostructured Electro-Active Polymer Actuators as Smart Muscles for Incontinence Treatment

Bekim Osmani[1, a], Tino Töpper[1, b], Christian Deschenaux[2, c], Jiri Nohava[2, d], Florian M. Weiss[1, e], Vanessa Leung[1, f], and Bert Müller[1, g]

[1] *Biomaterials Science Center, University of Basel, c/o University Hospital, 4031 Basel, Switzerland*
[2] *Anton Paar TriTec SA, Rue de la Gare 4, Galileo Center, 2034 Peseux, Switzerland*

a) Corresponding author: bekim.osmani@unibas.ch
b) tino.toepper@unibas.ch, c) christian.deschenaux@anton-paar.com, d) jiri.nohava@anton-paar.com,
e) florian.weiss@unibas.ch, f) vanessa.leung@unibas.ch, g) bert.mueller@unibas.ch

Abstract. Treatments of severe incontinence are currently based on purely mechanical systems that generally result in revision after three to five years. Our goal is to develop a prototype acting in a natural-analogue manner as artificial muscle, which is based on electro-active polymers. Dielectric actuators have outstanding performances including millisecond response times, mechanical strains of more than 10 % and power to mass densities similar to natural muscles. They basically consist of polymer films sandwiched between two compliant electrodes. The incompressible but elastic polymer film transduces the electrical energy into mechanical work according to the Maxwell pressure. Available polymer films are micrometers thick and voltages as large as kV are necessary to obtain 10 % strain. For medical implants, polymer films should be nanometer thin to realize actuation below 48 V. The metallic electrodes have to be stretchable to follow the strain of 10 % and remain conductive. Recent results on the stress/strain behavior of anisotropic EAP-cantilevers have shown dependencies on metal electrode preparation. We have investigated tunable anisotropic micro- and nanostructures for metallic electrodes. They show a preferred actuation direction with improved stress-strain behavior. The bending of the cantilever has been characterized by the laser beam deflection method. The impact of the electrode on the effective Young's Modulus is measured using an Ultra Nanoindentation Tester with an integrated reference system for soft polymer surfaces. Once ten thousand layers of nanometer-thin EAP actuators are available, devices beyond the envisioned application will flood the market.

INTRODUCTION

The treatment of severe fecal incontinence is a reasonable and growing market due to demographic changes in developed countries [1]. Current devices, usually consist of a pump with a liquid-filled inflating cuff, are slow and difficult to operate [2]. They improve incontinence but show considerable complication and revision rates [3].

We propose a device, which is based on dielectric electro-active polymers (EAP). These actuators can be designed to perform muscle-like actuations or imitate muscle functions.

Dielectric elastomer actuators (DEAs) are referred to artificial muscles because of the performance including millisecond response, mechanical strains of more than 10 %, and the power-to-mass densities similar to natural muscles [4, 5]. These actuators offer perspectives for bio-mimetic applications because of the large actuations [6] and sensing ability. Several examples are reported in robotics and haptic feedback devices [5]. However, key challenges like operation at low voltages, large-scale manufacturability and integrated sensing remain still unsolved to enable a breakthrough of this technology.

International Conferences and Exhibition on Nanotechnologies and Organic Electronics (NANOTEXNOLOGY 2014)
AIP Conf. Proc. 1646, 91-100 (2015); doi: 10.1063/1.4908588

The working principle of a DEA is shown in Fig. 1. Here, the elastomer films are sandwiched between compliant electrodes.

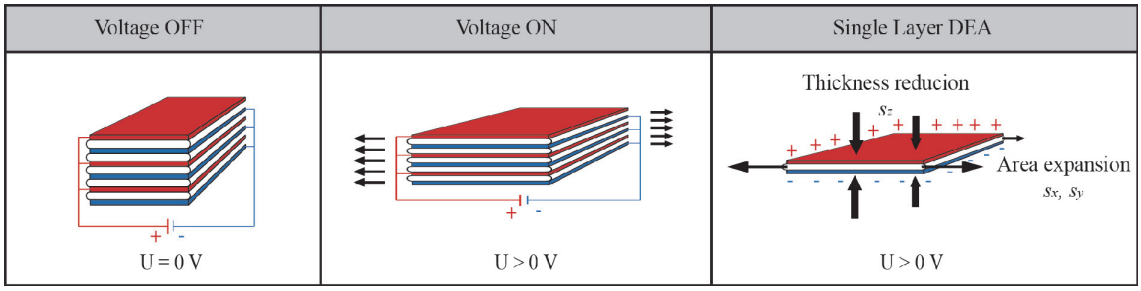

FIGURE 1. The sandwiched elastomer films respond to the electric field with a planar expansion.

Dielectric elastomer actuators transduce the applied voltage into mechanical work according to the Maxwell stress [7] often termed the actuation pressure p:

$$p = \varepsilon \cdot \varepsilon_o \cdot E^2 = \varepsilon \cdot \varepsilon_0 \cdot \frac{U^2}{t_{ef}^{\,2}} \qquad (1)$$

where ε is the dielectric constant of the elastomer, ε_0 the vacuum permittivity, E the induced electric field, U the applied voltage and t_{ef} the thickness of the elastomer film. The compressive strain s_z can be written as:

$$s_z = -\frac{\Delta t_{ef}}{t_{ef}} = -\varepsilon \cdot \varepsilon_0 \cdot \frac{U^2}{Y \cdot t_{ef}^{\,2}} = -\frac{p}{Y} \qquad (2)$$

Assuming that the elastomer is incompressible, with a bulk compressibility much higher than its elastic modulus Y and with a Poisson ratio of 0.5, we can write for the planar strains s_x and s_y:

$$s_{x,y} = -0.5 \cdot s_z = \varepsilon \cdot \varepsilon_0 \cdot \frac{U^2}{2 \cdot Y \cdot t_{ef}^{\,2}} \qquad (3)$$

For applications in medical implants we target driving voltages below 48 V. One would expect from the Eq. 3 that the planar strain for low voltages U can be achieved by simply reducing the elastomer film thickness t_{ef}. This is not the case since for thin layers, it is necessary to use the effective Young's modulus Y_{eff} of the stacked structure (electrode/ elastomer). For the uniform strain, Voigt [8] proposed the following model for sandwich materials:

$$Y_{eff} = Y_{ef} h_{ef} + Y_e h_e \qquad (4)$$

where h_{ef} is the normalized elastomer thickness and h_e the normalized electrode thickness, with $h_e + h_{ef} = 1$. For the uniform stress state, Reuss [9] introduced this expression for a two-phase material:

$$Y_{eff} = \frac{Y_{ef} \cdot Y_e}{Y_{ef} h_e + Y_e h_{ef}} \qquad (5)$$

Neither assumption is correct. For the Voigt model one would need two materials with the same Poisson ratio and for Reuss the interface between the two phases is not considered. Since these estimations are good as upper and lower bounds, the actual value is often taken as the average of the two [10], known also as the Voigt-Reuss-Hill average:

$$Y_{VRH} = \frac{1}{2} \cdot \left[\frac{Y_{ef} \cdot Y_e}{Y_{ef} h_e + Y_e h_{ef}} + (Y_{ef} h_{ef} + Y_e h_e) \right] \qquad (6)$$

The elastomer thickness can be scaled down to some hundred nanometers but there are restrictions for the electrode. A minimal thickness for a conductivity of < 10 Ω/square is needed to ensure a reaction time below 500 ms of the actuator. This leads to an increase of the electrode-to-elastomer ratio and therefore to an increase of the Y_{VRH} as shown in Fig. 2, especially for rigid electrodes.

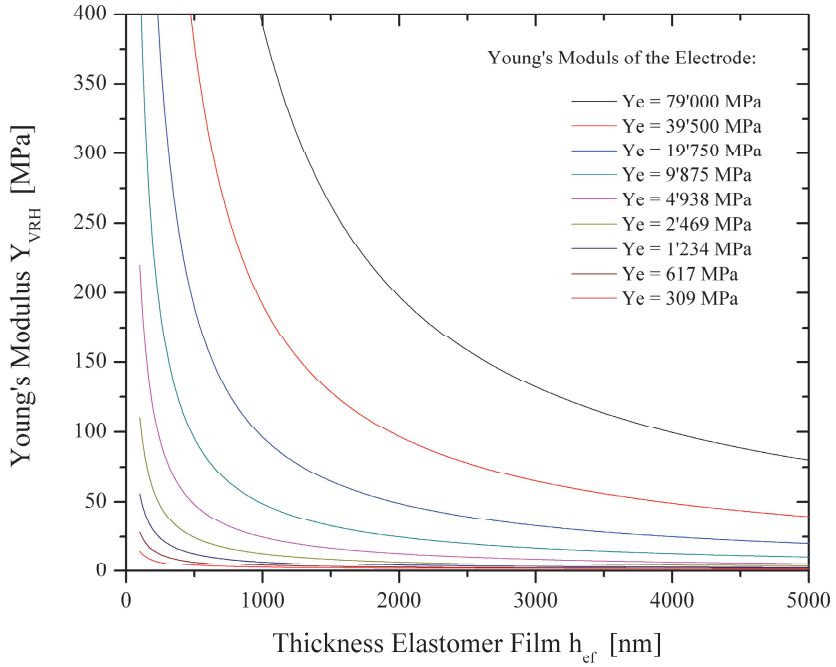

FIGURE 2. Plot for the Voigt-Reuss-Hill average as function of the elastomer thickness with a Young's Modulus Y_{ef} = 1 MPa for selected moduli Y_e of electrode with h_e = 10 nm.

For medical applications, DEAs should work at voltages as low as 6 to 48 V and elastomer thicknesses below 1000 nm to ensure actuation strains larger than 10%. To avoid a dominating stiffness of the electrode with respect to the elastomer films, the fabrication of highly stretchable or non-rigid electrodes is inevitable [10, 11].

We have investigated DEA cantilevers with planar and wrinkled electrodes using a custom-built cantilever beam bending apparatus. The electrodes were sputtered on a tunable wrinkled elastomer surface. It has been shown that uniaxial pre-stretched elastomer substrates form parallel wrinkles on the top due to the compressive strain between the deposited stiff film and the underlying soft substrate [12, 13]. The periodicity and amplitude of the wrinkled structures can be predicted for known film coatings and film thicknesses [13].

MATERIAL AND METHODS

Measurement of the Effective Young's Modulus

The effective Young's modulus of a single-layer dielectric actuator with an Au electrode was measured using an UNHT - Ultra Nano Indentation Tester (Anton Paar TriTec SA, Switzerland). The UNHT works with an integrated reference system, which can be placed on the rigid sample holder to prevent a possible sinking of the reference system into the soft elastomer film [14]. When the reference tip touches the surface, an indenter tip with a known geometry moves into the sample to be tested, applying an increasing normal load. The position of the indenter relative to the sample surface is monitored with a differential capacitive sensor (Fig. 3).

Two samples were cut and fixed on an adjustable holder. On the first sample, a 5 µm-thin polydimethylsiloxane (PDMS) film (Elastosil 745 A/B, Wacker Chemie AG, Munich, Germany) was spin-coated on a 3-inch Si wafer (Si-Mat Silicon Materials, thickness 381 ± 25 µm) and thermally cross-linked at a temperature of 80 °C for a period of 24 h. On the second sample, an additional electrode of 10 nm Au was magnetron sputtered (BALZERS UNION SCD 040 SYSTEM, Balzers, Lichtenstein). The edge of the sample holder was used as a fixed reference. The indenter with parameters given in the table of Fig. 3 was approaching the surface at a speed of 33 nm/s. At the maximum load of 15 µN, the indenter maintained this value for a period of 30 s to measure the creep into the elastomer. The power law method by Oliver & Pharr [14] was used to determine the hardness and elastic modulus of the material.

UNHT Parameters:

Indenter Type:	Spherico-Conical (SE-A19)
End-Radius:	20 µm
Cone Angle:	90°
Approach/ Retract Speed:	2000 nm/min
Approach Distance:	4000 nm
Fn Contact:	7 µN
Loading/ Unloading:	linear
Loading rate:	30 µN/min
Maximum Load:	15 µN
Holding time at max. load	30 s
Reference contact load	200 µN (on substrate)

Schematic of the UNHT head (patented design)

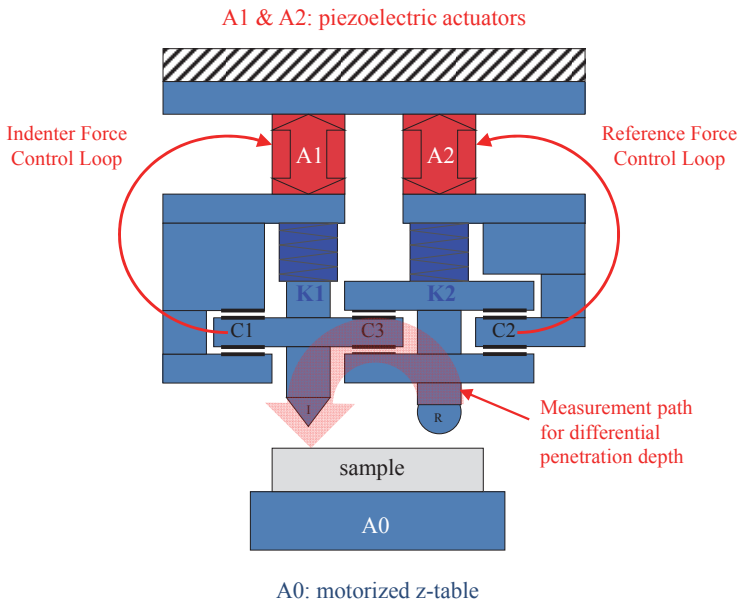

FIGURE 3. The parameters for the nano indentation tests are shown on the left. The schematic on the right gives an overview of the UNHT head with the indenter force F_N, the load cell capacitive sensors C1, C2, the penetration depth differential capacitive sensor C3 and the cell springs K1 and K2.

The displacement resolution was 0.0004 nm (noise floor of 0.03 nm) with a normal force resolution of 0.001 µN (noise floor of 0.1 µN).

Preparation of the DEA Cantilevers

The anisotropic cantilevers structures were prepared according to the steps shown in Fig. 4. Polyetheretherketone (PEEK) substrates (APTIV 2000, Victrex, Lancashire, UK) with a thickness of 25 µm were cut to the size of 3-inch wafers and cleaned with acetone (Merck KGaA, Darmstadt, Germany). Au (Lesker, East Sussex, United Kingdom) was sputtered (Balzers Union SCD 040 System, Balzers, Liechstenstein) on both sides of the PEEK film, 50 nm on the reflective side and 25 nm on the side of the actuator. The thickness was measured using a quartz crystal microbalance (QSG 301, Balzers, Liechtenstein).

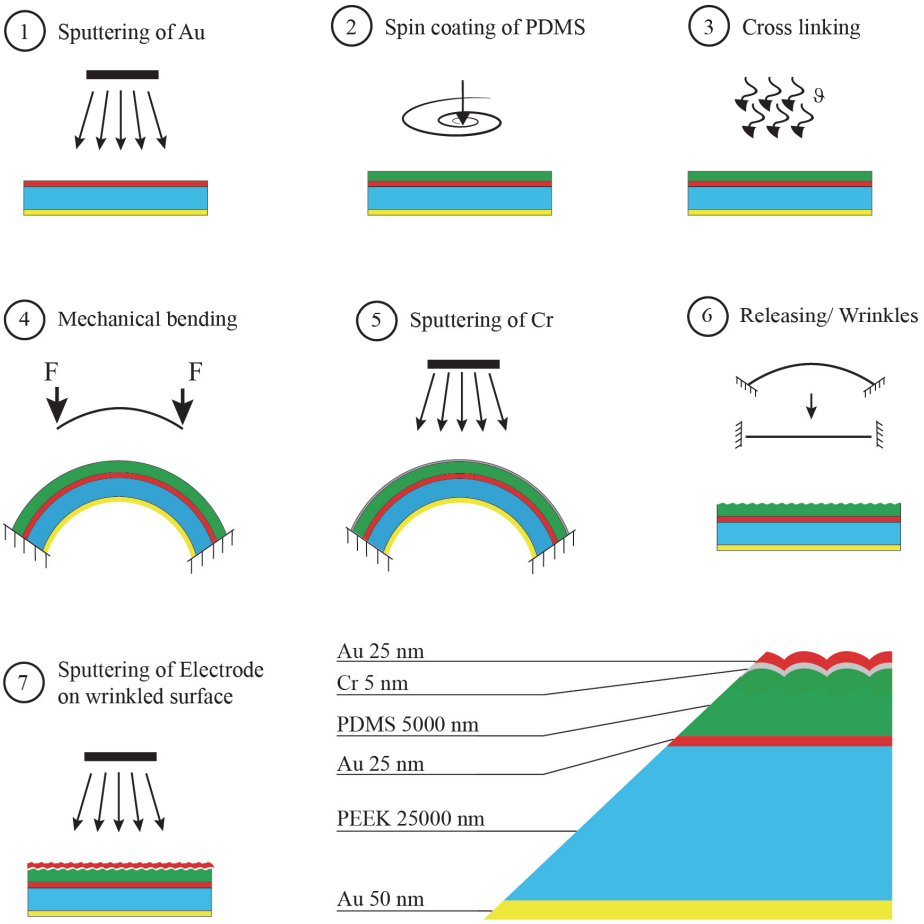

FIGURE 4. Preparation of the actuator with wrinkled electrode on the cantilever.

PDMS was mixed in a volume ratio 1:1 of component A and B and spin-coated at a rotational speed of 2000 rpm for 2 minutes, resulting in a film thickness of 5 µm. For a better access to the electrode, the substrate end (about 5 mm) was dip washed into ethyl acetate (Fisher Scientific, Reinach, Switzerland) to dissolve and wash off the PDMS. The remaining PDMS was thermally cross-linked at a temperature of 80 °C for a period of 24 hours.

The sample was mechanically bended to introduce a tensile strain on the PDMS film, where approximately 5 nm of Cr (Lesker, East Sussex, UK) were sputtered. After releasing, wrinkles appeared because of the inability of the Cr-film to follow the compressive strain on the PDMS [15, 16]. Finally, the conductive Au electrode was sputtered on the wrinkled surface. For reference measurements, we used a shadow mask to cover half of the 3 inch-wafer during the deposition of Cr and fabricated reference cantilevers with an Au electrode 25 nm thin.

Cantilever Bending Apparatus

Rectangular cantilevers with dimensions of 4 mm × 14 mm were cut out of the 3-inch wafer and fixed on a polytetrafluoroethylene (PTFE) holder. Both electrodes were contacted with flexible spring tips and connected to the power supply (Stanford Research System PS310, GMP SA, Lausanne, Switzerland). The cantilever holder was mounted inside a floatable and thermally decoupled chamber. The cantilever was hanging vertically to avoid a possible bending caused by the gravity.

The laser beam (Stream Line Laser System L2S-SL-660-1-S-A, Laser 2000, Germany) illustrated in Fig. 5 was adjusted to be reflected at a distance of 2 mm from the bottom of the Cantilever. The reflected laser beam hit the position sensitive photo detector (DUM-SpotOn Compact PSD Detector, Laser 2000, Germany) in the center. The PSD detector was mounted on an x-y-z-table and recorded the deflection of the laser beam during the actuation cycles. Voltage ramps were applied stepwise from 6 to 48 V. Cantilevers for the reference measurements were cut from the other half of the wafer without the wrinkled electrode on the top.

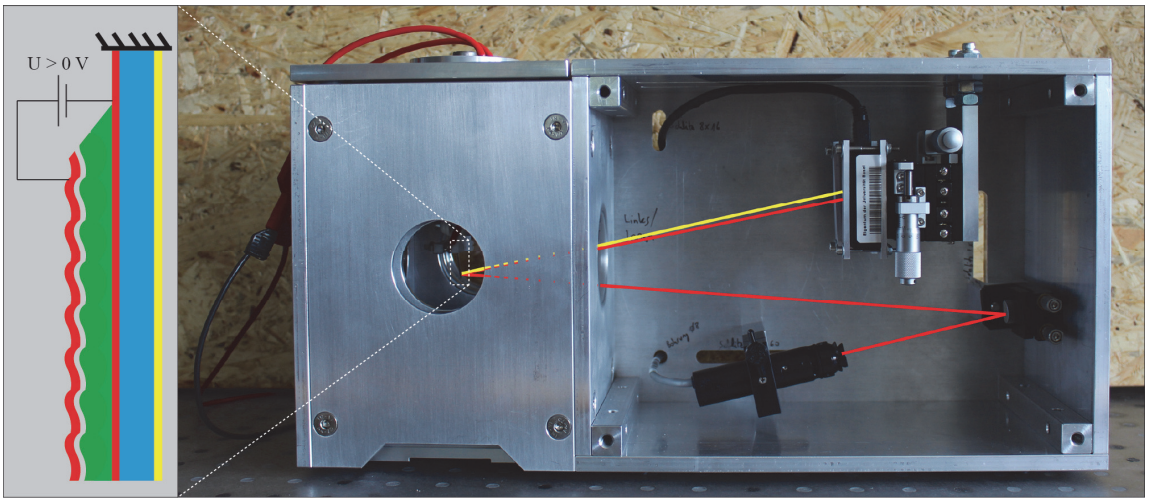

FIGURE 5. The custom-built apparatus is used for the characterization of mechanical properties of anisotropic EAP structures on PEEK cantilevers. The deflection of the laser beam is measured using a position sensitive photo detector.

RESULTS

Characterization of the Effective Young's Modulus

The average hardness H_{IT} shown in Table 1 is 0.128 ± 0.001 MPa for the single PDMS film and 0.235 ± 0.008 MPa for the PDMS + 10 nm Au electrode. The hardness H_{IT} is calculated from the measured maximum load F_{max} of the indenter head divided by the projected contact area $A_{p,hc}$ at the contact depth h_c:

$$H_{IT} = \frac{F_{max}}{A_{p,hc}} \qquad (7)$$

The Young's modulus of the sample Y_s (Eq. 8) is defined as a function of the reduced modulus and the modulus of the indenter Y_i. The reduced modulus Y_r of the indentation contact is a function of the contact stiffness (derivative at the peak load) and projected contact area $A_{p,hc}$. Since Oliver and Pharr's method does not consider any time effects, a creep analysis was performed to get additional information regarding the viscous behavior of the samples.

$$\frac{1}{Y_r} = \frac{1-\nu_i^2}{Y_i} + \frac{1-\nu_s^2}{Y_s} \qquad (8)$$

Fig. 6 shows selected indentation curves for both samples. The maximum penetration depths for the PDMS + 10 nm Au electrode were 849 nm and 881 nm, while for the PDMS films they were 1870 nm and 1927 nm. During the holding time of 30 s, the creeps for the PDMS + 10 nm Au electrode were approximately 11 nm and 6 nm, while for the PDMS films the measured creeps were 71 nm and 85 nm.

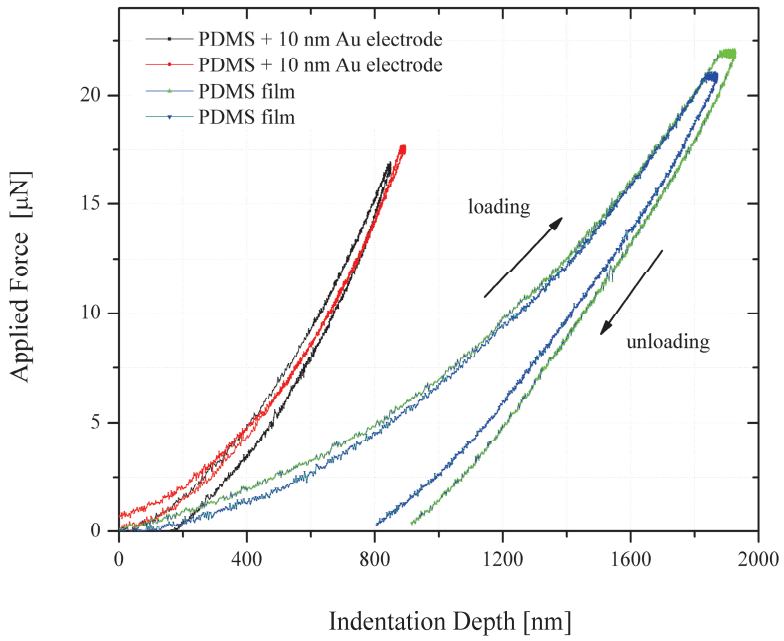

FIGURE 6. Indentation curves for PDMS film and PDMS + 10 nm Au electrode.

Comparing the results from Table 1 with the plots in Fig. 2 and Eq. 6, one can assume a Young's modulus of 3'000 MPa for the 10 nm Au electrode.

TABLE 1. Calculation of hardness H_{IT}, and the Young's modulus Y_S with and without creep.

Indentation		PDMS film [MPa]	PDMS + 10 nm Au electrode [MPa]
H_{IT} (O&P)	Sample 1	0.129	0.227
	Sample 2	0.127	0.243
	Mean	**0.128 ± 0.001**	**0.235 ± 0.008**
Y_S (O&P)	Sample 1	1.683	4.051
	Sample 2	1.691	3.861
	Mean	**1.687 ± 0.004**	**3.956 ± 0.095**
Y_S (Creep)	Sample 1	0.976	2.701
	Sample 2	1.015	2.623
	Mean	**0.996 ± 0.02**	**2.662 ± 0.039**

Actuator Performance

The cantilevers with wrinkled electrodes are shown in Fig. 7. The wrinkles have a periodicity of about 5.5 µm and an amplitude of 650 nm.

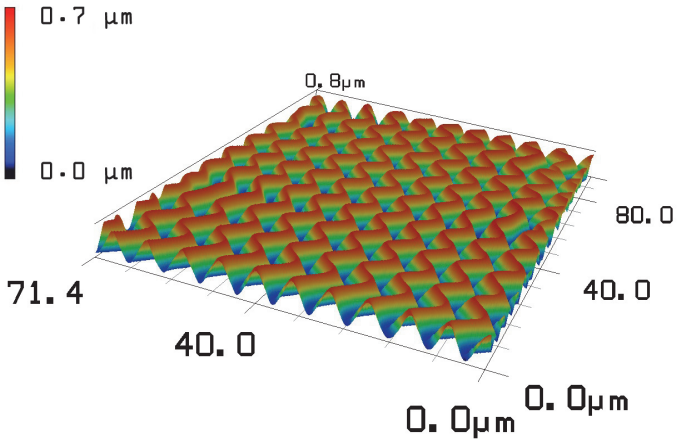

FIGURE 7. Scan with a 3D optical microscope from Keyence of a DEA cantilever with oriented wrinkles.

Measurements for voltage ramps of up to 48 V are shown in Fig. 8. The displacement on the PSD was for samples with wrinkled electrodes on average 65% larger than for the ones with planar electrodes. The fits for deflection curves are parabolic functions since the tensile strain s_x shown in Eq. 2, is also a function of U^2.

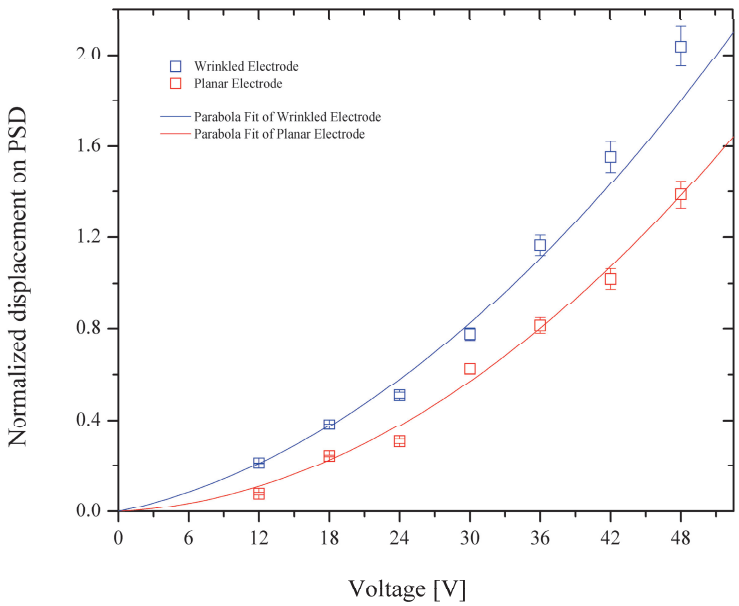

FIGURE 8. Analysis of the measured deflection.

Fig. 9 shows selected charging cycles for actuators with wrinkled and planar electrodes. The displacement of the reflected laser beam on the PSD was measured as a function of time for the maximum voltage of 350 V. Beside the reduced deflection seen in Fig. 8, one can measure a drift of 15 % for the actuator with planar electrodes within the time frame from 500 and 3800 ms. Actuators with wrinkled electrodes show a drift of about 2 %, maintaining the actuation within the oscillation peaks.

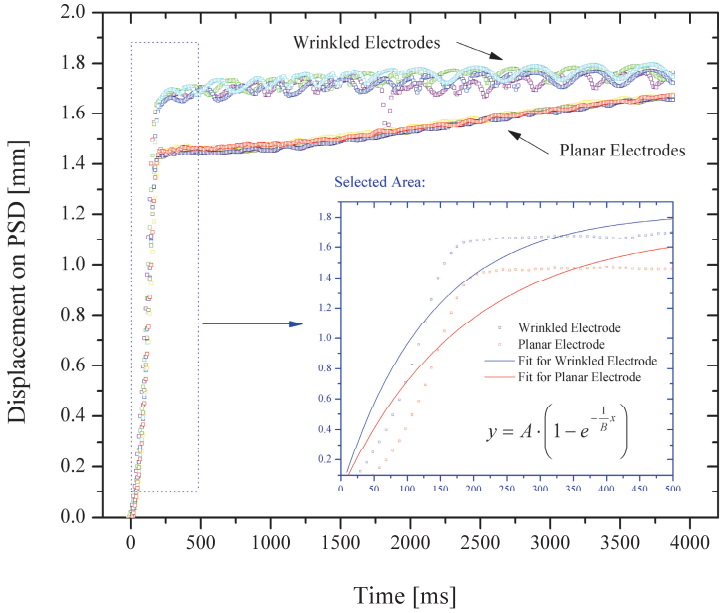

FIGURE 9. Charging curves of DEA Cantilevers.

As a simple model, DEAs can be considered as plate capacitors of two electrical conductors separated by a dielectric material. The fits of the charging curves in selected area (blue box) in Fig. 9 may be described by the charging behavior of a capacitor with a time constant τ=R*C:

$$Q(t) = Q_0 \cdot \left(1 - e^{-\frac{1}{RC}t}\right) \quad (9)$$

From the fits, the calculated time constant for the wrinkled electrode was found to correspond to τ = (134 ± 12) ms and for the planar electrode τ = (184 ± 22) ms.

DISCUSSION AND CONCLUSIONS

The stiffness and stretchability of conventionally fabricated actuators is dominated by planar metallic electrodes. We have shown that the stiffness of a single-layer actuator can successfully be measured using an Ultra Nano Indentation Tester. The penetration depth in pure PDMS was clearly larger than in the sample with an additional Au electrode. Measurements with the reference system on the PDMS were difficult because of the slightly sinking ball into the PDMS, even if the contact force was ≤ 200 μN (the penetration depth is measured relative to the height reference). The assumed Young's modulus of about 3 GPa for the 10 nm Au electrode can be a result of the cracks and also islands of the sputtered Au on the elastomer film. One has to perform further measurements for elastomer films between 100 and 1000 nm to verify the chosen model.

We have demonstrated that actuators with wrinkled electrodes show a larger actuation and an improved stress-strain behavior. We expect to adjust the wavelength and amplitude of the wrinkles by deposition of different film coatings on the elastomer surface Eq. 10 [13] and thereby to fabricate actuators for larger strains:

$$\lambda = 2 \cdot \pi \cdot h_e \cdot \left[\frac{(1-\nu_{el}^2) \cdot Y_e}{3 \cdot (1-\nu_e^2) \cdot Y_{el}} \right]^{\frac{1}{3}} \quad (10)$$

The drift in the deflection for actuators with planar electrodes in Fig. 9 can be a result of arising cracks in the Au electrode. The cracks could make it more stretchable and allow thereby a larger strain. For the wrinkled electrodes, we assume that the seen overlapped oscillations may be simple harmonic motions with a possible relation to the wavelength and the amplitude of the wrinkles.

The response time of the actuator with wrinkled electrodes seems to be faster than for the one without wrinkles. We can see from the fitted curves in Fig. 9 that the time constant τ for the wrinkled electrode is about 27 % smaller. The initial part of the actuation from 0 to 150 ms does not correspond well to the exponential fit. This could be due to inertia or other mechanical effects of the anisotropic cantilever.

ACKNOWLEDGMENTS

The authors gratefully acknowledge the funding of the Swiss National Science Foundation and the nano-tera.ch initiative (SmartSphincter). We thank Dr. Monica Schönenberger from the Nanotech Service Lab, Swiss Nanoscience Institute (SNI), Sascha Martin from the Mechanics Shop, Department of Physics, University of Basel and Victrex Europe for providing us with PEEK Cantilevers.

REFERENCES

1. C. W. McGrother, "Epidemiology of Urinary Incontinence," in Urinary and Fecal Incontinence, edited by H. D. Becker, A. Stenzl, D. Wallwiener and T. T. Zittel, (Springer-Verlag, Berlin Heidelberg, 2005), pp. 13-23.
2. K. D. Hong, G. Dasilva, S. N. Kalaskar, Y. Chong and S. D. Wexner, Journal of the American College of Surgeons 217 (4), 718-725 (2013).
3. M. Goos, U. Baumgartner, M. Löhnert, O. Thomusch and G. Ruf, BMC Surgery 13, p. 45 (2013).
4. S. Ashley, Scientific American 10, 52-59 (2003).
5. I. A. Anderson, T. A. Gisby, T. G. McKay, B. M. O'Brien and E. P. Calius, Journal of Applied Physics 112, 041101 (2012).
6. R. Pelrine, R. Kornbluh, Q. Pei and J. Joseph, Science 287 (5454), 836-839 (2000).
7. R. Pelrine, R. Kornbluh and J. Joseph, Sensors and Actuators A: Physical 64 (1), 77-85 (1998).
8. W. Voigt, Annalen der Physik 274 (12), 573-587 (1889).
9. A. Reuss, ZAMM - Journal of Applied Mathematics and Mechanics 9 (1), 49-58 (1929).
10. F. M. Weiss, X. Zhao, P. Thalmann, H. Deyhle, P. Urwyler, G. Kovacs and B. Müller, "Measuring the bending of asymmetric planar EAP structures," in Electroactive Polymer Actuators and Devices (EAPAD), Proceedings of SPIE 8687 (2013), 86871X-86871X-6.
11. F. M. Weiss, T. Töpper, B. Osmani, C. Winterhalter and B. Müller, "Impact of electrode preparation on the bending of asymmetric planar electro-active polymer microstructures," in Electroactive Polymer Actuators and Devices (EAPAD), Proceedings of SPIE 9056 (2014) 905607.
12. N. Bowden, S. Brittain, A. G. Evans, J. W. Hutchinson and G. M. Whitesides, Nature 393, pp. 146-149 (1998).
13. A. L. Volynskii, S. Bazhenov, O. V. Lebedeva and N. F. Bakeev, Journal of Materials Science 35, 547-554 (2000).
14. J. Nohava, N. X. Randall and N. Conté, Journal of Materials Research 24 (3), pp. 873-882 (2009).
15. S. Rosset and H. Shea, Applied Physics A 110 (2), 281-307 (2013).
16. X. Chen and J. W. Hutchinson, Journal of Applied Mechanics 71, 597-603 (2004).

2.4 Gold layers on elastomers near the critical stress regime

Interplay between functionalized, plasma-treated PDMS films and sputter-deposited metal electrodes enables the conservation of a thermally induced compressive stress on the very top of the PDMS film.

Insulator-metal transition occurring at only 10 nm Au electrodes enables the fabrication of very thin and conductive metal films.

Below electrode thicknesseses of 10 nm, nanoindentations reveal no stiffening of the Au/PDMS heterostructure.

AFM nanoindentations with sub-micrometer mapping reveal an anisotropy in elastic modulus for plasma treated PDMS films. The wrinkled film on top of the elastomer membrane shows stiffer nano-hills and softer nano-valleys.

DETs with compressed Au electrodes exhibit reduced electro-creasing, a significant contributor to structural failure of thin-film DETs.

Enhanced dielectric breakdown fields of up to 120 V/µm are achieved.

Published in Advanced Materials Technologies

FULL PAPER

ADVANCED MATERIALS TECHNOLOGIES

Soft Electrodes

www.advmattechnol.de

Gold Layers on Elastomers near the Critical Stress Regime

*Bekim Osmani, Hans Deyhle, Tino Töpper, Thomas Pfohl, and Bert Müller**

Soft electrodes are essential components of soft robotics, tunable optics, microfluidics, flexible electronics, neuroprosthetics, and dielectric elastomeric transducers (DET). The two main paths employed to increase an electrode's compliance involve the manipulation of either its intrinsic material properties or its structural features, such as the introduction of wrinkles, which arise above the critical stress of metal films on elastomeric substrates. Herein, this study demonstrates that the interplay between functionalized oxygen-plasma-treated polydimethylsiloxane (PDMS) films and sputter-deposited metal electrodes allows for conserving compressive stress within the electrode. Insulator–metal transition already occurs for 10 nm thin Au electrodes, and below this electrode thickness, atomic force microscopy nanoindentations with sub-micrometer resolutions reveal no stiffening of the Au/PDMS heterostructure. These DETs exhibit reduced electrocreasing, which is a significant contributor to structural failure, while their enhanced dielectric breakdown field of up to 120 V μm^{-1} enables calculated strains above 10% — a crucial requirement for thin-film DETs such as those used for artificial muscles.

1. Introduction

Recently, dielectric elastomer transducers (DET), also known as artificial muscles, have attracted broad interest, due to their versatile applicability as dielectric elastomer actuators (DEA), sensors, selfsensing actuators, and electric generators.[1–5] They are essential building blocks for applications in medicine, soft robotics, microfluidics, and flexible optoelectronics.[4,6–8] Very recently, Poulin et al. presented a fully printed 3 μm thin DEA, in which the operating voltage could be reduced from the kilovolt range to some hundreds of volts.[9] For future medical implants, however, nanometer-thin DEAs are required, as they can operate at physiologically acceptable voltages below 12 V.[10,11] Generally, planar DEAs are sandwich structures in which, for example, polydimethylsiloxane (PDMS) as an elastomeric film is embedded between soft electrodes and transduces electrical energy into mechanical work, as electrostatic pressure drives the elastomer to expand laterally by tens of percent.[12,13] A major goal is the development of nanometer-thin flexible and stretchable electrodes for a few micrometer- or sub-micrometer-thin DEAs. Many materials and related fabrication and characterization methods have been proposed for electrodes, including carbon powder, metallic thin films, or the implantation of metal nanoclusters.[14–18] Another approach to stretchable electronics, presented by Hirsch et al., is based on biphasic $AuGa_2$/Ga solid–liquid thin metal films. However, rigid 60 nm sputtered Au metallization is still required,[19] which significantly stiffens the overall thin-film DEA.[9,20] A related challenge is the low adhesion of Au to PDMS,[21] which can be improved via Cr or Ti layers but also increases the overall stiffness.[22] Atmaja et al. have shown that (3-mercaptopropyl)trimethoxysilane (MPTMS) can be used as a molecular adhesive to transfer atomically flat Au films to PDMS surfaces.[23] In addition, Mahapatro et al. have demonstrated that deposited Au on a self-assembled monolayer of MPTMS on an oxidized Si substrate has a root-mean-square surface roughness in the sub-nanometer scale.[24] MPTMS is a bifunctional molecule, its thiol head (−SH) binds to Au and the three methoxy ($-OCH_3$) functional groups bind to hydroxy PDMS (−OH) surfaces, which can be introduced by oxygen plasma or ultraviolet/ozone treatments.[20] Oxygen plasma forms a silica-like film on top of the PDMS layer,[25–27] thereby leading to a wrinkled surface, as its thermal expansion coefficient is several orders of magnitude lower compared to that of the underlying bulk PDMS.[28] Wrinkling is a universal phenomenon exhibited by a compressed film resting on a flexible substrate. Many approaches have been presented to control and even delaminate buckling films for enhanced stretchability.[29,30] As reported by Bowden et al., compressive stress in the SiO_x film has to exceed a critical stress for wrinkles to arise.[31,32] The critical stress can be described as a function of the elastic moduli of the upper film and the elastomer bulk.[33] Hendricks and Lee showed that by incorporating nanoparticles into the film, they were able to control and even prevent polymer films from buckling.[34] Herein, we illustrate that by depositing Au on MPTMS-functionalized and oxygen-plasma-treated PDMS (PDMS-O_x) films near the critical stress regime, we can conserve compressive stress and fabricate flat or wrinkled Au electrodes with a negligible stiffness increase in the overall Au/PDMS heterostructure. Using this technique, we have fabricated DEAs on polyethylene naphthalate (PEN) substrates and quantified actuation by using an in-house-built optical beam deflection device with applicable electrical fields up to 120 V μm^{-1}.[35]

B. Osmani, Dr. H. Deyhle, Dr. T. Töpper, Dr. T. Pfohl, Prof. B. Müller
Biomaterials Science Center
Department of Biomedical Engineering
University of Basel
Allschwil 4123, Switzerland
E-mail: bert.mueller@unibas.ch

The ORCID identification number(s) for the author(s) of this article can be found under https://doi.org/10.1002/admt.201700105.

DOI: 10.1002/admt.201700105

ADVANCED SCIENCE NEWS
www.advancedsciencenews.com

ADVANCED MATERIALS TECHNOLOGIES
www.advmattechnol.de

1.1. Fabrication of Compressed Au Electrodes on a Wrinkled PDMS Film

The wrinkling and buckling phenomena of films on elastomeric substrates are well understood.[32,33,36] Compressive or buckling stress σ_{comp} can be generated mechanically or thermally, as outlined in Equation (1)

$$\sigma_{comp} = \frac{E_f(\alpha_s - \alpha_f)(T_{dep} - T_{room})}{64(1-\nu_f^2)} \quad (1)$$

The thermal expansion coefficient of the bulk PDMS α_s is usually several orders of magnitude larger than that of a metallic- or a silica-like film α_f. The deposition of the metallic film as well as the plasma treatment of the PDMS substrate takes place at an elevated temperature T_{dep}, so the film may undergo buckling as the structure cools down to T_{room} in order to release compressive stress. It is reported that the film only wrinkles if the compressive stress is greater than a critical stress σ_{crit}, which is described as a function of the elastic moduli $E_{s,f}$ and the Poisson's ratios $\nu_{s,f}$ of the substrate and the film,[31,33] respectively

$$\sigma_{crit} = \left(\frac{9E_f E_s^2}{64(1-\nu_f^2)(1-\nu_s^2)^2}\right)^{1/3} \quad (2)$$

The orientation of the wrinkles on bulk PDMS is generally random, but the periodicity λ is reported to be proportional to the metal- or silica-like film height h_f[30–32]

$$\lambda = 2\pi h_f \left(\frac{(1-\nu_f^2)E_f}{3(1-\nu_s^2)E_s}\right)^{1/3} \quad (3)$$

Similar to the deposition of metallic films, during oxygen-plasma treatment, the PDMS surface is heated while a stiff, silica-like layer is formed.[26,32] During cooling, stress is released by forming wrinkle-like structures on top of the elastomer layer. The thickness of the silica-like layer is estimated on the basis of the buckling model for a bilayer system. Applying Equation (3) to selected PDMS films with Young's moduli of (1.0 ± 0.1) and (0.2 ± 0.1) MPa, the periodicities of the wrinkle patterns correspond to 2.6 and 4.5 µm, respectively. Assuming an elastic modulus for the silica-like layer of 1.5 GPa, as suggested by Béfahy et al.,[37] one finds a layer thickness of about 50 nm. Transmission electron microscopy (TEM) images of Béfahy et al.[37] show that the thickness of the silica-like layer can be controlled adjusting the plasma power and treatment time.

We show in **Figure 1**A the reformation of a thermally cured, plasma-treated PDMS layer (PDMS-O_x) with prominent wrinkles. The periodicity of the wrinkles was found to be λ = (2.0 ± 0.1) µm, using a 2D Fast Fourier Transform (2D FFT) analysis of the related atomic force microscopy (AFM) image. No preferential orientation of the wrinkles could be observed. The evaporation of a 30 nm thin Au electrode inside an ultra-high vacuum (UHV) chamber from a 45 cm-distant effusion source did not alter the periodicity or amplitude of the wrinkled pattern (Figure 1B). However, the sputtering of 30 nm thin Au

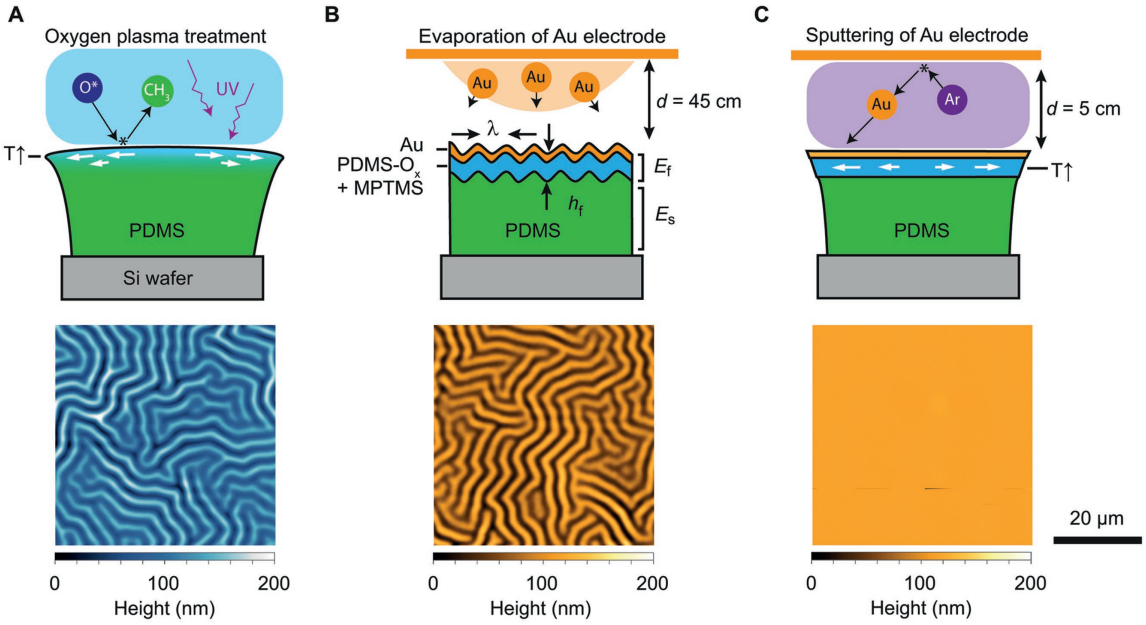

Figure 1. Fabrication of compressed Au electrodes on PDMS substrates. A) Schematic representation of PDMS surface modifications, using oxygen-plasma treatment (400 W, 120 s, 20 sccm oxygen flow). An AFM scan of a 50 × 50 µm² region after the oxygen-plasma treatment. The changed topography is due to induced stress in the silica-like layer on top of the PDMS layer. The characteristic wrinkles were prominent features with a periodicity of 2 µm and the amplitude of 90 nm. B) Thermal evaporation of 30 nm thin Au at a distance of 45 cm in UHV did not alter the wrinkled structure. C) Schematic representation of the sputtering process and AFM scan of a 50 × 50 µm² region after the sputtering of 30 nm thin Au, where the very top of the PDMS film is reheated and flattened during the sputter deposition of the Au electrode.

ADVANCED SCIENCE NEWS
www.advancedsciencenews.com

ADVANCED MATERIALS TECHNOLOGIES
www.advmattechnol.de

on the same substrate from a 5 cm-distant Au target flattened the surface completely (Figure 1C).

1.2. From Wrinkled to Flat Compressed Au/PDMS Heterostructures

We show in **Figure 2** that there is no abrupt change from wrinkling to nonwrinkling near the critical stress regime. The wrinkle amplitudes from the height histograms of the AFM scans were found to be (61 ± 3) nm for the oxygen plasma-treated PDMS. No preferential orientation of the wrinkles could be observed. After the subsequent sputtering of 5 nm Au, the wrinkles were maintained, cf. Figure 2B. 2D FFT analysis showed a slightly reduced periodicity of λ = (1.9 ± 0.1) µm, while the amplitude of the wrinkles was reduced to (33 ± 2) nm. For a 7 nm thin Au electrode, as shown in Figure 2C, the wrinkles almost disappeared. A cross-section revealed very flat wrinkles with an average height of (3 ± 1) nm and a periodicity of λ = (2.3 ± 0.1) µm. The mapping of the mechanical properties of the oxygen plasma-treated PDMS and Au/PDMS het erostructures revealed anisotropy on the sub-micrometer scale.

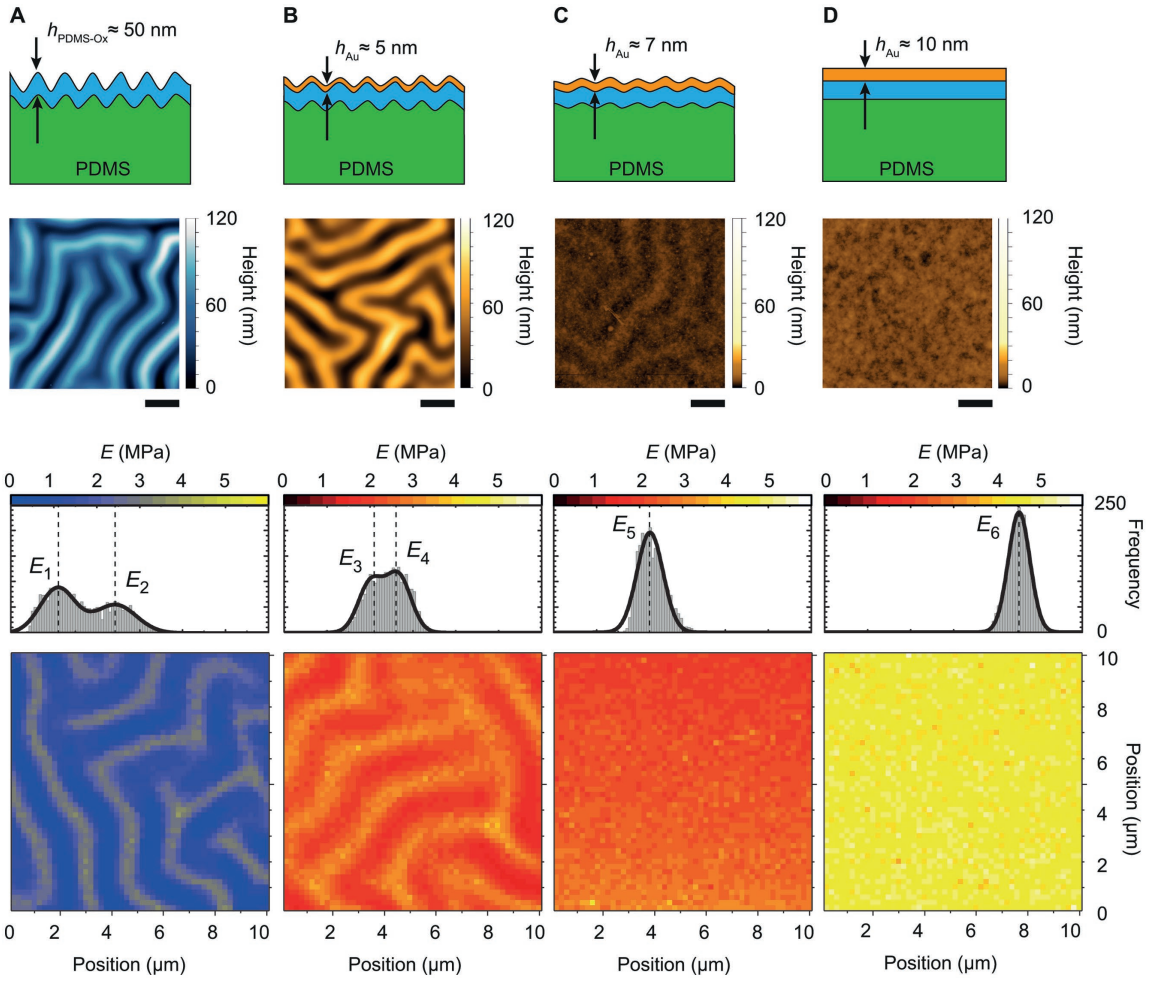

Figure 2. Evolution of oxygen-plasma-induced wrinkles toward compressed Au electrodes. A) Schematic of the oxygen-plasma-treated PDMS. The periodicity of the wrinkles was found to be (2.0 ± 0.1) µm with the average amplitude of (61 ± 3) nm as extracted from the AFM scan shown below. The bar corresponds to 2 µm. A stiffness histogram extracted from 2500 nanoindentations shows one peak at E_1 = (1.1 ± 0.5) MPa and a second peak at E_2 = (2.4 ± 0.5) MPa. The stiffness map with a sub-micrometer resolution identifies that the two peaks found in the histogram correspond to the softer material in valleys rather than on the hills. B) After the subsequent sputtering of 5 nm Au, the wrinkles were maintained with a slightly reduced periodicity of (1.9 ± 0.1) µm. The amplitude was reduced to (33 ± 2) nm. The related stiffness histogram shows a peak at E_3 = (2.1 ± 0.3) MPa and at E_4 = (2.7 ± 0.3) MPa. C) For a 7 nm Au electrode, the wrinkles were hardly recognized. The amplitude could not be extracted from the height histogram. Stiffness histograms show only one peak at E_5 = (2.2 ± 0.4) MPa. D) A deposition of 10 nm thin Au flattened the surface completely. Its mean surface roughness value of about 1 nm was similar to sputtered 10 nm thin Au on native PDMS. The related stiffness histogram shows only one peak at E_6 = (4.5 ± 0.3) MPa.

ADVANCED SCIENCE NEWS
www.advancedsciencenews.com

ADVANCED MATERIALS TECHNOLOGIES
www.advmattechnol.de

Probing of the wrinkled film with the AFM tip for each 200 nm shows that material in valleys is softer than that on hills. For the given plasma treatment parameters (RF power 200 W, treatment duration 120 s, oxygen pressure 0.3 mbar), valleys show an average elastic modulus of $E_1 = (1.1 \pm 0.5)$ MPa compared to hills with an elastic modulus of $E_2 = (2.4 \pm 0.5)$ MPa. The topological information required to discriminate between valleys and hills was extracted from the quasi height nanoindentation map. One can only speculate on the nature of the measured micrometer-scale modulations of the elastic modulus. Besides geometrical phenomena, the thickness modulation of the silica-like layer, possibly induced by the material transport,[38] is a plausible explanation. The nanoindentation depths were maximal 200 nm at a silica-like layer thickness of about 50 nm. The related histograms in Figure 2 show that after the sputter deposition of Au, compressive stress suppressed the stiffening effect, with $E_3 = (2.1 \pm 0.3)$ MPa, $E_4 = (2.7 \pm 0.3)$ MPa, and $E_5 = (2.2 \pm 0.4)$ MPa. As the surface was flattened totally, the additional sputtering of Au increased overall stiffness to $E_6 = (4.5 \pm 0.3)$ MPa.

1.3. Conservation of Compressive Stress within the Elastomeric Substrate — A Phenomenological Examination

Wrinkle patterns formed using the same plasma treatment parameters depend on the elastic modulus E_s of the PDMS film and evolve over time, as shown in **Figure 3**A. For a plasma-treated PDMS film with $E_s = 1$ MPa, wrinkles before Au deposition exhibited an amplitude of (90 ± 20) nm and a periodicity of (2.6 ± 0.2) µm. In Figure 3B, we show that compressive stress in the flattened electrode was maintained, as the subsequent peeling off of 30 nm sputtered Au electrode with adhesive tape returned the surface to a wrinkle pattern again. It showed a periodicity of (1.9 ± 0.1) µm and the amplitude of only (52 ± 5) nm. Compared to the wrinkling pattern before sputtering the Au electrode, the periodicity and amplitude are reduced by 27% and 42%, respectively. In addition, one observes a local alignment of wrinkles, cf. Figure 3B. We assume that an Au layer of a few nanometer remained on the PDMS, which was also visually observed when the sample was tilted against a light source, showing a golden shimmer. Figure 3C shows a closer look at the edge of Au/PDMS-O_x. In the region around the electrode, the wrinkles align parallel to each other and perpendicular to the electrode edge. They remain in this conformation along 100 µm, before returning to a randomly oriented arrangement. The amplitude of wrinkles rapidly increases in line with distance away from the electrode edge and reaches its equilibrium value within tens of micrometer, cf. Figure 3C. The periodicity of the oriented wrinkles was (2.4 ± 0.2) µm. The alignment of wrinkle patterns on the edges of PDMS surfaces has been reported by Bowden et al. as being due to stress relaxation at edges.[32] The presence of nonoriented wrinkle patterns prior to the sputter deposition of Au indicates that a rearrangement of the wrinkles occurs during the sputtering process outside the deposition area. We assume that the heat load during sputtering caused the film to expand, and as the structure cooled down, it gave rise to wrinkles that were aligned with respect to the electrode edge.

An in situ study of the Au/MPTMS/SiO_x/PDMS heterostructure is presented in **Figure 4**. The extinction coefficient k and the real part ε' of the dielectric function are determined with respect to the Au film thickness in Figure 4B of the thermally evaporated Au on the multilayered PDMS/SiO_x/MPTMS nanostructure, as schematically illustrated in Figure 4A. These parameters of the dielectric function allow for the detailed investigation of Au film formation processes and for the quantification of the film morphology after deposition.[39] The extinction coefficient reveals a broad plasmon absorbance band at a wavelength of 950 nm for Au film thicknesses below 3 nm. This is accompanied by a negative shift in the real part of the dielectric function, characteristic of confined electron oscillations on gold nanoparticles.[40] However, at Au film thicknesses above 3 nm, this absorbance band vanishes while a sharp absorbance peak occurs at a wavelength around 600 nm. The increased mean path of electron oscillations for the first Au monolayers can be accounted by its enhanced adhesion to the MPTMS, thereby promoting confluent film growth. The sudden blue shift of the plasmon resonance indicates a pronounced Vollmer–Weber growth mode toward Au nanoparticles instead of confluent film formation for Au film thicknesses above 3 nm.[39] With increased Au film thickness, this absorbance peak redshifts back toward the near infrared of the detected spectrum, thus indicating the coalescence of Au nanoparticles. The derived Au film thickness h_{Au} is higher compared to the expected film thickness, adjusted by the evaporator temperature. This fact underlines the Vollmer–Weber growth mode.[40] The derived growth rate h_{Au}' in Figure 4E asymptotically approaches the adjusted growth rate d', exhibiting an insulator–metal transition (IMT) above a derived Au thickness of (14 ± 2) nm.[39] The IMT threshold coincides with a rapid redshift of the absorbance feature within extinction coefficient spectra for film Au thicknesses above 12 nm, indicating the onset of free electron oscillations. Thus, this detected percolation threshold for Au growth on MPTMS/SiO_x/PDMS is well below that of Au growth on untreated PDMS at 22 nm.[39] This is in accordance with the improved conductivity of Au electrodes on MPTMS/SiO_x/PDMS compared to Au electrodes on untreated PDMS, verified by a four-point probe measurement.[20] The sharp absorbance feature around a wavelength of 400 nm is related to scattering on the surface's wrinkled microstructure. The negligible shift of this absorbance indicates stable wrinkled morphology during Au deposition.

1.4. Long-Term Stability of Compressed Au Electrodes

In **Figure 5**, we compare AFM topography scans of a sputtered 30 nm thin Au electrode on the native PDMS and on the MPTMS/SiO_x/PDMS surfaces. The calculated root-mean-square roughness value for a 2×2 µm^2 area was found to be (1.5 ± 0.2) nm for the sputtered 30 nm Au electrode on native PDMS, whereas the same Au electrode on MPTMS/SiO_x/PDMS showed a value of (0.5 ± 0.1) nm. Long-term observations show that the poor adhesion of the initially flat Au electrode on native PDMS leads to the formation of Au nanoclusters with dome-like structures having an average diameter of 100 nm and a height up to 50 nm. In addition, DEAs with

ADVANCED SCIENCE NEWS
www.advancedsciencenews.com

ADVANCED MATERIALS TECHNOLOGIES
www.advmattechnol.de

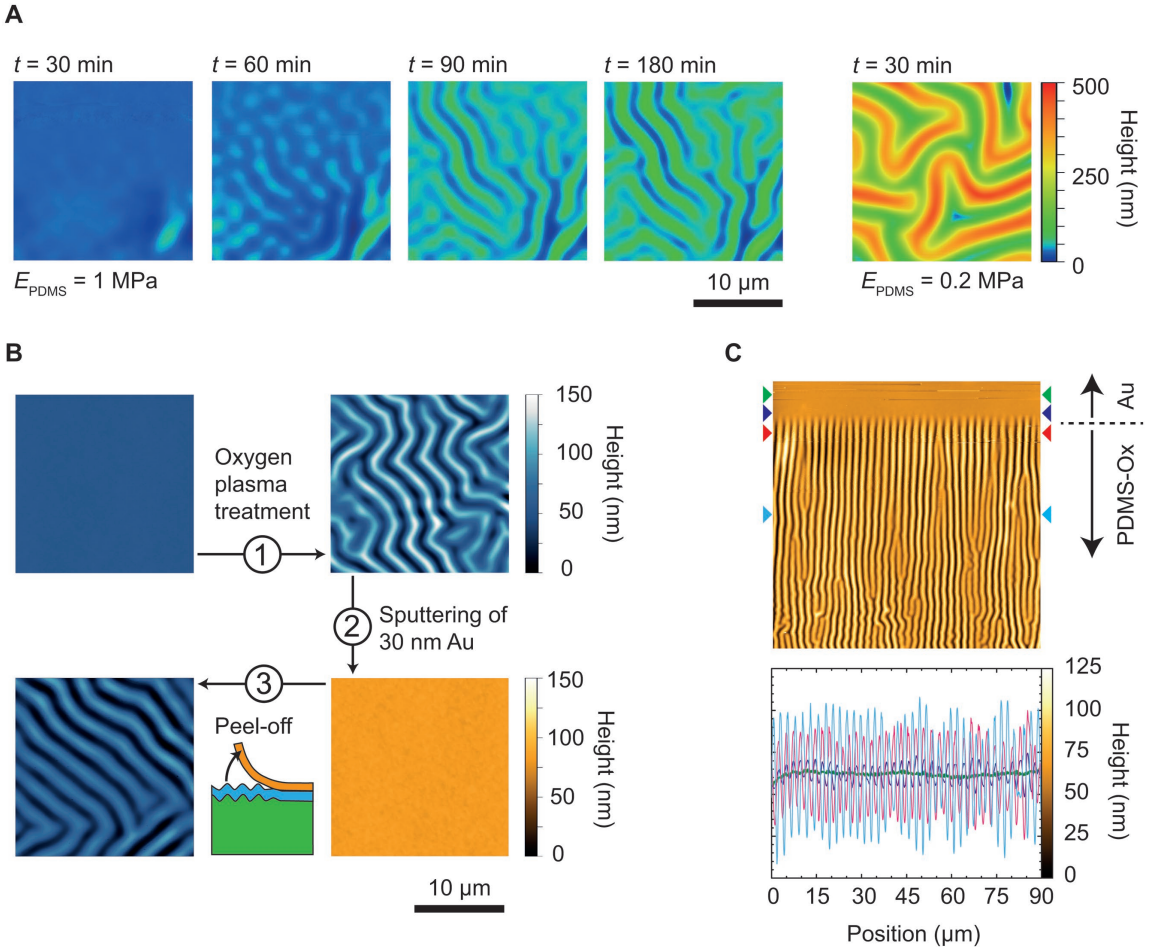

Figure 3. Relaxation of a compressed Au electrode on an elastomeric substrate to a wrinkled pattern after peeling off the Au electrode. A) Reformation of the PDMS surface, with $E_{S1} = (1.0 \pm 0.1)$ MPa and $E_{S2} = (0.2 \pm 0.1)$ MPa after oxygen-plasma treatment. Reformation is finished much faster for the softer PDMS with E_{S2}. B) The prestressed structure with a 30 nm Au on top of a wrinkled surface went back to a wrinkled structure again after peeling off the thin Au layer. C) An AFM scan at step Au/PDMS-O_x electrode. The wrinkles were aligned parallel to each other and perpendicular to the Au electrode edge. This conformation is found for a region of about 100 µm. Profile cuts with locations indicated by the colored arrowheads show that the wrinkle amplitude rapidly increases in line with distance to the electrode edge, which implies that the wrinkles are flattened and not filled with Au, due to material transport phenomena. Insulator-to-metal transition of Au on a compressed and MPTMS-functionalized PDMS-O_x surface.

compressed Au electrodes were still ready for operation after a period of nine months.

1.5. Fabrication and Actuation of DEAs with Compressed Au Electrodes

Substrate-based thin-film DEAs, using MPTMS as an interface between PDMS-O_x and an Au electrode, were fabricated as shown in **Figure 6**A. The actuation of the DEA was measured by detecting the curvature k_s of the underlying PEN cantilever as a function of the applied voltage U, using an optical beam deflection technique, cf. Figure 6B. This technique permits the measurement of actuation forces in dielectric elastomeric transducers with elastomer layers as thin as 1 µm.[35] The asymmetric cantilevers consisted of 8 µm thin DEAs (15 nm Au/8 µm PDMS/15 nm Au) deposited on 50 µm thick PEN substrates. The application of a voltage generated electrostatic pressure that was translated to an in-plane expansion of the DEA. The torque of this asymmetric actuation bent the PEN cantilever. The real-time response of the curvature k_s in Figure 6C corresponded well to the predicted model with the square dependence to the applied voltage U

$$k_s = \frac{1}{R} = U^2 \frac{6\varepsilon_0 \varepsilon_p (1-\nu_s)(h_p + h_s)}{E_s h_p h_s^3} \quad (4)$$

where thickness h_p and permittivity ε_p are parameters of the PDMS membrane, and thickness h_s, the elastic modulus E_s, and Poisson's ratio ν_s are parameters of the PEN substrate. The

ADVANCED SCIENCE NEWS
www.advancedsciencenews.com

ADVANCED MATERIALS TECHNOLOGIES
www.advmattechnol.de

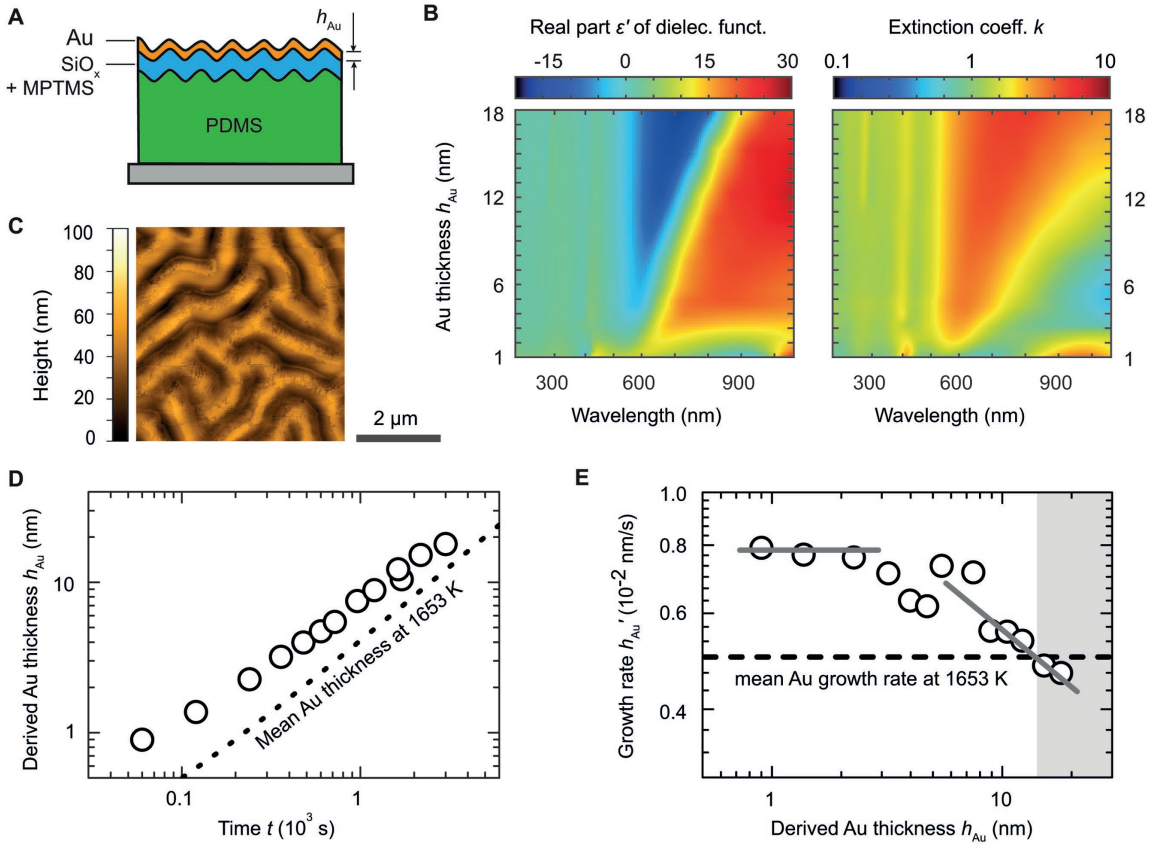

Figure 4. Insulator-to-metal transition for thermally evaporated Au on MPTMS/SiO_x. A) Schematic description of the stacked nanostructures. B) The evolution of the extinction coefficient k and the real part ε' of the dielectric function with respect to Au film thickness on a wrinkled MPTMS/SiO_x/PDMS surface. The color code for the extinction coefficient k and the real part ε' of the dielectric function is displayed logarithmically and linearly, respectively. C) AFM scan of the evaporated Au electrode. D) The ellipsometry-derived Au film thickness h_{Au} at representative time points for Au growth on the wrinkled MPTMS/SiO_x/PDMS surface. The dotted line represents the mean Au thickness adjusted by the evaporator temperature at 1653 K. E) Ellipsometry-derived growth rates h_{Au}' of Au with respect to the derived Au thickness h_{Au}. The expected mean growth rate for an evaporation temperature of $T = 1653$ K is marked as a dashed line.

applied electrical field perpendicular to the PDMS layer was 120 V µm^{-1} with leakage currents below the detection limit of 10 µA. This value is 50% higher than in previous reports for the same PDMS.[35,41] The results are consistent with recently performed simulations, which show that the surface tension increase leads to a significant improvement of the critical electrical field for instabilities to occur in constrained dielectric elastomer films.[42]

2. Conclusions

We have demonstrated an innovative approach to realize soft Au electrodes on silicone substrates. Our results, combining topological and mechanical film properties, shed light on the formation and reformation of wrinkles associated with the intrinsic compression of metal films. More generally, the interplay between a metal electrode and an elastomer substrate allows for tuning local morphology and related mechanics. Especially important is the ability to suppress the stiffness impact of the thin metal electrode on the entire sandwich nanostructure. Once the electrode has a thickness at which wrinkles disappear, maximal compliance is reached. Ultrathin-film dielectric elastomer transducers, which can be operated at low voltages, require such intrinsic-compressed, soft electrodes. Especially for dielectric elastomer actuators with thousands of nanometer-thin layers, this approach to suppress any rise in stiffness is productive.

3. Experimental Section

Preparation of the DEA Structures: PDMS (Dow Corning 184 Silicone Elastomer Kit, Dow Corning Europe S.A, Belgium) was prepared by mixing the prepolymer (component A) and the crosslinker (component B) at a volume ratio of 10:1, degassing for a period of 30 min, and then spin-coating on a 2 in. Si wafer at a rotation speed of 6000 rpm for a period of 120 s. The PDMS films were thermally cured at a temperature of 75 °C for a period of 24 h. For the in situ ellipsometry measurements

ADVANCED SCIENCE NEWS
www.advancedsciencenews.com

ADVANCED MATERIALS TECHNOLOGIES
www.advmattechnol.de

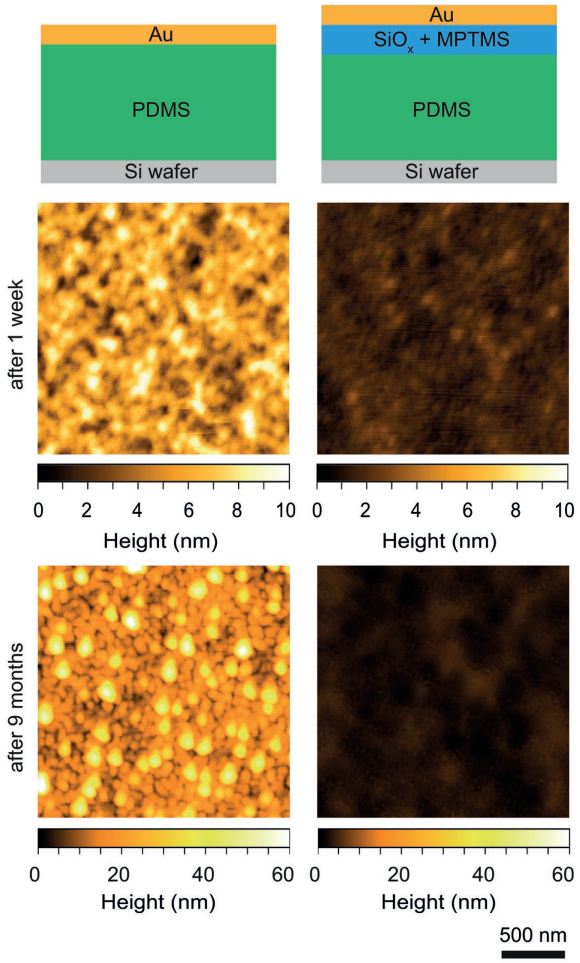

Figure 5. ULong-term stability of compressed Au electrodes. AFM scans of 30 nm thin sputtered Au electrodes. The Au electrode on native PDMS shows the characteristic morphology related to Au clusters, whereas the compressed Au electrode is flat with a roughness of 0.5 nm. The formation of Au nanoclusters on PDMS after nine months' storage in air at room temperature is suppressed for the compressed Au electrode.

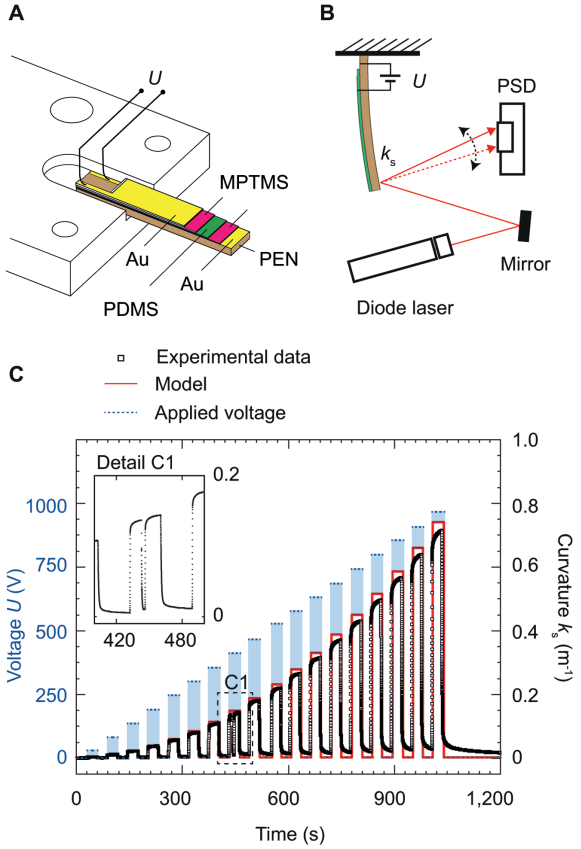

Figure 6. Actuation characteristics of bending DEA cantilever structures with compressed electrodes. A) Preparation of the DEA/PEN cantilever with a free-hanging area of 4 × 12 mm^2. B) Schematic illustration of the optical beam deflection method. For small deflections, curvature k_s can be calculated from the displacement of the laser beam on the PSD. C) Real-time response of the actuation up to an applied electrical field of 120 V μm^{-1}. The model originates from Equation (4). Detail C1 shows a selfclearance effect occurring at 53 V μm^{-1}, where the DEA structure recovered after a short breakdown due to defects in the dielectric layer.

in Figure 4, vinyl-terminated PDMS DMS-V05 (Gelest Inc., Morrisville, PA, USA) was evaporated at a temperature of (160 ± 5) °C and deposited on a 2 in. Si wafer inside a UHV chamber at a base pressure of 10^{-7} mbar, using low-temperature effusion sources (NTEZ, Dr. Eberl MBE Komponenten GmbH, Weil der Stadt, Germany) with a 25 cm^3 crucible. Crucible temperature was well below the temperature required to thermally degrade vinyl end groups.[43] The Si wafer was mounted at a distance of 400 mm away from the crucibles. The plasma treatments were performed on a 40 kHz RF system (PICO System, Diener Electronics, Ebhausen, Germany). The chamber was floated with oxygen at a flow rate of 20 sccm (Carbagas AG, Gümligen, Switzerland), keeping the partial pressure constant at 0.3 mbar. MPTMS of a purity ≥94.5% (Sigma-Aldrich, Switzerland, CAS Number: 4420-74-0, formula: $C_6H_{16}O_3SSi$, formula weight: 196.34 g mol^{-1}) was deposited on the hydroxyl PDMS surface by floating the vacuum chamber at 0.1 mbar for a period of 60 min. Excess MPTMS was removed by putting the sample in an ethyl acetate bath (Merck KGaA, Darmstadt, Germany). The Au electrodes (Lesker, East Sussex, UK) were sputtered using a DC sputter coater (SCD040, Balzers Union, Liechtenstein) at a discharge current of 15 mA. The sputter chamber was floated with Ar, and the pressure was kept at 0.05 mbar (Carbagas AG, Gümligen, Switzerland). The thickness of the Au electrodes was monitored using a quartz crystal microbalance (QSG 301, Balzers Union, Liechtenstein). The actuation measurements of DEAs were performed using a high-voltage supply (Stanford Research System PS310, GMP SA, Lausanne, Switzerland) with a current resolution of 10 µA.

AFM Imaging and Nanoindentation: AFM images were acquired by raster scanning the region of interest with a soft AFM probe (Tap190Al-G probe, NanoAndMore GmbH, Wetzlar, Germany) in tapping mode (FlexAFM C3000, Nanosurf AG, Liestal, Switzerland). The raw data were leveled by subtracting a mean plane and a polynomial background of second degree. Root-mean-square roughness values were calculated using the open source software for SPM data analysis, Gwyddion, Version 2.41. AFM nanoindentation measurements using a spherical tip with a radius of (522 ± 4) nm (B500FMR, Nanotools GmbH, Germany) were carried out to assess the mechanical properties of the soft heterostructures. Areas of 10 × 10 μm^2 were partitioned into 2500 domains, each serving as a nanoindentation site. The elastic modulus

ADVANCED SCIENCE NEWS
www.advancedsciencenews.com

ADVANCED MATERIALS TECHNOLOGIES
www.advmattechnol.de

at each site was calculated from the related force–distance curve by means of the Hertz contact model, as implemented in the FLEX-ANA software (Automated Nanomechanical Analysis, Nanosurf AG, Liestal, Switzerland). Substrate effects could be ignored, since the indentation depths were well below 500 nm.

Real-Time Spectroscopic Ellipsometry: To extract the optical properties of the nanostructures formation in situ, a spectroscopic ellipsometer (SE801, Sentech, Berlin, Germany) with SpectraRay3 software was utilized. The ellipsometric Ψ and Δ values from light with wavelengths ranging from 190 to 1050 nm were monitored at a frequency of 0.5 Hz at an incident angle of 70° to the normal of the substrate's surface. The 4 mm diameter of the incident beam led to a 4×10 mm^2 spot area on the substrate. The obtained Ψ and Δ values were related to the complex Fresnel reflection coefficients r_p and r_s of p- and s-polarized light and their ratio ρ by

$$\rho = \frac{r_p}{r_s} = e^{-i\Delta} \tan\Psi \tag{5}$$

Based on the obtained Fresnel reflection coefficient ratio, it was possible to extract the wavelength-dependent dielectric function $\varepsilon(\lambda)$

$$\begin{aligned}\langle\varepsilon\rangle &= \langle\varepsilon'\rangle + i\langle\varepsilon''\rangle = \langle\tilde{n}\rangle^2 = \left[\langle n\rangle + i\langle k\rangle\right]^2 \\ &= \varepsilon_0 \sin(\varphi_0)^2 \left[1 + \tan(\varphi_0)^2 \left(\frac{1-\rho}{1+\rho}\right)^2\right]\end{aligned} \tag{6}$$

with an angle of incidence φ_0, vacuum permittivity $\varepsilon_0 = 1$, and $n(\lambda)$ the real and $k(\lambda)$ the imaginary parts of the refractive index, respectively. The dielectric function of the evaporated PDMS was modeled with the Tauc–Lorentz dispersion formula.[44] To model the dielectric function of Au, a combination of two dispersion types was applied, named the "Drude–Lorentz oscillator model". Here, the Drude oscillator described the absorption of free-charge carriers, assuming that they acted in phase in response to the applied electrical field, while the Lorentz oscillator effectively modeled electrons bound to a positive core.[45] For the assessment of the model, the mean square error of the model fit and the experimentally measured $\Psi^{\mathrm{mod,exp}}$ and $\Delta^{\mathrm{mod,exp}}$ were calculated as

$$\mathrm{MSE} = \frac{1}{N}\sqrt{\sum_{i=1}^{N}\left[\left(\frac{\Psi_i^{\mathrm{mod}} - \Psi_i^{\mathrm{exp}}}{\sigma_{\Psi,i}^{\mathrm{exp}}}\right)^2 + \left(\frac{\Delta_i^{\mathrm{mod}} - \Delta_i^{\mathrm{exp}}}{\sigma_{\Delta,i}^{\mathrm{exp}}}\right)^2\right]} \tag{7}$$

with the random and systematic error σ^{exp}.

Supporting Information

Supporting Information is available from the Wiley Online Library or from the authors.

Acknowledgements

The authors acknowledge the financial support of the nano-tera.ch initiative, project SmartSphincter, as well as the Swiss Nanoscience Institute (SNI) for the financial contribution to the AFM. The authors thank Nanotools GmbH, Germany, for kindly providing them with two extra B500 AFM cantilevers, Frederikke Bahrt Madsen at the Technical University of Denmark, Florian M. Weiss and Vanessa Leung at the University of Basel for their helpful discussions and feedback on the paper.

Conflict of Interest

The authors declare no conflict of interest.

Keywords

AFM nanoindentations, dielectric elastomer transducers, metal-on-elastomer films, oxygen-plasma treatment of PDMS, soft electrodes

Received: April 27, 2017
Revised: June 6, 2017
Published online:

[1] R. Pelrine, R. Kornbluh, Q. Pei, J. Joseph, *Science* **2000**, *287*, 836.
[2] Y. Bar-Cohen, *Electroactive Polymer (EAP) Actuators as Artificial Muscles: Reality, Potential, and Challenges*, SPIE Press, Bellingham, **2004**.
[3] P. Brochu, Q. Pei, *Macromol. Rapid Commun.* **2010**, *31*, 10.
[4] I. A. Anderson, T. A. Gisby, T. G. McKay, B. M. O'Brien, E. P. Calius, *J. Appl. Phys.* **2012**, *112*, 041101.
[5] G. Rizzello, D. Naso, A. York, S. Seelecke, *Smart Mater. Struct.* **2016**, *25*, 035034.
[6] F. Carpi, D. De Rossi, R. Kornbluh, R. E. Pelrine, P. Sommer-Larsen, *Dielectric Elastomers as Electromechanical Transducers: Fundamentals, Materials, Devices, Models and Applications of an Emerging Electroactive Polymer Technology*, Elsevier, Amsterdam, **2008**.
[7] D. Rus, M. T. Tolley, *Nature* **2015**, *521*, 467.
[8] E. Fattorini, T. Brusa, C. Gingert, S. Hieber, V. Leung, B. Osmani, M. D. Dominietto, P. Büchler, F. Hetzer, B. Müller, *Ann. Biomed. Eng.* **2016**, *44*, 1355.
[9] A. Poulin, S. Rosset, H. R. Shea, *Appl. Phys. Lett.* **2015**, *107*, 244104.
[10] T. Töpper, F. M. Weiss, B. Osmani, C. Bippes, V. Leung, B. Müller, *Sens. Actuators, A* **2015**, *233*, 32.
[11] F. M. Weiss, T. Töpper, B. Osmani, S. Peters, G. Kovacs, B. Müller, *Adv. Electron. Mater.* **2016**, *2*, 1500476.
[12] R. Pelrine, R. Kornbluh, J. Joseph, R. Heydt, Q. Pei, S. Chiba, *Mater. Sci. Eng., C* **2000**, *11*, 89.
[13] F. B. Madsen, A. E. Daugaard, S. Hvilsted, A. L. Skov, *Macromol. Rapid Commun.* **2016**, *37*, 378.
[14] I. M. Graz, D. P. J. Cotton, S. P. Lacour, *Appl. Phys. Lett.* **2009**, *94*, 071902.
[15] S. Rosset, H. R. Shea, *Appl. Phys. A* **2013**, *110*, 281.
[16] R. Seghir, S. Arscott, *Sci. Rep.* **2015**, *5*, 14787.
[17] J. Tang, H. Guo, M. Zhao, J. Yang, D. Tsoukalas, B. Zhang, J. Liu, C. Xue, W. Zhang, *Sci. Rep.* **2015**, *5*, 16527.
[18] D. McCoul, W. Hu, M. Gao, V. Mehta, Q. Pei, *Adv. Electron. Mater.* **2016**, *2*, 1500407.
[19] A. Hirsch, H. O. Michaud, A. P. Gerratt, S. Mulatier, S. P. Lacour, *Adv. Mater.* **2016**, *28*, 4507.
[20] B. Osmani, H. Deyhle, F. M. Weiss, T. Töpper, M. Karapetkova, V. Leung, B. Müller, *Proc. SPIE* **2016**, *9798*, 979822.
[21] Y.-L. Loo, R. L. Willett, K. W. Baldwin, J. A. Rogers, *Appl. Phys. Lett.* **2002**, *81*, 562.
[22] T. Adrega, S. P. Lacour, *J. Micromech. Microeng.* **2010**, *20*, 055025.
[23] B. Atmaja, J. Frommer, J. C. Scott, *Langmuir* **2006**, *22*, 4734.
[24] A. K. Mahapatro, A. Scott, A. Manning, D. B. Janes, *Appl. Phys. Lett.* **2006**, *88*, 151917.
[25] H. Hillborg, J. F. Ankner, U. W. Gedde, G. D. Smith, H. K. Yasuda, K. Wikström, *Polymer* **2000**, *41*, 6851.
[26] K. Efimenko, W. E. Wallace, J. Genzer, *J. Colloid Interface Sci.* **2002**, *254*, 306.
[27] D. Bodas, C. Khan-Malek, *Sens. Actuators, B* **2007**, *123*, 368.
[28] D. B. H. Chua, H. T. Ng, S. F. Y. Li, *Appl. Phys. Lett.* **2000**, *76*, 721.
[29] D. Y. Khang, J. A. Rogers, H. H. Lee, *Adv. Funct. Mater.* **2009**, *19*, 1526.
[30] A. Schweikart, A. Fery, *Microchim. Acta* **2009**, *165*, 249.

[31] N. Bowden, S. Brittain, A. G. Evans, J. W. Hutchinson, G. M. Whitesides, *Nature* **1998**, *393*, 146.
[32] N. Bowden, W. T. S. Huck, K. E. Paul, G. M. Whitesides, *Appl. Phys. Lett.* **1999**, *75*, 2557.
[33] Y. Shao, M. A. Brook, *J. Mater. Chem.* **2010**, *20*, 8548.
[34] T. R. Hendricks, I. Lee, *Nano Lett.* **2007**, *7*, 372.
[35] B. Osmani, E. A. Aeby, B. Müller, *Rev. Sci. Instrum.* **2016**, *87*, 053901.
[36] W. T. S. Huck, N. Bowden, P. Onck, T. Pardoen, J. W. Hutchinson, G. M. Whitesides, *Langmuir* **2000**, *16*, 3497.
[37] S. Béfahy, P. Lipnik, T. Pardoen, C. Nascimento, B. Patris, P. Bertrand, S. Yunus, *Langmuir* **2010**, *26*, 3372.
[38] B. Osmani, G. Gerganova, B. Müller, *Eur. J. Nanomed.* **2017**, *9*, 69.
[39] T. Töpper, S. Lörcher, B. Osmani, V. Leung, H. Deyhle, T. Pfohl, B. Müller, *Adv. Electron. Mater.* **2017**, 1700073.
[40] T. W. H. Oates, L. Ryves, M. M. M. Bilek, *Opt. Express* **2008**, *16*, 2302.
[41] D. Gatti, H. Haus, M. Matysek, B. Frohnapfel, C. Tropea, H. F. Schlaak, *Appl. Phys. Lett.* **2014**, *104*, 052905.
[42] S. Seifi, H. S. Park, *Int. J. Solids Struct.* **2016**, *87*, 236.
[43] T. Töpper, S. Lörcher, F. M. Weiss, B. Müller, *APL Mater.* **2016**, *4*, 056101.
[44] H. Fujiwara, *Spectroscopic Ellipsometry: Principles and Applications*, John Wiley & Sons, Hoboken, NJ, USA, **2007**.
[45] T. W. H. Oates, H. Wormeester, H. Arwin, *Prog. Surf. Sci.* **2011**, *86*, 328.

2.5 Nanomechanical probing of thin-film dielectric elastomer transducers

AFM nanoindentations on DC-powered DETs show increased indenting depths by 42 % with respect to the field-free condition, implying an electro-mechanically driven elastic softening of the DET.

Experimental results agree with related nonlinear, dynamic finite element model simulations.

Pull-off forces rise from (23 ± 7) to (46 ± 15) nN implying a nanoindentation imprint after the unloading.

Root-mean-square roughness of Au electrode raised by 11 % at an electrical field of 12 V/µm demonstrating that the electrode's morphology change is an undervalued factor in the fabrication of DET structures.

Published in Applied Physics Letters

Nanomechanical probing of thin-film dielectric elastomer transducers

Bekim Osmani, Saman Seifi, Harold S. Park, Vanessa Leung, Tino Töpper, and Bert Müller

Citation: Appl. Phys. Lett. **111**, 093104 (2017); doi: 10.1063/1.5000736
View online: http://dx.doi.org/10.1063/1.5000736
View Table of Contents: http://aip.scitation.org/toc/apl/111/9
Published by the American Institute of Physics

APPLIED PHYSICS LETTERS 111, 093104 (2017)

Nanomechanical probing of thin-film dielectric elastomer transducers

Bekim Osmani,[1] Saman Seifi,[2] Harold S. Park,[2] Vanessa Leung,[1] Tino Töpper,[1] and Bert Müller[1,a)]
[1]*Biomaterials Science Center, Department of Biomedical Engineering, University of Basel, Allschwil 4123, Switzerland*
[2]*Department of Mechanical Engineering, Boston University, Boston, Massachusetts 02215, USA*

(Received 4 May 2017; accepted 13 August 2017; published online 31 August 2017)

Dielectric elastomer transducers (DETs) have attracted interest as generators, actuators, sensors, and even as self-sensing actuators for applications in medicine, soft robotics, and microfluidics. Their performance crucially depends on the elastic properties of the electrode-elastomer sandwich structure. The compressive displacement of a single-layer DET can be easily measured using atomic force microscopy (AFM) in the contact mode. While polymers used as dielectric elastomers are known to exhibit significant mechanical stiffening for large strains, their mechanical properties when subjected to voltages are not well understood. To examine this effect, we measured the depths of 400 nanoindentations as a function of the applied electric field using a spherical AFM probe with a radius of (522 ± 4) nm. Employing a field as low as 20 V/μm, the indentation depths increased by 42% at a load of 100 nN with respect to the field-free condition, implying an electromechanically driven elastic softening of the DET. This at-a-glance surprising experimental result agrees with related nonlinear, dynamic finite element model simulations. Furthermore, the pull-off forces rose from (23.0 ± 0.4) to (49.0 ± 0.7) nN implying a nanoindentation imprint after unloading. This embossing effect is explained by the remaining charges at the indentation site. The root-mean-square roughness of the Au electrode raised by 11% upon increasing the field from zero to 12 V/μm, demonstrating that the electrode's morphology change is an undervalued factor in the fabrication of DET structures. [http://dx.doi.org/10.1063/1.5000736]

Thin-film dielectric elastomer transducers (DETs) are emerging in applications such as haptics, tunable optics, soft robotics, and biomedical devices.[1] In their most primitive version, they are composed of a soft elastomeric film, sandwiched between two compliant electrodes. The elastomer film, often polydimethylsiloxane (PDMS), undergoes an expansion perpendicular to the applied electric field as a result of the Coulomb attraction of the oppositely charged electrodes. DETs show an actuation strain larger than muscles in the human body[2] and millisecond response time[3] and have energy densities well comparable to human muscle tissue.[4,5] In addition, composed of elastomers,[6] they can self-heal[7] and can provide sensing feedback.[8] Thus, DETs could become medical devices to substitute the function of human muscles.[9] The generated force of a thin-film DET with an area of about a square-centimeter was found to be 100 mN and could be quantified using an optical beam-deflection technique.[10] Therefore, thousands of layers would be required to generate forces of several Newtons, which is required for artificial muscles to treat urinary or fecal incontinence. A recent work describes the fabrication of a 12-layer stacked DET that allows significant actuations without pre-stretching at voltages between 1 and 2 kV.[11] Major efforts have been invested to reduce the operation voltage by one or two orders of magnitude. One approach relies on elastomer films with a submicron thickness which are prepared by thin-film techniques such as molecular beam deposition (MBD) techniques and electrospraying.[12,13] The surface roughness of thermally evaporated metal/PDMS sandwich structures can be controlled on the nanometer scale;[14] however, their applicability for DETs is still restricted. First, the evaporation of viscous PDMS pre-polymers in vacuum is limited to oligomers with a molecular weight of 6100 g/mol (Ref. 15); second, the growth rate below one layer per hour confines the fabrication of stacked DETs.[16] Electrospraying of dissolved PDMS in ethyl acetate exhibits increased deposition rates of one layer per minute but leads to comparably rough PDMS sub-micrometer films. However, it is easily scalable and promising for large-scale fabrication of low-voltage DETs. The performance of electrosprayed DETs with inhomogeneous PDMS films has not been investigated yet. Recently, it has been shown that for thin-film DETs, the impact of electrode's topology and stiffness increase of the overall DET by a metal electrode, such as Au, is essential.[17] In a previous study, these mechanical properties have been determined by nanoindentation (NI) measurements with a spherical indenter using atomic force microscopy (AFM).[18] The elastic modulus of the thin-film DET sandwich structure increased by a factor of three after the deposition of a 10 nm Au electrode. The observed force-distance-curves allow us not only to extract the mechanical properties of thin polymeric films but also to study the related adhesion forces.[19–22] Several research teams have investigated the electromechanical behavior for larger deformations using experimental

a)Author to whom correspondence should be addressed: bert.mueller@unibas.ch

methods and simulations including finite element (FE) analysis.[23–26]

In this communication, we elucidate that probing a DC-powered thin-film DET with a spherical AFM tip leads to increased indentation depths by several tens of percent, as verified by dynamic FE models. Furthermore, we investigate how far the roughness of the Au electrode increases owing to the actuation. This effect is highly beneficial and can be used in anisotropic DET structures with electrodes containing parallel wrinkles to generate unilateral actuation.

Single-layer DET specimens, as shown in Fig. 1(a), were fabricated on polyethylene naphthalate (PEN) polymeric substrates. The related materials and fabrication methods are presented in a previous work.[10] For the nanoindentation (NI) measurements, the 10 nm-thin Au electrodes were connected to the DC power supply and set to selected voltages between 0 and 160 V. The voltage Φ was set to the preselected value and kept constant until the completion of the 400 NI measurements. For all experiments, we used only one AFM cantilever with a spherical electron-beam processed carbon tip (B500 FMR, Nanotools GmbH, Germany). The tip radius has been measured using scanning electron microscopy and is found to be (522 ± 4) nm. The nominal spring constant of the AFM cantilever was calculated using the Sader method and was found to be $k = (1.9 \pm 0.1)$ N/m. According to the Global Calibration Initiative by Sader *et al.*, we get for this cantilever a standardized spring constant of $k_{\text{Sader}} = (2.1 \pm 0.2)$ N/m ($f_r = 88.9$ kHz, $Q = 132$, B500 FMR).[27] The deflection sensitivity was calibrated using a Si wafer serving as a substrate with an infinite stiffness. An area of $10 \times 10\ \mu\text{m}^2$ contains 400 subdomains, each serving as a NI site. An automated data acquisition and analysis software (Flex-ANA, Nanosurf AG, Switzerland) running on an AFM system (FlexAFM C3000, Nanosurf AG, Switzerland) was used to extract the indentation depths δ for each measurement. The nanoindentation speed was set to 3 μm/s. PDMS can be approximated to be purely elastic.[21] Characteristic force-distance curves for $P = 100$ nN and $\Phi = 0$ V shown in the supplementary material clearly indicate that the PDMS-layer shows an almost perfectly elastic behavior as the loading and unloading curve coincide.

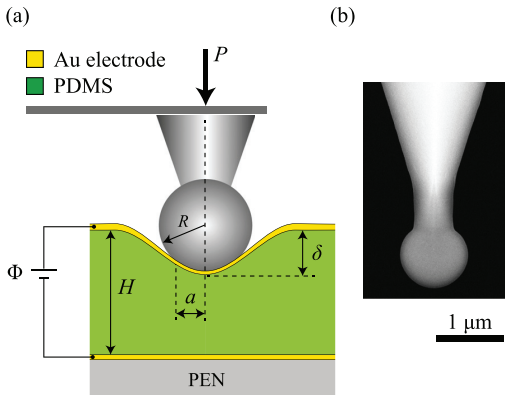

FIG. 1. AFM nanoindentation on the activated DET structure. (a) Schematic of the experimental setup consisting of an 8 μm-thin elastomer film, sandwiched between two 10 nm-thin Au electrodes. The nanoindentation depth δ is measured at selected voltages Φ and loads P using an AFM probe with a well-defined radius R. The spherical tip gives rise to the contact radius a used for the JKR model.[28] (b) SEM image of the used spherical probe with a radius of (522 ± 4) nm. Reproduced with permission from Nanotools GmbH, Munich, Germany. Copyright 2017 Nanotools GmbH.

NIs on DETs without applying a voltage, $\Phi = 0$ V, were employed to determine the average elastic modulus E_{DET}. The dimensionless Tabor parameter $\mu = (R\gamma^2/E_{DET}^2\varepsilon^3)^{1/3}$ supports selecting the contact model.[28] Here, R is the probe radius, γ the adhesion work, and ε the equilibrium separation, typically around 0.5 nm. For $\mu > 5$, the Johnson-Kendall-Roberts (JKR) contact model is recommended.[28,29] Using $R = 522$ nm and the average pull-off force $F_0 = 23$ nN, the adhesion work $\gamma = F_0/(3\pi R/2)$ is found to be 9.3 mJ/m^2. With $E_{\text{DET}} = 1.6$ MPa, the Tabor parameter can be calculated to be $\mu = 52$. For $\Phi = 0$ V, the experimental data clearly uncover the two-layer DET structure consisting of the 10 nm-thin electrode and the elastomeric bulk. For a small load of $P = 25$ nN, the calculated average elastic modulus using the JKR model corresponds to $E_{\text{DET}} = (2.1 \pm 0.3)$ MPa. It decreases to (1.8 ± 0.2), (1.7 ± 0.2), and (1.6 ± 0.2) MPa for loads of $P = 50$, 75, and 100 nN, respectively. The nanoindentation depths for $\Phi = 0$ V are listed in Table I. The elastic modulus decreases with the indentation depth for the two-layer structure. We assume that local strains on the 10 nm-thin Au electrode rise for larger penetration depths minimizing the stiffness increase due to the stiff electrode. It was shown, however, that the surface layer of PDMS is stiffer than the PDMS below.[30] As reported previously, the nanometer-thin Au electrode is not confluent and forms nanoclusters with a nominal size of (20 ± 10) nm.[31] NI results on actuated DETs operated at voltages of $\Phi = 0$, 40, 80, 120, and 160 V are summarized in Table I for applied loads of $P = 25$, 50, 75, and 100 nN. The resulting mean indentation depth δ including the measurements at $\Phi = 0$ V were fitted using a Gaussian function.

For a constant indentation load P, the indentation depth δ increases with respect to the applied voltage Φ. We assume that the indentation depth increases with the applied voltage due to an increased charge density at the indentation site. It is shown that the electric charge density at a point on a given conductor surface increases with its local curvature $1/R$.[32] These experimental results were surprising at first glance, as one might expect a stiffening effect due to the applied Maxwell pressure generated.[2] For $P = 25$ nN, the indentation depth is increased by 17 nm, whereas for $P = 100$ nN, the average increase was found to be 50 nm. The variance of measured data increased as well. The nonlinear, dynamic

TABLE I. Indentation depths δ of a spherical AFM probe on a single-layer thin-film DET at selected loads P and applied voltages Φ. The derived parameters are grouped and fitted using a Gaussian.

Indentation load P (nN)	Indentation depth δ (nm)[a]				
	$\Phi = 0$ V	$\Phi = 40$ V	$\Phi = 80$ V	$\Phi = 120$ V	$\Phi = 160$ V
25	38 ± 4	40 ± 5	46 ± 5	51 ± 5	55 ± 6
50	74 ± 6	75 ± 6	83 ± 8	93 ± 8	114 ± 16
75	103 ± 6	106 ± 7	113 ± 8	125 ± 9	143 ± 11
100	117 ± 4	132 ± 6	140 ± 7	151 ± 8	167 ± 11

[a]The error corresponds to the standard deviation of the Gaussian fit.

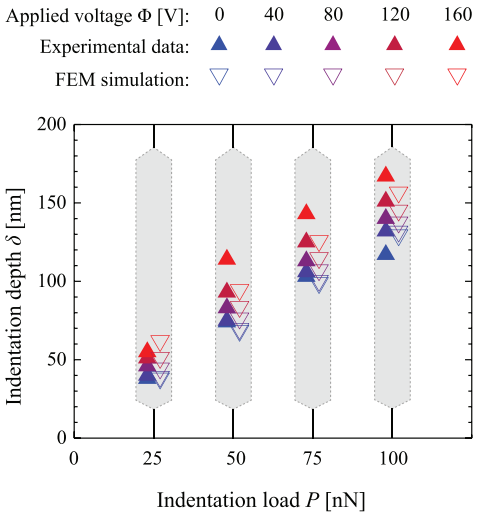

FIG. 2. Indentation depth δ as a function of the applied load P for selected voltages Φ. The FE simulations explain the experimental data.

finite element (FE) simulations, as shown in Fig. 2, agree with the experimental results. The FE simulations were carried out using a previously developed dynamic FE formulation for DETs.[33] 2D plane strain FE simulations were performed on DETs with the same material properties. The voltage at the bottom surface was kept at zero, while the voltage was increased linearly on the top surface in Fig. 1 and the voltage was increased sufficiently slowly to mimic quasi-static loading conditions. After the voltage reached the target value, the DET was indented by moving the indenter towards the DET with fixed velocity. The reaction force as a function of indentation depth was then measured, and the FE simulations were repeated for the voltages, as in the experiments. We have observed that at higher loads P, the experimental data are pulled apart more strongly than the values observed from the FE simulation. The indentation depths δ from FE simulations overshoot the experimental data at smaller voltages and fall below the experimental data at higher voltages Φ. This is likely because the FE models assume "ideal dielectric behavior," i.e., the polarization of the dielectric is like a fluid or isotropic.

The loading curves of NI experiments include both the contact and adhesion forces. From the unloading force-distance curves, however, the pull-off force F_0, also termed adhesion force at the time of separation, is extracted. The pull-off force F_0 is given as[29]

$$F_0 = 2\pi R(\gamma_1 + \gamma_2 - \gamma_{12}), \quad (1)$$

where R is the indenter radius and γ_1, γ_2, and γ_{12} are the free surface energies of the indentation sphere, the electrode and the interface, respectively. In Fig. 3, we show the categorized pull-off forces from 400 nanoindentations at a fixed load of $P = 100$ nN. The histograms were consistently fitted using OriginPro 2015 (OriginLab Corporation, Northampton, USA) and pro Fit 6.2.11 (QuantumSoft, Uetikon am See, Switzerland) to one Gaussian with the three relevant parameters including their error bars by means of the Levenberg-Marquardt algorithm.

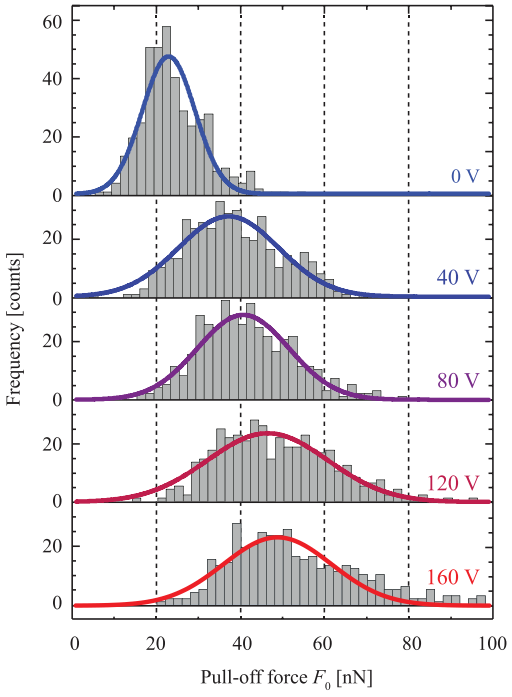

FIG. 3. Histograms of pull-off forces F_0 at the time of separation extracted from the unloading force distance curves for an applied load of $P = 100$ nN. The obtained values are fitted with a Gaussian function, upon which for the mean values we find $F_0 = (23.0 \pm 0.4)$, (37.2 ± 0.6), (40.7 ± 0.5), (46.4 ± 0.7), and (49.0 ± 0.7) nN for $\Phi = 0$, 40, 80, 120, and 160 V, respectively.

We have observed more than a doubling of the pull-off forces from (23.0 ± 0.4) to (49.0 ± 0.7) nN with increased operation voltages from $\Phi = 0$ to 160 V. Equation (1) illustrates the proportionality of pull-off force to the size of the indenter sphere. Therefore, we assume that the increased pull-off forces are related to an increased contact area at the instant of time when the indenter is being separated from the Au electrode. We hypothesize that a *nano-indentation imprint* remains after the measurement due to charge accumulation at the indentation site of the activated DET structure. Although our AFM instrumentation does not allow direct scanning of the topology after indentation, it is a reasonable hypothesis because adhesion measurements on stiff Au-coated Si wafers show that the pull-off forces are independent of the applied load and indentation speed. An electrostatic field between the cantilever and the top gold electrode layer can be excluded as they were connected at a single point to avoid an electrical potential. The related data are given in the supplementary material. As reported by Rabinovich *et al.*, the adhesion forces decrease with respect to the surface roughness.[34] Therefore, in the present experiment, one can definitely exclude any increase in the adhesion force as a result of enhanced surface roughness. However, doubling the applied voltage Φ from 80 to 160 V, the pull-off force F_0 only increases by 20%, i.e., from (40.7 ± 0.5) to (49.0 ± 0.7) nN.

Figure 4 shows AFM surface scans of planar electrodes for $\Phi = 0$ and 100 V. The scans were performed in the tapping mode (Budget Sensors Tap 190-G, Nano and More GmbH, Wetzler, Germany) with an amplitude of 1 V and a

set point of 60%. The typical Volmer-Weber growth mode of Au on PDMS leads to nanoclusters with an average size of (20 ± 10) nm. At applied voltages of 100 V, the detected surface roughness increased by 11%. The charge distribution on the electrode of a powered DET is expected to be strongly dependent on the topology of the electrode. Due to charge accumulation within the valleys, the electric field becomes inhomogeneous on the nanometer scale. This effect could be related to the indentation depth, which increases with the voltage applied, as elucidated by the experimental data shown in Fig. 2.

As recently published, we were able to follow the compressive strain of a DET structure using the AFM in real time.[35] For this, the upper electrode was scanned in the contact mode with a comparably soft spherical AFM tip (B150 CONTR, $k = 0.2$ N/m) at the low set point of 8 nN to minimize the penetration of the tip into the DET structure. The calculated contact pressure was found to be 0.48 MPa. The radius of the AFM tip was measured using scanning electron microscopy and was found to be $R = (152 \pm 2)$ nm. To ensure a verifiable contact between the AFM tip and the electrode, we have fabricated DET structures with parallel aligned wrinkles as seen in Fig. 5(a). DET structures were fabricated on 2-in. Si substrates with a 100 nm SiO_2 coating using a Mo mask with 12×0.4 mm^2 windows. As Bowden *et al*. have shown, wrinkles align perpendicular to steps and edges.[36] Due to the oriented wrinkle structure over the whole width, at one end of the DET, the upper electrode was displaced by $s_x = (80 \pm 3)\,\mu$m in one direction, as observed with the built-in top camera of the AFM system. The compressive strain was extracted via two profile cuts as seen in Fig. 5(b). The profile cuts were fitted using a constant revealing an actuation of (180 ± 20) nm. This value corresponds to a strain of only 2.3%, as the DET structure was fabricated on a rigid Si wafer. The calculated RMS value for $\Phi = 0$ V and $\Phi = 100$ V of the AFM scan shown in Fig. 5(b) increased from 23 to 28 nm.

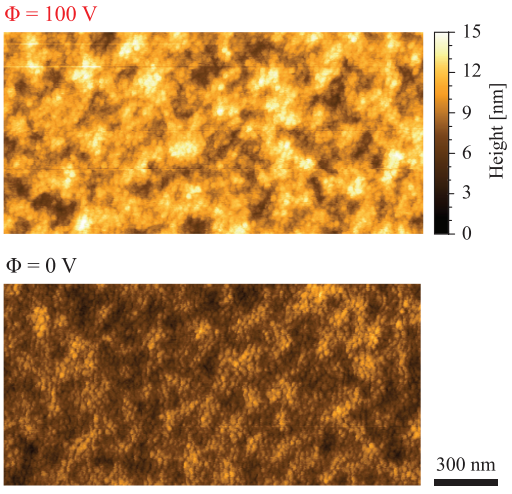

FIG. 4. AFM surface scan of a 2×1 μm^2 spot of the top Au electrode for a non-powered and powered DET. For a voltage of $\Phi = 100$ V, which corresponds to an electric field of 12 V/μm, the root-mean-square roughness increased by 11%, from 1.35 to 1.50 nm. The height color bar is valid for both AFM scans.

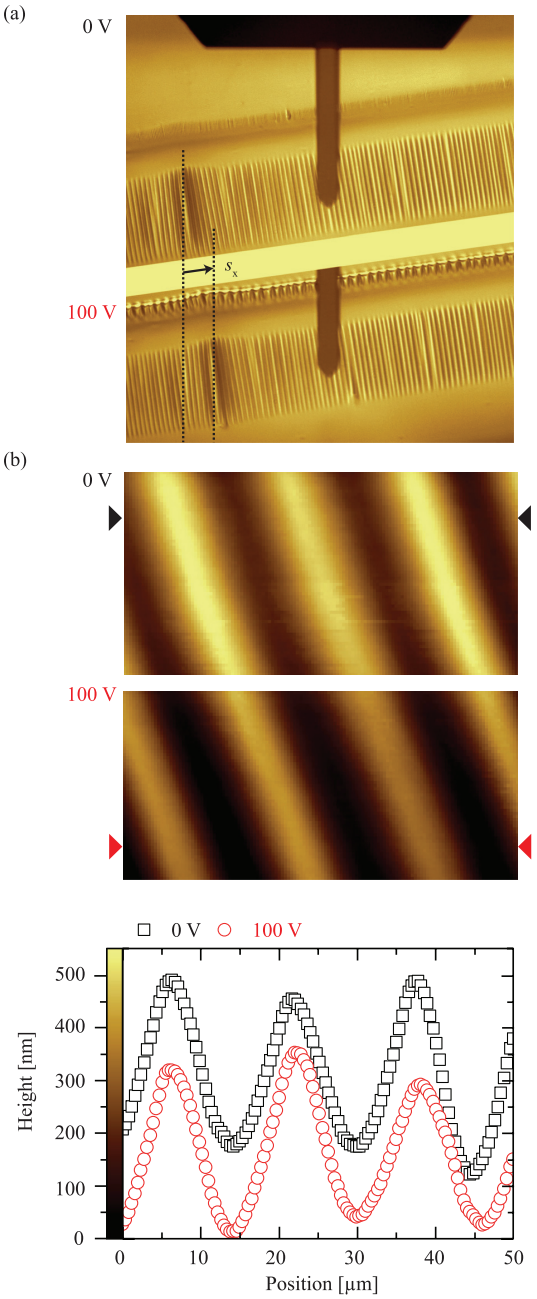

FIG. 5. Actuation measurement of a substrate bonded single-layer DET using an AFM in the contact mode. (a) Observation of the lateral displacement $s_x = (80 \pm 3)\,\mu$m of the wrinkled electrode using the built-in top camera of the AFM. (b) AFM scan in the contact mode of the wrinkled electrode using a spherical AFM tip with a large radius of $R = (152 \pm 2)$ nm for $\Phi = 0$ and 100 V. Profile cuts reveal a compressive actuation of only (180 ± 20) nm, corresponding to a strain of only 2.3%, as the DET structure was fabricated on a rigid Si wafer. The height color bar for the AFM scans is shown on the left side/ordinate of the graph containing the profile cuts.

In summary, we have shown that probing a DC-powered thin-film DET with an AFM spherical tip leads to increased indentation depths by several tens of percent, as verified by dynamic FE models. We address the apparent softening

effect of the DET structure as a result of the expected charge accumulation at the nanoindentation site, which is the consequence of the impression by the tip.[32] Furthermore, AFM scans revealed increased roughness of the Au electrode as a result of the voltage applied to the DET. In conclusion, electrodes with a controlled topology can be prepared to trigger a preferred direction of the actuation.

See supplementary material for details on the sample preparation, characteristic force-distance curves, average elastic modulus using the JKR contact model for the DET-structure at four selected loads, and pull-off forces for a spherical AFM tip with a radius of (499 ± 4) nm on a 50 nm-thin Au-coated Si wafer.

This work was conducted with financial support from the Swiss Research Program Nano-Tera.ch as well as from the Swiss Nanoscience Institute (SNI). HSP and SS acknowledge funding from the ARO, grant W911NF-14-1-0022.

[1]S. Rosset and H. R. Shea, Appl. Phys. Rev. **3**(3), 031105 (2016).
[2]R. Pelrine, R. Kornbluh, Q. Pei, and J. Joseph, Science **287**(5454), 836 (2000).
[3]J. Kun, L. Tongqing, and T. J. Wang, Sens. Actuators, A **239**, 8 (2016).
[4]A. O'Halloran, F. O'Malley, and P. McHugh, J. Appl. Phys. **104**(7), 071101 (2008).
[5]I. A. Anderson, T. A. Gisby, T. G. McKay, B. M. O'Brien, and E. P. Calius, J. Appl. Phys. **112**(4), 041101 (2012).
[6]D. Rus and M. T. Tolley, Nature **521**(7553), 467 (2015).
[7]S. Hunt, T. G. McKay, and I. A. Anderson, Appl. Phys. Lett. **104**(11), 113701 (2014).
[8]G. Rizzello, D. Naso, A. York, and S. Seelecke, Smart Mater. Struct. **25**(3), 035034 (2016).
[9]E. Fattorini, T. Brusa, C. Gingert, S. E. Hieber, V. Leung, B. Osmani, M. D. Dominietto, P. Büchler, F. Hetzer, and B. Müller, Ann. Biomed. Eng. **44**, 1355 (2016).
[10]B. Osmani, E. A. Aeby, and B. Müller, Rev. Sci. Instrum. **87**(5), 053901 (2016).
[11]M. Duduta, R. J. Wood, and D. R. Clarke, Adv. Mater. **28**(36), 8058 (2016).
[12]F. M. Weiss, T. Töpper, B. Osmani, H. Deyhle, G. Kovacs, and B. Müller, Langmuir **32**, 3276 (2016).
[13]T. Töpper, F. M. Weiss, B. Osmani, C. Bippes, V. Leung, and B. Müller, Sens. Actuators, A **233**, 32 (2015).
[14]T. Töpper, S. Lörcher, H. Deyhle, B. Osmani, V. Leung, T. Pfohl, and B. Müller, Adv. Electron. Mater. **3**, 1700073 (2017).
[15]T. Töpper, S. Lörcher, F. Weiss, and B. Müller, APL Mater. **4**(5), 56101 (2016).
[16]F. M. Weiss, T. Töpper, B. Osmani, S. Peters, G. Kovacs, and B. Müller, Adv. Electron. Mater. **2**, 1500476 (2016).
[17]A. Poulin, S. Rosset, and H. R. Shea, Appl. Phys. Lett. **107**(24), 244104 (2015).
[18]B. Osmani, H. Deyhle, F. M. Weiss, T. Töpper, M. Karapetkova, V. Leung, and B. Müller, Proc. SPIE **9798**, 979822 (2016).
[19]K. Miyake, N. Satomi, and S. Sasaki, Appl. Phys. Lett. **89**(3), 031925 (2006).
[20]M. Galli and M. L. Oyen, Appl. Phys. Lett. **93**(3), 031911 (2008).
[21]F. Carrillo, S. Gupta, M. Balooch, S. J. Marshall, G. W. Marshall, L. Pruitt, and C. M. Puttlitz, J. Mater. Res. **20**(10), 2820 (2005).
[22]H. J. Butt, B. Cappella, and M. Kappl, Surf. Sci. Rep. **59**(1), 1 (2005).
[23]M. Wissler and E. Mazza, Sens. Actuators, A **138**(2), 384 (2007).
[24]S. Seifi and H. S. Park, Int. J. Solids Struct. **87**, 236 (2016).
[25]H. S. Park, Z. Suo, J. Zhou, and P. A. Klein, Int. J. Solids Struct. **49**(15–16), 2187 (2012).
[26]X. Zhao and Q. Wang, Appl. Phys. Rev. **1**(2), 021304 (2014).
[27]J. E. Sader, R. Borgani, C. T. Gibson, D. B. Haviland, M. J. Higgins, J. I. Kilpatrick, J. Lu, P. Mulvaney, C. J. Shearer, A. D. Slattery, P. A. Thorén, J. Tran, H. Zhang, H. Zhang, and T. Zheng, Rev. Sci. Instrum. **87**(9), 093711 (2016).
[28]Yu. M. Efremov, D. V. Bagrov, M. P. Kirpichnikov, and K. V. Shaitan, Colloids Surf., B **134**, 131 (2015).
[29]D. Tabor, J. Colloid Interface Sci. **58**(1), 2 (1977).
[30]W. Xu, N. Chahine, and T. Sulchek, Langmuir **27**(13), 8470 (2011).
[31]B. Osmani, T. Töpper, M. Siketanc, G. Kovacs, and B. Müller, Proc. SPIE **10163**, 101631E (2017).
[32]K. Bhattacharya, Phys. Scr. **91**(3), 035501 (2016).
[33]H. S. Park, Q. Wang, X. Zhao, and P. A. Klein, Comput. Methods Appl. Mech. Eng. **260**, 40 (2013).
[34]Y. I. Rabinovich, J. J. Adler, A. Ata, R. K. Singh, and B. M. Moudgil, J. Colloid Interface Sci. **232**(1), 17 (2000).
[35]T. Töpper, B. Osmani, S. Lörcher, and B. Müller, Proc. SPIE **10163**, 101631F (2017).
[36]N. Bowden, W. T. S. Huck, K. E. Paul, and G. M. Whitesides, Appl. Phys. Lett. **75**(17), 2557 (1999).

2.6 Biomimetic nanostructures for the silicone-biosystem interface: tuning oxygen-plasma treatments of polydimethylsiloxane

Fabrication and cross-linking of nanometer-thin PDMS films using oxygen plasma for vinyl-terminated PDMS prepolymers with a molecular weight of 800 g/mol.

The amplitude and periodicity of the wrinkles on nanometer-thin PDMS films can be tuned. It depends on the film thickness, plasma power, treatment duration and the partial oxygen pressure within the chamber.

The extracted mechanical properties of plasma-treated PDMS film show that the average elastic modulus can be set to a few MPa.

Nanoindentations on wrinkled PDMS films with sub-micrometer mapping reveal softer nano-valleys and stiffer nano-hills.

The hydrophobic recovery of nanostructured PDMS surfaces, as assessed by dynamic contact angle measurements, scales with nanostructure's fineness.

Published in European Journal of Nanomedicine

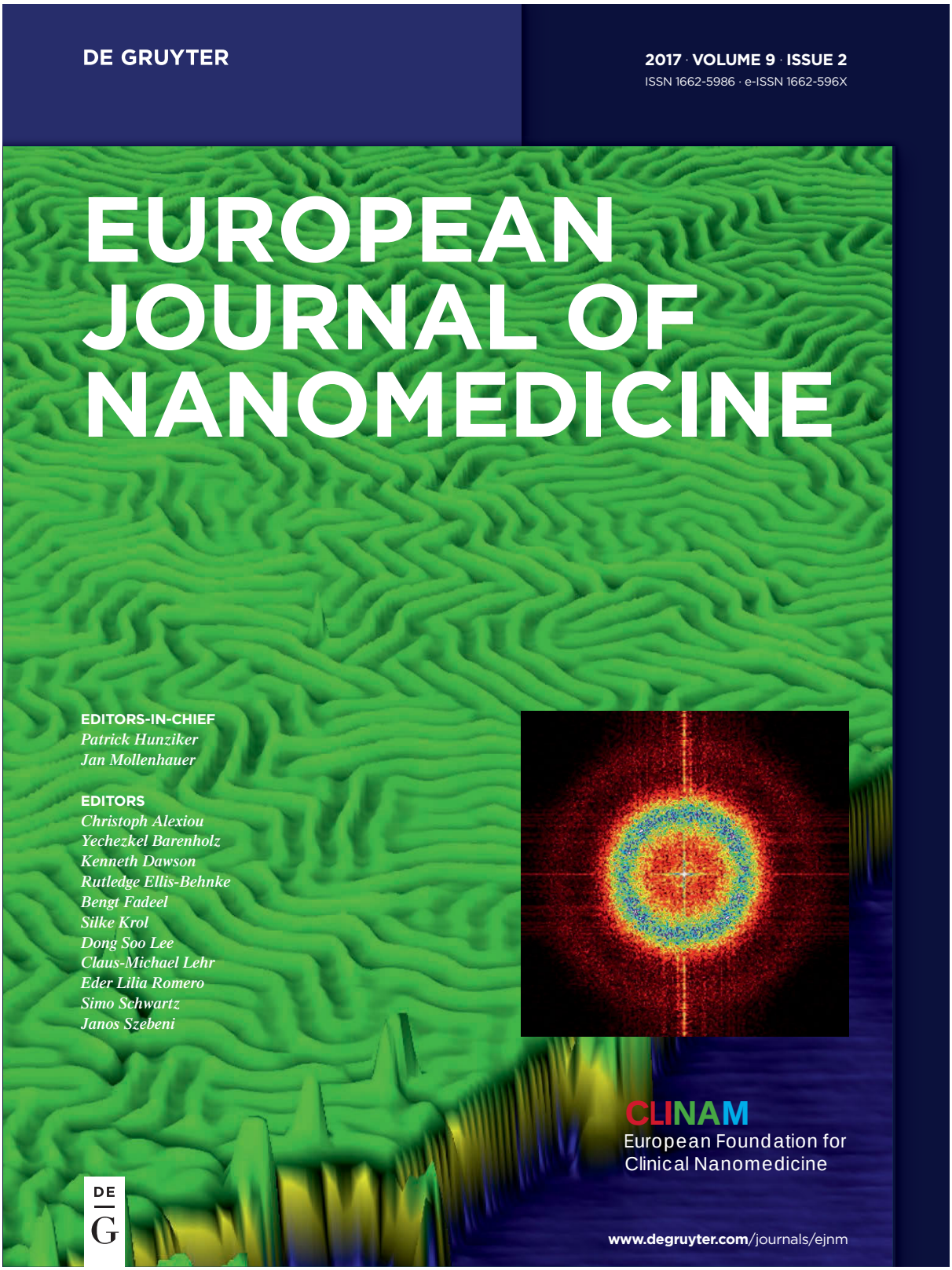
DE GRUYTER
2017 · VOLUME 9 · ISSUE 2
ISSN 1662-5986 · e-ISSN 1662-596X
EUROPEAN JOURNAL OF NANOMEDICINE
EDITORS-IN-CHIEF
Patrick Hunziker
Jan Mollenhauer
EDITORS
Christoph Alexiou
Yechezkel Barenholz
Kenneth Dawson
Rutledge Ellis-Behnke
Bengt Fadeel
Silke Krol
Dong Soo Lee
Claus-Michael Lehr
Eder Lilia Romero
Simo Schwartz
Janos Szebeni
CLINAM
European Foundation for Clinical Nanomedicine
DE G
www.degruyter.com/journals/ejnm

DE GRUYTER Eur. J. Nanomed. 2017; aop

Bekim Osmani*, Gabriela Gerganova and Bert Müller

Biomimetic nanostructures for the silicone-biosystem interface: tuning oxygen-plasma treatments of polydimethylsiloxane

DOI 10.1515/ejnm-2017-0002
Received February 2, 2017; accepted March 2, 2017

Abstract: Polydimethylsiloxanes (PDMS) have drawn attention because of their applicability in medical implants, soft robotics and microfluidic devices. This article examines the formation of dedicated nanostructures on liquid submicrometer PDMS films when exposed to oxygen-plasma treatment. We show that by using a vinyl-terminated PDMS prepolymer with a molecular weight of 800 g/mol, one can bypass the need of solvent, copolymer, or catalyst to fabricate wrinkled films. The amplitude and periodicity of the wrinkles is tuned varying the thickness of the PDMS film between 150 and 600 nm. The duration of the plasma treatment and the oxygen pressure determine the surface morphology. The amplitude was found between 30 and 300 nm with periodicities ranging from 500 to 2800 nm. Atomic force microscopy was used to measure film thickness, amplitude and wrinkle periodicity. The hydrophobic recovery of the nanostructured PDMS surface, as assessed by dynamic contact angle measurements, scales with nanostructure's fineness, associated with an improved biocompatibility. The mechanical properties were extracted out of 10,000 nanoindentations on 50×50-μm^2 spots. The mechanical mapping with sub-micrometer resolution reveals elastic properties according to the film morphology. Finally, we tailored the mechanical properties of a 590 ± 120-nm-thin silicone film to the elastic modulus of several MPa, as required for dielectric elastomer actuators, to be used as artificial muscles for incontinence treatments.

Keywords: dielectric elastomer actuators; dynamic contact angle measurements on PDMS; local mechanical properties of thin polymer films; nanometer-thin polymer films; oxygen-plasma-tuned wrinkles.

***Corresponding author: Bekim Osmani,** Department of Biomedical Engineering, Biomaterials Science Center, University of Basel, Gewerbestrasse 14, 4123 Allschwil, Switzerland,
E-mail: bekim.osmani@unibas.ch
Gabriela Gerganova and Bert Müller: Department of Biomedical Engineering, Biomaterials Science Center, University of Basel, Gewerbestrasse 14, 4123 Allschwil, Switzerland

Introduction

Polydimethylsiloxane (PDMS) elastomers are inexpensive, flexible, biocompatible, optically transparent materials and their manifold fabrication techniques, such as spin coating, electrospraying, molecular beam deposition, 3D printing and molding, have led to a numerous applications (1–6). They are widely used in soft robotics, flexible electronics, microfluidic devices, medical implants, cell culture substrate and dielectric elastomer actuators, as shown in Figure 1 (3, 7–14). Its native hydrophobic surface exhibits a water contact angle of $120° \pm 4°$ and is mainly determined by the CH_3 groups. It can easily become hydrophilic by the introduction of silanol functional groups on the PDMS surface via oxygen-plasma or ultraviolet/ozone treatments (15–18). The hydrophilicity decays with time, if stored in air, due to the migration of the smaller polymer chains from the bulk to the surface, reorientation of the polar groups and condensation of hydroxyl groups (18). The oxygen-plasma treatment forms a silica-like surface layer and its thickness increases with treatment duration and RF plasma power (19). The oxygen plasma does not only change the wettability but also alters the surface topography (20). Wavy patterns arise due to the mismatch of the thermal expansion coefficient of the formed silica-like layer and the bulk PDMS. The heating originates from the plasma itself and causes the PDMS layer to expand. Upon cooling, the bulk PDMS shrinks much more than the stiff silica-like film and exerts a compressive stress on the stiff film on top.

This stress is released by forming a wrinkling pattern on the elastomeric substrate. For thermally cross-linked PDMS films, the wrinkles can be tailored in amplitude and periodicity (21–23). It has been shown that nanostructures of plasma-treated submicrometer-thin liquid films of dissolved PDMS prepolymers with a molecular weight of 139,000 g/mol can vary with the thickness of

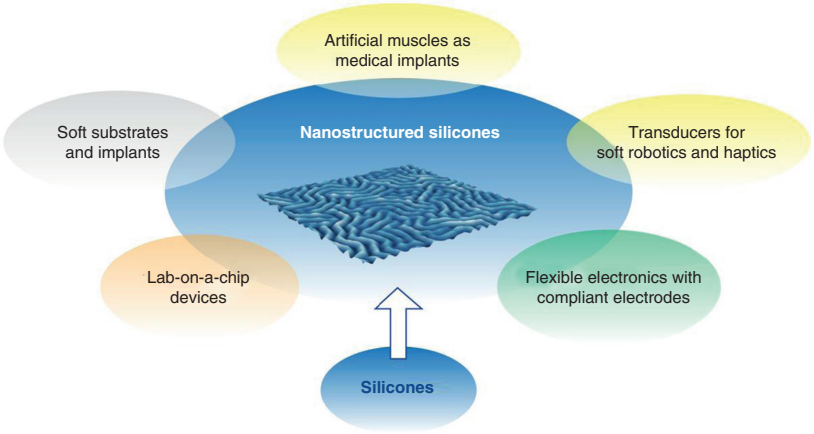

Figure 1: Applications of silicone (PDMS) elastomers: their biocompatibility, ease of use and manifold fabrication techniques have led to developments for flexible electronics, lab-on-a-chip devices, soft substrates and implants and artificial muscles as medical implants or transducers for soft robotics and haptics.

the film (24). In addition, many communications report on the estimated elastic modulus for the silica-like surface layer, which was found to be between 4 MPa and 1.5 GPa (15, 19).

The interface between man-made material and the human body is critical for the functionality of a medical implant. In general, the body recognizes the implant as foreign body resulting in encapsulation. Several researchers have demonstrated, however, that nanostructures similar to the hydroxyapatite crystallites promote protein adsorption and can reduce the inflammatory reactions (25–29). Nanostructures on plasma-treated polymer polyetheretherketone can even support osteogenic differentiation of human mesenchymal stem cells in vitro (30, 31). Another key parameter that affects cell behavior is the substrate elasticity (32). Consequently, the present study on tailoring the surface morphology and elasticity tuning the plasma treatment is an essential step to realize next-generation silicone implants.

Here, we show that using a vinyl-terminated PDMS prepolymer with a molecular weight of 800 g/mol, we can bypass the need of a solvent or a cross-linking agent to fabricate PDMS films in the nanometer range. The amplitude and the periodicity of the wrinkles were tuned decreasing the film thickness, adapting the treatment duration and the oxygen pressure. Finally, we have extracted the mechanical properties of a plasma-treated PDMS film with a submicrometer resolution and showed that the average elastic modulus can be set to a few MPa, as required for low-voltage dielectric elastomer actuators as proposed for artificial muscles (33).

Materials and methods

Preparation of PDMS films

Vinyl-terminated PDMS (V05, Gelest, Inc., Morrisville, PA, USA) with a number average molecular weight of 800 g/mol and a kinematic viscosity of 6 ± 2 cSt was spun (WS-400B-6NPP/LITE/AS, Laurell Technologies Corporation, North Wales, PA, USA) onto 2-inch silicon wafers as supplied (SIEGERT WAFER GmbH, Germany). The thickness of the PDMS films was determined by scanning an edge using atomic force microscopy (AFM) in tapping mode as shown in Figure 2.

The PDMS films were prepared by pre-selected rotational speeds and spin durations to realize a variety of film thicknesses. The film thickness of 590 ± 120 nm was found at a speed of 3000 rpm applied for 2 min. Increasing the speed to 6000 rpm and applying the same duration, we have found a thickness of 350 ± 50 nm. The thickness was reduced to 150 ± 20 nm using a speed of 7000 rpm for 4 min.

Oxygen-plasma treatment of PDMS films

The specimens were oxygen-plasma treated using a power of 200 W for durations of 18, 36, 72 and 144 s and a frequency of 40 kHz (PICO System, Diener Electronics, Ebhausen, Germany). The oxygen partial pressure (Carbagas, Gümligen, Switzerland) was controlled varying the oxygen flow rate from 15 to 40 sccm. The application of an oxygen-plasma treatment alters the surface topography as schematically shown in Figure 3.

Dynamic contact angle measurements

The specimens were aged for a period of 180 days prior to contact angle measurements to study the hydrophobic recovery of the nanometer-thin films. They were placed on a tiltable stage of a contact angle goniometry device (OCA 15 EC, Version 2.1, DataPhysics

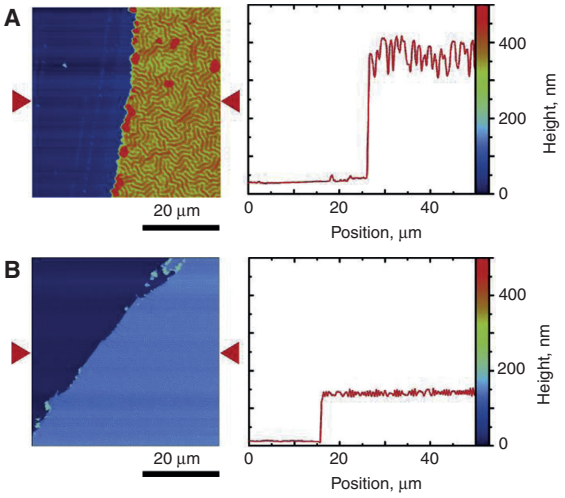

Figure 2: Determination of the PDMS film thickness: (A) AFM scan of a spin-coated and oxygen-plasma treated PDMS at a rotation speed of 6000 rpm for a duration of 2 min.
The profile cut according to the triangle directions on the left image shows that the wrinkling is present only on top of the film and does not affect the underlying bulk PDMS layer. (B) AFM scan and profile cut of a plasma-treated and spin-coated PDMS at a rotation speed of 7000 rpm for a duration of 4 min.

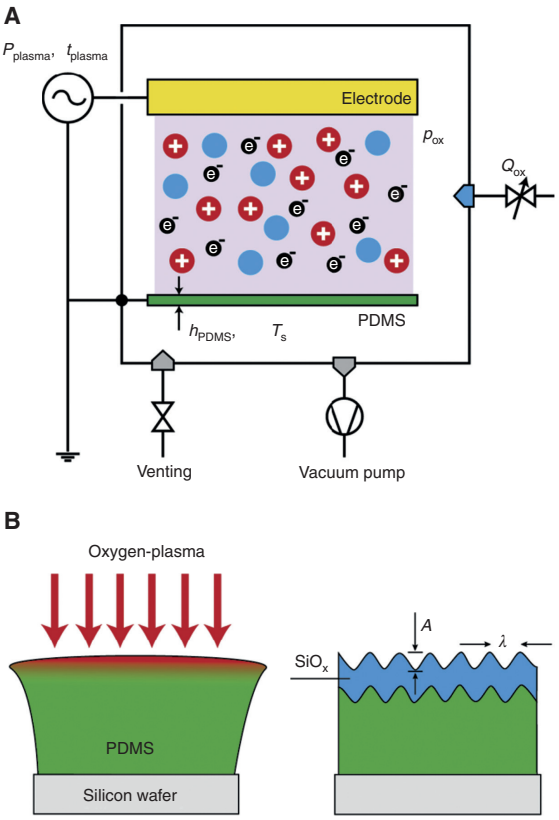

Figure 3: Formation of anisotropic and wrinkled PDMS films through oxygen plasma.
(A) Schematic of a plasma chamber showing the main parameters: power P_{plasma}, treatment duration t_{plasma}, oxygen pressure p_{ox}, PDMS film thickness h_{PDMS} and substrate temperature T_s. (B) Schematic of oxygen-plasma-treated PDMS film with the amplitude A and the wavelength/periodicity λ.

Instr. GmbH, Germany) supplied with LED illumination and a USB camera for video recording. Deionized water of high purity was used as the probing liquid (Elga, Purelab UHQ II, UK). A droplet of 5 µL was dispensed with a glass syringe and taken up on the surface of the polymer by raising the sample stage upwards. Care was taken not to touch the needle tip with the stage.

For dynamic contact angle measurements, the tilting base unit TBU 90E (DataPhysics Instr. GmbH) was set up to perform a tilt angle of the platform from $\alpha = 0°$ to $\alpha = 95°$. The relative velocity of the rotation was set to 4.5° per second with a grabbing rate of 20 frames per second. Video-based optical evaluation of the tilting was used to obtain the advancing contact angle θ_a and the receding contact angle θ_r, represented in the diagrams of Figure 4. Therefore, the hysteresis $\Delta\theta = \theta_a - \theta_r$ for rolling drops, describing the difference between the advancing and receding contact angles, is calculated for $\alpha = 90°$.

The SCA 20 software (DataPhysics Instr. GmbH) was used to record and analyze all contact angle measurements. The static contact angle was recorded prior to the dynamic measurements. The apparent contact angle θ between the sessile drop and the surface of the polymer was measured by imaging the water droplet from a side view and applying a software contouring technique to calculate the angle. Droplets were visually assessed from a top view for axisymmetry before measurement.

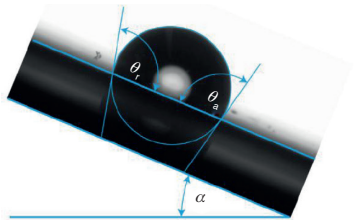

Figure 4: Schematic representation of the dynamic contact angle measurement setup, where the advancing contact angle θ_a and the receding contact angle θ_r are acquired for tilting angles α between 0° and 95°.

Determination of the elastic modulus *E*

The elastic modulus of the oxygen-plasma treated PDMS films was assessed by AFM nanoindentation (NI) techniques (FlexAFM C3000, Nanosurf AG, Switzerland). For this purpose, 10,000 NIs were applied on 50 µm × 50 µm spots using a spherical tip with a radius of 522±2 nm (B500_FMR, Nanotools GmbH, Germany). The nominal spring constant of the AFM cantilever was found to be 1.9±0.1 N/m as determined by the Sader method (34). During a single NI measurement, the sample was moved toward the AFM tip until the previously defined force of $F = 200$ nN was achieved. The additional information of the z-piezo allowed to extract the indentation depth and calculate the mean elastic

modulus E using the Hertz contact model, which is implemented in the FLEX-ANA® software (Automated Nanomechanical Analysis, Nanosurf AG, Switzerland). Potential substrate effects were neglected since the indentation depths were less than 20% of the total film thickness.

AFM imaging

AFM images were acquired by raster-scanning a soft AFM-probe with a radius smaller than 10 nm (Tap190Al-G probe, NanoAndMore GmbH, Wetzlar, Germany) in tapping mode (vibration amplitude 2.0 V, set point 60%) using a FlexAFM System (Nanosurf AG, Liestal, Switzerland). A total of 512 lines at a speed of 1 s per line were acquired for each image. The raw data were leveled by subtracting a mean plane and removing a polynomial background of the first degree. Root-mean-square (RMS) roughness values were calculated by the open source software Gwyddion, Version 2.41.

Results

AFM scans and dynamic contact angle measurements of the oxygen-plasma treated PDMS films ($P_{plasma}=200$ W, $t_{plasma}=60$ s, $p_{ox}=45$ Pa, $T_s=25°C$) are shown in Figure 5. The amplitude A, as extracted out the height distribution diagram and the periodicity/wavelength λ of the wrinkles are summarized in Table 1. The periodicity λ is calculated using 2D fast Fourier transform (2D FFT) of the related AFM image. The periodicity λ and the amplitude A decrease with film thickness.

We show in Figure 6 dynamic contact angle measurements and AFM images of surfaces of 350 ± 50 nm PDMS films, which were oxygen-plasma treated ($P_{plasma}=200$ W, $t_{plasma}=60$ s, $T_s=25°C$) at oxygen pressures from $p_{ox}=18$ to $p_{ox}=45$ Pa. The amplitude A, as extracted out the height distribution diagram and the periodicity/wavelength λ of the wrinkles are summarized in Table 2. It is found that the periodicity λ and the amplitude A increase at lower oxygen pressures p_{ox}.

PDMS films with a thickness of 350 ± 50 nm were oxygen-plasma treated ($P_{plasma}=200$ W, $p_{ox}=45$ Pa, $T_s=25°C$) by varying the treatment duration from 18 to 144 s are shown in Figure 7. The amplitude A, as extracted out the height

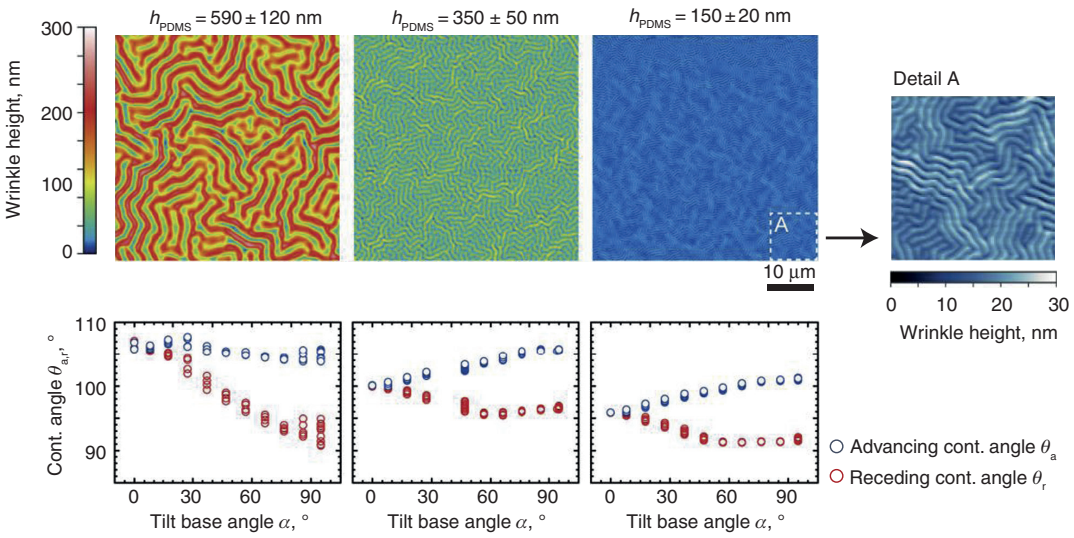

Figure 5: AFM scans and dynamic contact angle measurements of PDMS films with varying film thicknesses h_{PDMS}.
The amplitude A and periodicity λ of the wrinkles show a positive correlation with the film thickness. The contact angle θ decreased with decrement in film thickness from $107°\pm1°$ to $96°\pm1°$ and the hysteresis $\Delta\theta$ shows a tendency towards smaller values.

Table 1: Contact angle, periodicity and amplitude of plasma-treated PDMS films ($P_{plasma}=200$ W, $t_{plasma}=60$ s, $p_{ox}=45$ Pa, $T_s=25°C$) for selected film thicknesses.

Film thickness h_{PDMS}, nm	Contact angle θ, deg	Hysteresis $\Delta\theta$ at $\alpha=90°$, deg	Periodicity of the wrinkles λ, nm	Amplitude A, nm	Ratio amplitude to film thickness A/h_{PDMS}
590 ± 120	107 ± 1	11 ± 1	2800 ± 200	≈200	≈1/3
350 ± 50	99 ± 1	10 ± 1	1100 ± 100	≈90	≈1/4
150 ± 20	96 ± 1	9 ± 1	500 ± 100	≈30	≈1/5

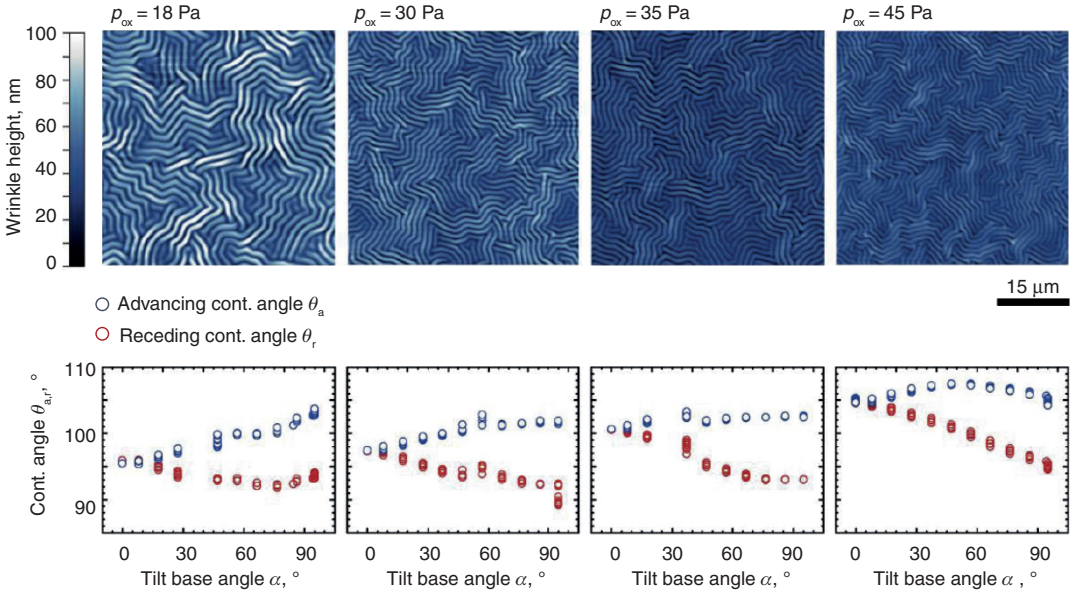

Figure 6: AFM images and dynamic contact angle measurements of 350 ± 50 nm PDMS films at oxygen pressures p_{ox} indicated. The amplitude A and periodicity λ of the wrinkles reversely relate with the oxygen pressure p_{ox}. The initial contact angle θ increased slightly with increment in oxygen pressure p_{ox} from 96° ± 1° to 105° ± 1° and the hysteresis $\Delta\theta$ at $\alpha = 90°$ remained constant at 10° ± 1°.

distribution diagram, and the periodicity/wavelength λ of the wrinkles are listed in Table 3. The periodicity λ was calculated using 2D fast Fourier transform (2D FFT) of the related AFM images and are found to remain constant at 1100 ± 100 nm for the selected conditions.

A PDMS film with a thickness of 590 ± 120 nm was plasma-treated at an RF power $P_{plasma} = 200$ W for a total duration of $t_{plasma} = 60$ s. The mechanical mapping with submicrometer resolution, shown in Figure 8, reveals topology-dependent elastic properties. It exhibits elastic moduli of 1.8 ± 0.6 and 3.9 ± 1.7 MPa, which are in the range of interest for dielectric elastomer actuators. Substrate effects can be neglected because the PDMS film was 590 ± 120 nm thick, which is large compared to the NI depth of 150 ± 50 nm. We can also exclude geometrical artifacts because the spherical tip has a radius of 522 ± 2 nm, which is small with respect to the periodicity of the wrinkles corresponding to 2800 ± 200 nm. In addition, the map reveals that the material on the hills is significantly stiffer with respect to the one located in the valleys.

Discussion and conclusions

Our results show that using a vinyl-terminated PDMS prepolymer with a number average molecular weight of 800 g/mol, one can easily bypass the use of any solvent or curing agent to fabricate nanostructured PDMS elastomer films as thin as hundreds of nanometer.

As plasma treatments do not only change the surface morphology but also influence the chemistry and the related mechanics of the surface layers, the cross-linking

Table 2: Changing the oxygen pressure p_{ox} and keeping all the other parameters constant for plasma-treated 350 ± 50 nm PDMS films [$P_{plasma} = 200$ W, $t_{plasma} = 60$ s, $h_{PDMS} = 350 \pm 50$ nm, $T_s = 25$°C].

Oxygen pressure p_{ox}, Pa	Contact angle θ, deg	Hysteresis $\Delta\theta$ at $\alpha = 90°$, deg	Periodicity of the wrinkles λ, nm	Amplitude A, nm
18	96 ± 1	10 ± 1	1800 ± 200	≈80
30	98 ± 1	10 ± 1	1400 ± 150	≈70
35	96 ± 1	10 ± 1	1300 ± 150	≈30
45	105 ± 1	10 ± 1	1100 ± 100	≈25

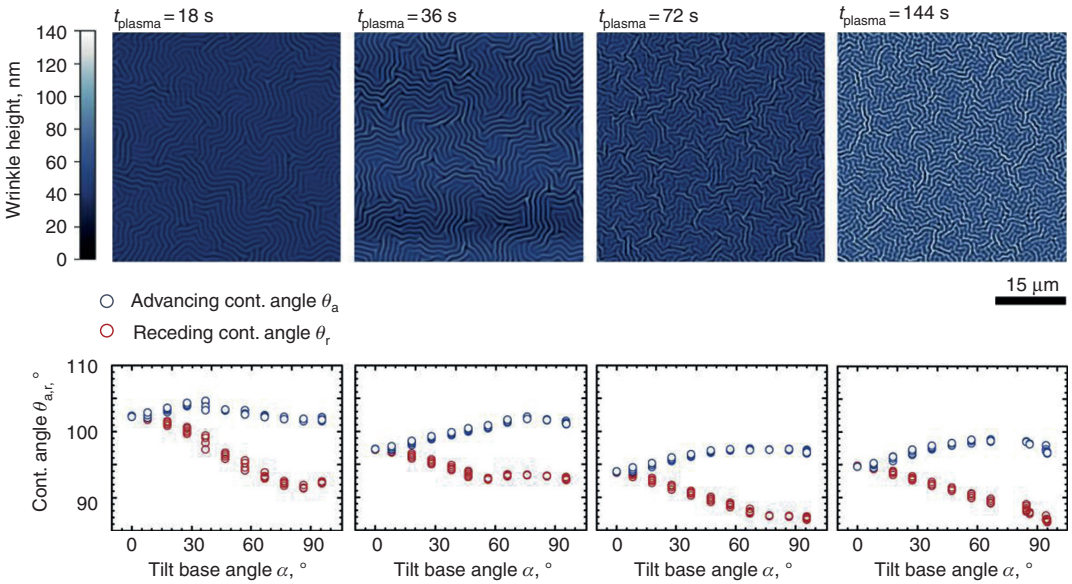

Figure 7: AFM scans and dynamic contact angle measurements of 350 ± 50 nm PDMS films, plasma treated for different durations t_{plasma}. The amplitude A increased 10-fold up to 100 nm for t_{plasma} = 144 s, whereas the periodicity λ remained constant at 1100 ± 100 nm. The contact angle θ decreased from 102° ± 1° to 95° ± 1° and the hysteresis $\Delta\theta$ at α = 90° remained constant at 10° ± 1°.

Table 3: Increasing the treatment duration leads to larger amplitudes.

Treatment duration t_{plasma}, s	Contact angle θ, deg	Hysteresis $\Delta\theta$ at α = 90°, deg	Periodicity of the wrinkles λ, nm	Amplitude A, nm
18	102 ± 1	10 ± 1	1100 ± 100	≈10
36	97 ± 1	9 ± 1	1100 ± 100	≈40
72	94 ± 1	10 ± 1	1100 ± 100	≈60
144	95 ± 1	10 ± 1	1100 ± 100	≈100

All other parameters were kept constant for the plasma-treated PDMS films [P_{plasma} = 200 W, p_{ox} = 45 Pa, h_{PDMS} = 350 ± 50 nm, T_s = 25°C].

mechanism via reactive species generated through photoionization and ion bombardments have to be considered. As previously shown, the irradiation of PDMS with light at wavelengths of approximately 170 nm leads to scissions of the Si-CH_3 and Si-CH_2-H bonds. The resulting unsaturated bonds give rise to a three-dimensional elastomer network (33, 35). It should be noted that we observed a strong adherence of the PDMS films to the Si wafer. It cannot be removed simply by wiping or by washing out in ethyl acetate. This effect could be associated with the comparably low wrinkle periodicity of the thinner films because the plasma treatment also affects layers well below the surface.

The wrinkling phenomena of a simple bilayer system are understood (36). It has been shown that a compressed film on a much less stiff elastomer undergoes wrinkling to relieve the intrinsic compressive stress. The orientation of the wrinkles is generally random. Buckling models can precisely predict the periodicity of these randomly oriented wrinkles λ (21):

$$\lambda = 2\pi h_f \left(\frac{(1-\nu_f^2)E_f}{3(1-\nu_s^2)E_s} \right)^{1/3}, \quad (1)$$

where h_f corresponds to the thickness of the stiffer film, $E_{s,f}$ and $\nu_{s,f}$ are the elastic moduli and the Poisson's ratios of the two components, respectively. This two-layer model, however, does only partially account for the plasma-treated PDMS. The plasma treatment does not only produce a nanometer-thin film of increasing thickness but probably also changes the elastic properties of the underlying elastomer. Assuming that unchanged plasma treatment conditions result in alike parameters

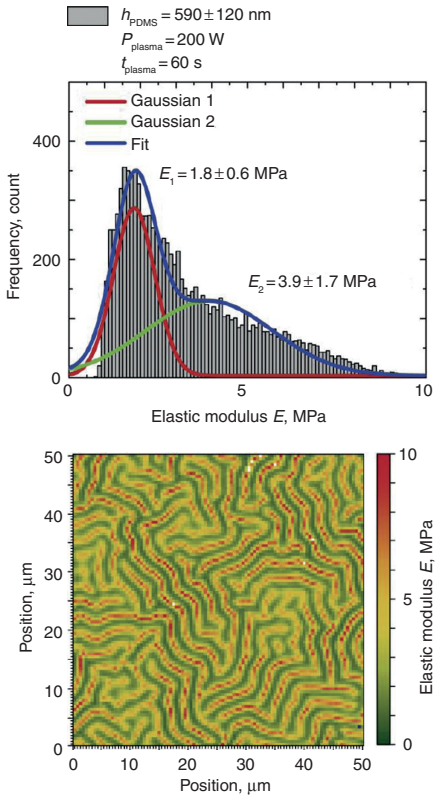

Figure 8: Stiffness histogram and map out of 10,000 NIs on a 50×50 µm² spot.
The submicrometer mechanical mapping of the spot reveals softer valleys with an elastic modulus of $E_1 = 1.8 \pm 0.6$ MPa compared to hills showing an elastic modulus of $E_2 = 3.9 \pm 1.7$ MPa. Substrate effects can be neglected since the NIs depth were below 200 nm.

h_f and E_f and the thinner films are more intensely plasma-treated resulting in an increased E_s, according to Equation (1), the ratio E_f/E_s becomes smaller, giving rise to a shorter periodicity. We have observed such a behavior, as listed in Table 1 and represented in Figure 5. The periodicity λ decreases with the decrement in film thickness. The amplitude A of the wrinkling pattern is proportional to the square root of the buckling strain ε (36). Neglecting the impact of the Poisson coefficients, one finds

$$\varepsilon = \left(\frac{9E_s^2}{64E_f^2} \right)^{1/3}. \quad (2)$$

As the treatment duration t_{plasma} could influence the bulk elastic modulus E_s, the model correlates well with our findings. For $t_{plasma} = 144$ s, we have demonstrated a 10-fold amplitude increase. According to Equation (1), one should observe a periodicity decrease. Instead, the experiments show a constant value. Here, we speculate that the thickness h_f is increasing with treatment duration. Reducing the oxygen pressure p_{ox}, as given by the data in Table 2 and Figure 6, one can reasonably assume that E_s increases. Therefore, both the amplitude A and the periodicity λ are similarly influenced, as described by means of Equations (1) and (2).

The mechanical properties of a plasma-treated PDMS film locally measured with submicrometer precision reveals that the elastic modulus of the material in valleys differs from that on hills. The difference by a factor of two is surprisingly high. So far, one can only speculate on the reasons. We know the cross-sectional profiles of wrinkle's networks. Geometrical phenomena related to the sinusoidal microstructure could be a reason but probably do not explain such a large effect. We further know that the wrinkle formation is associated with significant material transport (37). Therefore, one can reasonably assume a thickness modulation of the silicate layer according to the wrinkle structure.

The wetting of the aged, nanostructured PDMS films, as studied by contact angle goniometry, was improved for the ones with smaller amplitude and wrinkle periodicity.

Smaller contact angles are also found on samples treated at lower oxygen pressures. This could be due to the higher SiO_x concentration on the surface exposed to increased number of ion bombardments at lower oxygen pressures p_{ox}. The hysteresis $\Delta\theta$ at $\alpha = 90°$ is found to be constant for all samples showing a value of $10° \pm 1°$. All samples were stored under ambient conditions for a period of 180 days. The contact angle of water on a surface plasma-treated with $P_{plasma} = 200$ W, $t_{plasma} = 18$ s, $T_s = 20$°C and $p_{ox} = 45$ Pa corresponded $49° \pm 1°$ several hours after fabrication and increased to $77° \pm 1°$ and $85° \pm 1°$ after 2 and 3 weeks, respectively. It is worth mentioning that plasma-polymerized PDMS films recover similarly to plasma-treated cross-linked PDMS films. Further investigations are required to analyze the prospects and challenges of these wrinkled elastomer films to serve as a support for stretchable electrodes and their integration in the field of artificial muscles and medical implants.

Acknowledgments: The financial support of the nanotera.ch initiative (grant/award no. "SmartSphincter RTD2013"), project SmartSphincter, as well as the Swiss Nanoscience Institute (SNI) for the financial contribution to the AFM is gratefully acknowledged. The authors also

thank Dr. Thomas Pfohl and Dr. Tino Töpper for the discussion of the results presented.

Conflict of interest statement: Authors state no conflict of interest. All authors have read the journal's publication ethics and publication malpractice statement available at the journal's website and hereby confirm that they comply with all its parts applicable to the present scientific work.

References

1. Poulin A, Rosset S, Shea HR. Printing low-voltage dielectric elastomer actuators. Appl Phys Lett 2015;107:244104.
2. Hinton TJ, Hudson A, Pusch K, Lee A, Feinberg AW. 3D printing PDMS elastomer in a hydrophilic support bath via freeform reversible embedding. ACS Biomater Sci Eng 2016;2:1781–6.
3. Rosset S, Shea HR. Small, fast, and tough: Shrinking down integrated elastomer transducers. Appl Phys Rev 2016;3:031105.
4. Weiss FM, Madsen FB, Töpper T, Osmani B, Leung V, Müller B. Molecular beam deposition of high-permittivity polydimethylsiloxane for nanometer-thin elastomer films in dielectric actuators. Mater Des 2016;105:106–13.
5. Weiss FM, Töpper T, Osmani B, Deyhle H, Kovacs G, Müller B. Thin film formation and morphology of electrosprayed polydimethylsiloxane. Langmuir 2016;32:3276–83.
6. Weiss FM, Töpper T, Osmani B, Peters S, Kovacs G, Müller B. Electrospraying nanometer-thin elastomer films for low-voltage dielectric actuators. Adv Electron Mater 2016;2:1500476.
7. Sia SK, Whitesides GM. Microfluidic devices fabricated in poly(dimethylsiloxane) for biological studies. Electrophoresis 2003;24:3563–76.
8. Lee JN, Jiang X, Ryan D, Whitesides GM. Compatibility of mammalian cells on surfaces of poly(dimethylsiloxane). Langmuir 2004;20:11684–91.
9. O'Halloran A, O'Malley F, McHugh P. A review on dielectric elastomer actuators, technology, applications, and challenges. J Appl Phys 2008;104:071101.
10. Brochu P, Pei Q. Advances in dielectric elastomers for actuators and artificial muscles. Macromol Rapid Commun 2010;31:10–36.
11. Shepherd RF, Ilievski F, Choi W, Morin SA, Stokes AA, Mazzeo AD, et al. Multigait soft robot. Proc Natl Acad Sci USA 2011;108:20400–3.
12. Anderson IA, Gisby TA, McKay TG, O'Brien BM, Calius EP. Multifunctional dielectric elastomer artificial muscles for soft and smart machines. J Appl Phys 2012;112:041101.
13. Osmani B, Töpper T, Deschenaux C, Nohava J, Weiss FM, Leung V, et al. Micro- and nanostructured electro-active polymer actuators as smart muscles for incontinence treatment. AIP Conf Proc 2015;1646:91–100.
14. Fattorini E, Brusa T, Gingert C, Hieber S, Leung V, Osmani B, et al. Artificial muscle devices: innovations and prospects for fecal incontinence treatment. Ann Biomed Eng 2016;44:1–15.
15. Hillborg H, Ankner JF, Gedde UW, Smith GD, Yasuda HK, Wikström K. Crosslinked polydimethylsiloxane exposed to oxygen plasma studied by neutron reflectometry and other surface specific techniques. Polymer 2000;41:6851–63.
16. Efimenko K, Wallace WE, Genzer J. Surface modification of sylgard-184 poly(dimethyl siloxane) networks by ultraviolet and ultraviolet/ozone treatment. J Colloid Interface Sci 2002;254:306–15.
17. Lawton A, Price CR, Runge AF, Doherty WJ, Saavedra SS. Air plasma treatment of submicron thick PDMS polymer films: effect of oxidation time and storage conditions. Colloids Surf A 2005;253:213–5.
18. Bodas D, Khan-Malek C. Hydrophilization and hydrophobic recovery of PDMS by oxygen plasma and chemical treatment – an SEM investigation. Sens Actuators B 2007;123:368–73.
19. Béfahy S, Lipnik P, Pardoen T, Nascimento C, Patris B, Bertrand P, et al. Thickness and elastic modulus of plasma treated PDMS silica-like surface layer. Langmuir 2010;26:3372–5.
20. Bowden N, Brittain S, Evans AG, Hutchinson JW, Whitesides GM. Spontaneous formation of ordered structures in thin films of metals supported on an elastomeric polymer. Nature 1998;393:146–9.
21. Bowden N, Huck WT, Paul KE, Whitesides GM. The controlled formation of ordered, sinusoidal structures by plasma oxidation of an elastomeric polymer. Appl Phys Lett 1999;75:2557–9.
22. Chua DB, Ng HT, Li SF. Spontaneous formation of complex and ordered structures on oxygen-plasma-treated elastomeric polydimethylsiloxane. Appl Phys Lett 2000;76:721–3.
23. Tserepi A, Gogolides E, Tsougeni K, Constantoudis V, Valamontes ES. Tailoring the surface topography and wetting properties of oxygen-plasma treated polydimethylsiloxane. J Appl Phys 2005;98:113502.
24. Evensen HT, Jiang H, Gotrik KW, Denes F, Carpick RW. Transformations in wrinkle patterns: cooperation between nanoscale cross-linked surface layers and the submicrometer bulk in wafer-spun, plasma-treated polydimethylsiloxane. Nano Lett 2009;9:2884–90.
25. Müller B. Natural formation of nanostructures: from fundamentals in metal heteroepitaxy to applications in optics and biomaterials science. Surf Rev Lett 2001;08:169–228.
26. Müller B, Riedel M, Michel R, De Paul SM, Hofer R, Heger D, et al. Impact of nanometer-scale roughness on contact-angle hysteresis and globulin adsorption. J Vac Sci Technol B 2001;19:1715–20.
27. Riedel M, Müller B, Wintermantel E. Protein adsorption and monocyte activation on germanium nanopyramids. Biomaterials 2001;22:2307–16.
28. Dalby MJ, Gadegaard N, Tare R, Andar A, Riehle MO, Herzyk P, et al. The control of human mesenchymal cell differentiation using nanoscale symmetry and disorder. Nat Mater 2007;6:997–1003.
29. Kolind K, Leong KW, Besenbacher F, Foss M. Guidance of stem cell fate on 2D patterned surfaces. Biomaterials 2012;33:6626–33.
30. Waser-Althaus J, Padeste C, Köser J, Pieles U, Peters K, Müller B. Nanostructuring polyetheretherketone for medical implants. Eur J Nanomed 2012;4:7–15.
31. Waser-Althaus J, Salamon A, Waser M, Padeste C, Kreutzer M, Pieles U, et al. Differentiation of human mesenchymal stem cells on plasma-treated polyetheretherketone. J Mater Sci Mater Med 2014;25:515–25.
32. Engler AJ, Sen S, Sweeney HL, Discher DE. Matrix elasticity directs stem cell lineage specification. Cell 2006;126:677–89.
33. Töpper T, Weiss FM, Osmani B, Bippes C, Leung V, Müller B. Siloxane-based thin films for biomimetic low-voltage dielectric actuators. Sens Actuators A 2015;233:32–41.

34. John ES, James WM, Paul M. Calibration of rectangular atomic force microscope cantilevers. Rev Sci Instrum 1999;70:3967–9.
35. Vasilets VN, Kovalchuk AV, Ponomarev AN. Photooxidation of siloxane polymers under vacuum ultraviolet irradiation. J Photopolym Sci Technol 1994;7:165–74.
36. Schweikart A, Fery A. Controlled wrinkling as a novel method for the fabrication of patterned surfaces. Microchim Acta 2009;165:249–63.
37. Müller B, Deyhle H, Mushkolaj S, Wieland M. The challenges in artificial muscle research to treat incontinence. Swiss Med. Wkly 2009;139:591–5.

Bionotes

Bekim Osmani
Department of Biomedical Engineering, Biomaterials Science Center, University of Basel, Gewerbestrasse 14, 4123 Allschwil, Switzerland
bekim.osmani@unibas.ch

Bekim Osmani is a PhD student at the Biomaterials Science Center at the University of Basel. He did his BSc in Mechanical Engineering and his MSc in Biomedical Engineering and Robotics at the Swiss Federal Institute of Technology in Zurich (ETHZ) in 2002. After several years of experience in academia and industry, he is currently working toward his PhD degree in nanosciences. His research interests include molecular beam deposition and electrospraying of nanometer thin elastomer films, atomic force microscopy, nanoindentation techniques and mechanical properties of nanometer thin film, polymeric implants and biomedical applications for low-voltage dielectric elastomer actuators.

Gabriela Gerganova
Department of Biomedical Engineering, Biomaterials Science Center, University of Basel, Gewerbestrasse 14, 4123 Allschwil, Switzerland

Gabriela Gerganova, 22 years old, is an integrated master's student of pharmacology at University of Glasgow. She performs her placement year at the Biomaterials Science Centre under the direction of Prof. Bert Müller. Her research focus is on the formulation, characterization and safety of liposome-based nanocontainers for targeted drug delivery. During her internship, she has expanded her practical skills in biomedical engineering with the help of on-site laboratory facilities.

Bert Müller
Department of Biomedical Engineering, Biomaterials Science Center, University of Basel, Gewerbestrasse 14, 4123 Allschwil, Switzerland

Bert Müller received a diploma in mechanical engineering, Berlin 1982, followed by MSc degrees in Physics and English both from the Dresden University of Technology in 1989. In 1994, he obtained a PhD in experimental physics from the University of Hannover, Germany. For his achievements, he was granted with the Morton M. Traum Award of the American Vacuum Society in 1994. From 1994 to 2001, he worked as a researcher at the Paderborn University, Germany, as Feodor Lynen Fellow and research associate at the EPF Lausanne, Switzerland and as team leader at the Physics Department, Materials Department and Department of Information Technology and Electrical Engineering at ETH Zurich, Switzerland. He became a faculty member of the Physics Department at ETH Zurich in April 2001. After his election as Thomas Straumann-Chair for Materials Science in Medicine at the University of Basel, Switzerland and his appointment at the Surgery Department of the University Hospital Basel in September 2006, he founded the Biomaterials Science Center in March 2007. Currently, this center hosts more than 20 researchers dealing with nanotechnology-based artificial muscles for incontinence treatment, smart nanocontainers to treat cardiovascular diseases, high-resolution X-ray imaging to visualize the human body down to the molecular level, computational sciences of tissues in health and disease and other applications of nanosciences in medicine. The mission of the research team can be summarized by using physical principles for human health. Professor Müller teaches physics and materials science at the ETH Zurich and the University of Basel and currently supervises doctoral students from medicine, dentistry, physics, nanosciences and biomedical engineering. He was elected as Fellow of SPIE in 2014 and as an active member of the European Academy of Sciences and Arts in 2015.

2.7 Electrospraying and ultraviolet light curing of nanometer-thin polydimethylsiloxane membranes for low-voltage dielectric elastomer transducers

Compared to previous studies, stable single-cone jet electro-spraying enabled the fabrication of elastomer membranes in less than one minute.

Confluent SH-functionalized PDMS films were obtained at thicknesses > 220 nm using 1 vol % solutions. Smooth elastomer films were observed at thicknesses of about 1 µm.

UV-polymerization of SH-PDMS without photo-initiators enables the fabrication of homogeneously cross-linked PDMS membranes.

Elastic modulus increases with the UV-irradiation time and could be set to values between 165 and 1'300 kPa.

Peel-off tests demonstrate that adhesive layers between the electrode and elastomer are not required. Au nanoclusters form covalent bonds to the SH-groups of the elastomer network.

Published in Proceedings of SPIE

PROCEEDINGS OF SPIE

SPIEDigitalLibrary.org/conference-proceedings-of-spie

Electrospraying and ultraviolet light curing of nanometer-thin polydimethylsiloxane membranes for low-voltage dielectric elastomer

Bekim Osmani
Tino Töpper
Matej Siketanc
Gabor M. Kovacs
Bert Müller

SPIE.

Electrospraying and ultraviolet light curing of nanometer-thin polydimethylsiloxane membranes for low-voltage dielectric elastomer transducers

Bekim Osmani*[a], Tino Töpper[a], Matej Siketanc[a], Gabor Kovacs[b], and Bert Müller[a]
[a]Biomaterials Science Center, Department of Biomedical Engineering, University of Basel, 4123 Allschwil, Switzerland; [b]Swiss Federal Laboratories for Materials Science and Technology, Überlandstrasse 129, 8600 Dübendorf, Switzerland.

ABSTRACT

Dielectric elastomer transducers (DETs) have attracted interest as actuators, sensors, and even as self-sensing actuators for applications in medicine, soft robotics, and microfluidics. To reach strains of more than 10 %, they currently require operating voltages of several hundred volts. In medical applications for artificial muscles, however, their operation is limited to a very few tens of volts, which implies high permittivity materials and thin-film structures. Such micro- or nanostructures can be prepared using electro-spraying, a cost-effective technique that allows upscaling using multiple nozzles for the fabrication of silicone films down to nanometer thickness. Deposition rates of several micrometers per hour have already been reached. It has been recently demonstrated that such membranes can be fabricated by electro-spraying and subsequent ultraviolet light irradiation. Herein, we introduce a relatively fast deposition of a dimethyl silicone copolymer fluid that contains mercaptopropyl side chains in addition to the methyl groups. Its elastic modulus was tuned with the irradiation dose of the 200 W Hg-Xe lamp. We also investigated the formation of elastomer films, using polymer concentrations in ethyl acetate of 1, 2, 5 and 10 vol%. After curing, the surface roughness was measured by means of atomic force microscopy. This instrument also enabled us to determine the average elastic modulus out of, for example, 400 nanoindentation measurements, using a spherical tip with a radius of 500 nm. The elastomer films were cured for a period of less than one minute, a speed that makes it feasible to combine electro-spraying and *in situ* curing in a single process step for fabricating low-voltage, multilayer DETs.

Keywords: dielectric elastomer actuators, electro-spraying, thiol-functionalized polymers, ultraviolet light curing, nanoindentation, nanometer-thin films, atomic force microscopy.

1. INTRODUCTION

Soft dielectric elastomer transducers (DETs) are used for a growing number of applications, including tunable optics, microfluidics, soft robotics, and haptic devices [1-5]. Their main drawback is still the driving voltage of several hundred volts. In medical applications such as artificial muscles, however, their operation is limited to a very few tens of volts. Many research groups report approaches on how to reduce the operating voltage, either by increasing the dielectric constant, using fillers such as TiO_2 or $BaTiO_3$, or by reducing the thickness of the elastomeric layer [6-9]. A recent work describes the combination of a curable liquid acrylic composition and multilayer fabrication method that allows actuation without pre-stretching, though the elastomer layers

Electroactive Polymer Actuators and Devices (EAPAD) 2017, edited by Yoseph Bar-Cohen, Proc. of SPIE
Vol. 10163, 101631E · © 2017 SPIE · CCC code: 0277-786X/17/$18 · doi: 10.1117/12.2258214

were more than 35 m thick and required several kilovolts for operation [10]. As the compressive strain s_z is inversely proportional to the square of the film thickness h_p [11]:

$$s_z = -\frac{\varepsilon_0 \varepsilon}{E}\left(\frac{U}{h_p}\right)^2, \quad (1)$$

with its relative permittivity ε, elastic modulus E, and operating voltage U, we target the fabrication of soft, micrometer-thin elastomer layers, which can be operated at a few tens of volts.

Thin polydimethylsiloxane (PDMS) films can be prepared by spin-coating, electro-spraying, or molecular beam deposition (MBD) techniques. Although the homogeneity of thermal evaporation of PDMS film is superior with respect to spin-coating or electro-spraying, its applicability for DETs is restricted. The evaporation of liquid PDMS pre-polymers is limited to oligomers at low deposition rates, due to the thermal degradation of the used polymer [12]. As shown recently, electro-spraying of vinyl-terminated PDMS with an average molecular weight of 6,000 g/mol leads initially to a partially coalescent drop-like film with an average thickness of about 150 nm [13]. The confluent layers shown here were covered only by 75 %. Even a subsequent deposition for 588 s resulted in 500 nm films and did not fully cover the substrate. In addition, long-lasting ultraviolet (UV) irradiation for around 15 minutes was necessary to cure the PDMS film at a distance as low as 2 cm. The crosslinking mechanism was based on the scissions of Si-CH_3 and –CH_2-H bonds using a deuterium broad-band UV lamp with its maximum intensity at a wavelength of 210 nm.

Another challenge for thin-film DETs is the low adhesion of the Au electrode to the PDMS membrane. It can be increased by the introduction of an adhesive layer of Cr or Ti, but this implementation increases the overall stiffness by orders of magnitude [14]. Another approach is based on oxygen plasma treatment and the functionalization of the PDMS surface using the molecular glue 3-mercaptopropyltrimethoxysilane (MPTMS) [15]. This bifunctional molecule interfaces the relatively stiff Au electrode and the relatively soft elastomer layer. Furthermore, its thiol or mercaptan head (-SH) can form covalent bonds to Au, whereas the three methoxy (-O-CH3) functional groups bind to silanized PDMS (-OH) surfaces, which are introduced via oxygen plasma or UV/ozone treatments [16].

Here, we show that by using an SH-functionalized PDMS with a low molecular weight of 3'600 g/mol, one can fabricate smooth dielectric films at one-micrometer in thickness. An adhesive layer between the electrode and the elastomer is not required, as the Au clusters form strong covalent bonds to the existing SH groups within the elastomer network. We also show than PDMS films can be cured in air, using a high-power Xe-Hg lamp, and tune the elastic modulus between 165 and 1'300 kPa in less than a minute, a speed that allows for combining electro-spraying and *in situ* UV curing in a single process step for fabricating low-voltage, multilayer DETs.

2. EXPERIMENTAL

2.1 Preparation of GP367 silicone films

The equipment for the fabrication of the PDMS films is shown in Figure 1. A dimethyl silicone copolymer fluid, containing mercaptopropyl (-SH) side groups with an average molecular weight of 3'600 g/mol (GP-367, Genesee Polymers Corporation, USA), was dissolved in ethyl acetate (laboratory reagent grade, Fisher Scientific, Loughborough, UK) to obtain 1 %, 2 %, 5 %, and 10 vol% spray solutions. A 3 mL glass syringe with a metallic Luer-lock (Eternal-Matic, Sanitex, HUBERLAB, Aesch, Switzerland) was used to introduce

the spray solutions into the electro-spray chamber through a custom-built PEEK flange and a stainless steel needle (25 ga, 20 mm, pst 3, Hamilton, Bonaduz, Switzerland) with an inner diameter of 260 m. The syringe pump (Aladdin AL1600-220Z, World Precision Instruments Germany GmbH, Berlin, Germany) was set to a constant flow rate of 10 l/min. A rectangular alternating voltage signal at a frequency of 1 Hz (Tektronix AFG3021C, Linktronix AG, Thalwil, Switzerland) was amplified to ±1.5 kV using a high-voltage power amplifier (TREK 10/40A, TREK INC., Lockport, NY, USA). The optimal gap between the nozzle and the 2-inch Si substrate (2P0/1-10/ 279 ± 25, Siegert Wafer, Aachen, Germany) was found to be 50 mm. Post UV curing was performed with a 200 W Hg-Xe UV lamp (super-quiet mercury-xenon lamp L2423, Hamamatsu Photonics K.K., Hamamatsu, Japan) at a distance of 50 cm.

The built-in lens and mirror adjustments allowed for broadening the beam and irradiating the entire 2-inch specimen in one shot. To improve the homogeneity of the UV-cured films, the samples were irradiated on a rotating stage at a speed of 60 rpm. All experiments were carried out in ambient conditions.

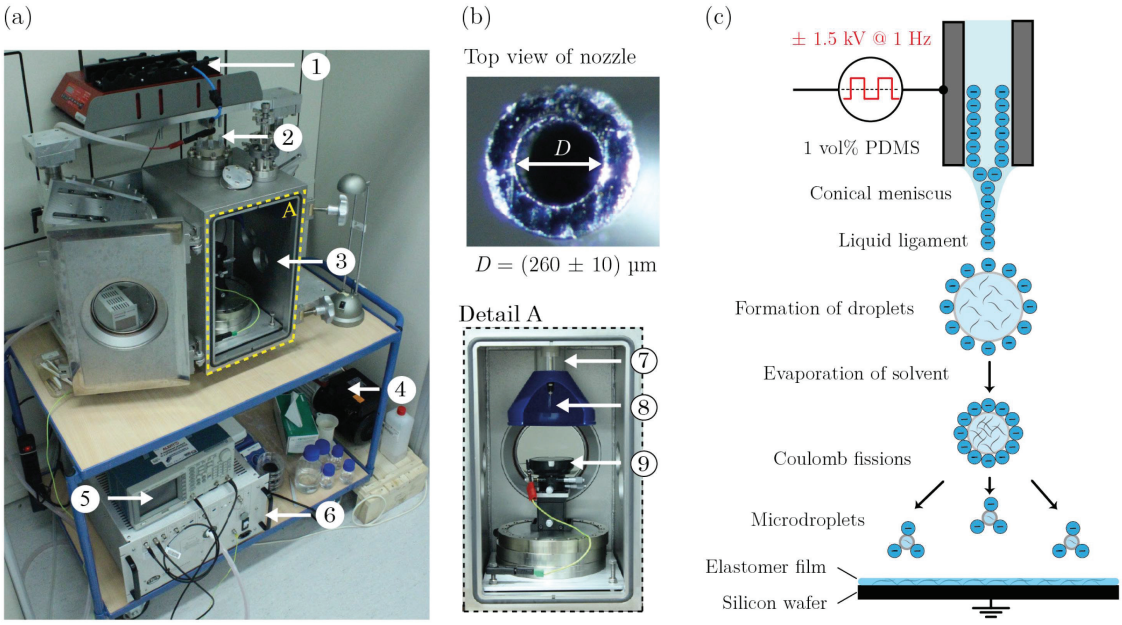

Figure 1. Electro-spraying of PDMS films. (**a**) Photograph of the experimental setup consisting of: (1) Syringe pump, (2) DN63 PEEK flange for the metallic nozzle feed-through, (3) Floatable vacuum chamber to guarantee well-defined conditions, (4) Rotary vane pump, (5) Function generator, (6) High-voltage power amplifier, (7) Plexiglas tube, (8) Stainless steel nozzle, and (9) Si wafer; (**b**) Optical micrograph of the used nozzle; (**c**) Scheme representing the formation of the conical meniscus and the droplet breakup into finer droplets. The repulsion forces caused the fine droplets to self-disperse.

2.2 Morphology of the PDMS films

Non-contact measurements on crosslinked GP-367 films were performed with a Keyence confocal 3D laser microscope (Keyence VK-X200, Keyence International, Belgium), using the supplier's VK Viewer acquisition

software. Scans were taking using a 20× objective at a pixel resolution of 690 nm in the two lateral directions and a pitch of 100 nm in the third direction.

2.3 Thickness measurements and surface scans using AFM

AFM scans in tapping mode were performed on manually induced scratches (Budget Sensors Tap190-G, Nano and More GmbH, Wetzler, Germany) to determine the film thickness. The vibration amplitude was set to 4 V, using a set point of 60 % on a FlexAFM system (Nanosurf AG, Liestal, Switzerland). For the mean surface roughness on 2 × 2 m^2 spots, the vibration amplitude was set to 900 mV and the set point to 90 %.

2.4 Nano-indentations on PDMS films

AFM nanoindentations (FlexAFM C3000, Nanosurf AG, Switzerland) were applied on 10 × 10 m^2 spots using an AFM cantilever with a spherical tip ($R = (490 \pm 5)$ nm, B500 FMR, Nanotools GmbH, Germany), as shown in Figure 2. The spring constant $k = (2.6 \pm 0.1)$ Nm of the AFM cantilever was determined using the Sader method [17]. Each spot was partitioned into 400 subdomains, serving as a nanoindentation site. The elastic modulus for each subdomain was calculated from the force distance curves. It has been reported that the nanoindentation measurements using large spheres on soft polymers are affected significantly by adhesion forces F_{adh} [18]. The Johnson-Kendall-Roberts (JKR) contact model takes into account F_{adh} and can be described by the following equation [19]:

$$E_f = \sqrt{\frac{S^3(1-\upsilon_f^2)^2}{6R}\left(\frac{1}{P+2F_{adh}+2F_{adh}\sqrt{\left(\frac{P}{F_{adh}}+1\right)}}\right)}, \quad (2)$$

where P is the applied load, R is the radius of the spherical tip, υ_f is the Poisson ratio of the silicone film, and F_{adh} is the maximum adhesive pull-off force between the tip and the sample during unloading. Stiffness S represents the slope of the unloading curve. The JKR model is implemented in FLEXANA® software (FLEXANA, Nanosurf AG, Switzerland), offering a fully automated post-processing and analysis of the data.

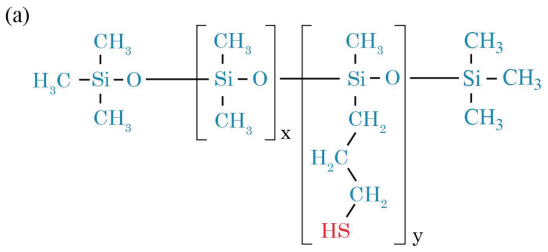

x	y	Molecular weight	SH content
36	6	3'600 g/mol	5.2 wt%

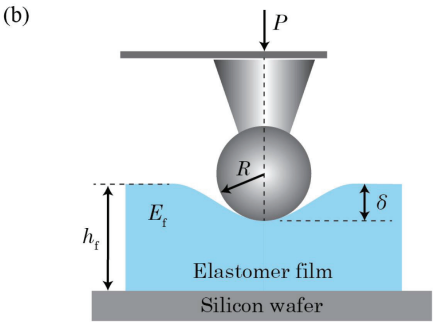

Figure 2. (**a**) Structure of dimethyl silicone copolymer fluid GP367 containing mercaptopropyl SH-side chains in addition to the conventional CH_3-methyl groups. (**b**) Scheme of the AFM nanoindentation using a spherical tip with a radius $R = (490 \pm 5)$ nm. The elastic modulus E_f of the silicone film was calculated from the force distance curves and the applied load using the Johnson-Kendall-Roberts contact model.

2.5 Evaporation of the Au electrode

The 15 nm-thin Au electrodes were thermally evaporated in ultra-high-vacuum conditions at a residual pressure of 10^{-7} mbar. High-temperature effusion cells (HTEZ, Dr. Eberl MBE Komponenten GmbH, Weil der Stadt, Germany) with 10 cm^3 PBN crucibles served as molecular beam sources. The evaporation temperature was set to 1'440 °C, corresponding to a deposition rate of 0.5 nm per minute. The substrate was mounted at a distance of 40 cm away from the crucibles and rotated at a speed of 10 rpm to obtain a homogenous film and to minimize the thermal impact of the source on the underlying PDMS film.

2.6 Contact angle measurements

The specimens were placed on the stage of a contact angle goniometry device (OCA 15 EC, DataPhysics Instr. GmbH, Germany), supplied with LED illumination and a USB camera for video-recording. High-purity water droplets at a volume of 5 µL (Elga, Purelab UHQ II, UK) were dispensed by a glass syringe and taken up on the surface of the polymer by raising the stage upwards. The SCA 20 software (DataPhysics Instr. GmbH) was used to record and analyze the data.

3. RESULTS AND DISCUSSION

3.1 From islanding to confluent elastomer films

First, we tuned the electro-spray's deposition parameters, namely the applied alternating high voltage, its frequency, the flow rate through the nozzle, and the distance between the nozzle and the substrate, to create a stable and reproducible mono-dispersed, single-cone jet.

In a next step, we varied polymer concentration from 1 to 10 vol% and investigated film formation with respect to deposition time, as displayed in Figure 3. After depositing for a duration of 10 s, we observed islands but no confluent film for the polymer concentrations used herein. The island heights corresponded to about 30 nm for the 1 vol% and increased to 750 nm for the 10 vol% solution. Nevertheless, the islands were rather flat and exhibited a diameter-to-height ratio of about 500.

For the 1 vol% solution, the films became percolated after a deposition period of 50 s. The average film thickness reached (220 ± 70) nm after a deposition period of 75 s and resulted in a clearly present irregular thickness, even for deposition periods exceeding 100 s. These thickness modulations reflect the still micrometer-sized droplets landing on the substrate. Note that the islands were high with respect to film thickness. The images represented in Figure 3 further indicate that an increase in concentration to 10 vol% resulted in an earlier transition to the percolation threshold and to confluent films.

Confluent films are required in the preparation of functional elastomer films in DETs. Therefore, the minimal deposition time is 75 s (with an exception at 10 vol%, which equates to 50 s). Related average film thickness, however, depends linearly on polymer concentration, as indicated by the numbers above the images. These numbers are red-colored for the films that only partially cover the substrate. Numbers in black mark the layers that cover the entire substrate and are suitable for building DET structures. Our experiments clearly demonstrate that using a polymer concentration of 5 or 10 vol% only allows for fabricating micrometer-thick films, whereas lower concentrations enable us to build nanometer-thin confluent elastomer films.

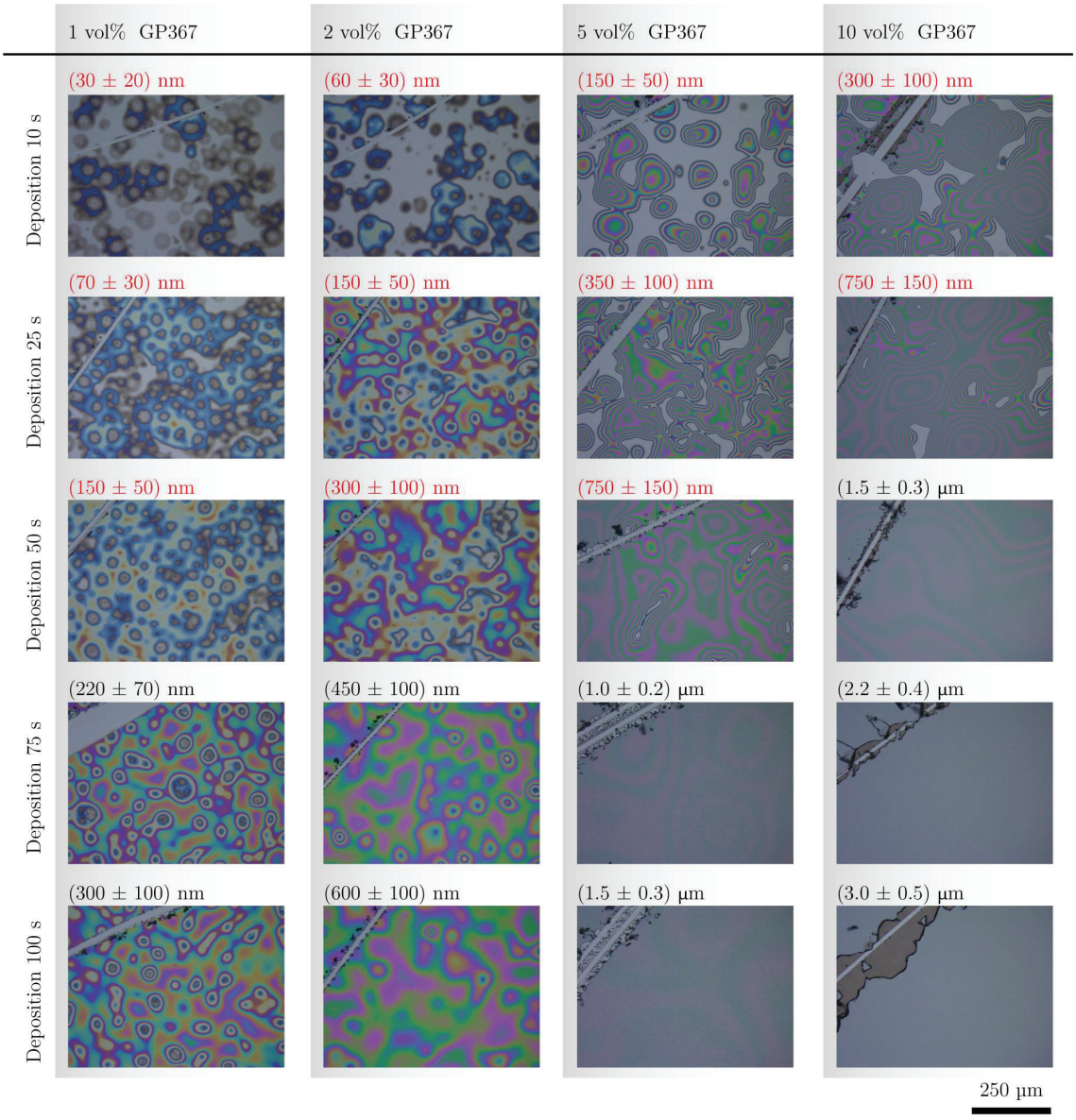

Figure 3. Optical micrographs of AC electro-sprayed and UV-cured PDMS films on Si wafers. PDMS was dissolved in ethyl acetate to realize concentrations between 1 and 10 vol%. The PDMS ethyl acetate solution was electro-sprayed for deposition times ranging from 10 to 100 s. More or less interconnected islands, which do not fully cover the substrate, are formed during the early stages of deposition and marked in red color. They will result in a short-circuit fault in the DET structures. For 1 and 2 vol% concentrations, confluent films were found even at nanometer thicknesses. These films, however, were rough. Smoother PDMS films were found for a thickness above 1 m. Note: The scratches were built on purpose.

The nanometer-thin films, however, are comparably rough and only qualify partially for the preparation of DETs. The film roughness reflects the micrometer-sized droplets. For a 5 vol% concentration, the average radius of the micro-droplets was (7 ± 2) m, which could be reduced to (3 ± 1) m for the 1 vol% solution. For the micrometer-thick films, however, the roughness is comparably small and the impact of droplets less obvious.

As previously reported [20], voltages of ±5 kV usually lead to unstable, multi-cone jets and therefore to local variances in deposition rate and film thickness. Flow rate and PDMS concentration determine the mean droplet size, whereas the other operation parameters, including applied voltage, nozzle diameter, and electrical conductivity of the solvent, seem to have a modest effect [21].

3.2 Thermal treatment of electro-sprayed elastomer films

The molecular weight of GP367 corresponds to 3'600 g/mol and is therefore relatively low. Thus, we investigated the influence of thermal processing on film morphology. For this purpose, a solution with an oligomer concentration of 5 vol% was sprayed over a period of 25 s to obtain a PDMS film that would partially cover the substrate. In the next step, these liquid-like films, with an average thickness in the sub-micrometer range, were processed at temperatures between 25 and 150 °C for a period of ten minutes.

The resulting morphology is best represented using the optical micrographs in Figure 4. Up to an annealing temperature of 100 °C, part of the Si substrate is visible. Annealing to 150 °C results in a film that covers the entire substrate. This film, at a thickness of (500 ± 150) nm, however, still exhibits height modulations of more than 100 nm, as identified by the interference pattern on the optical micrograph.

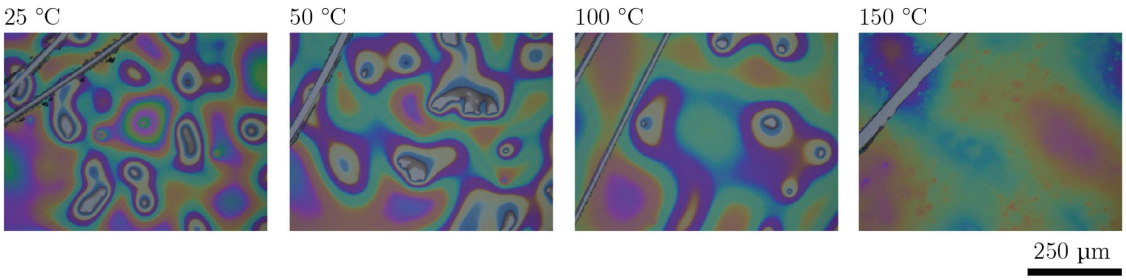

Figure 4. Optical micrographs of thermally treated liquid-like PDMS films at a mean thickness of (550 ± 150) nm. The holes were filled after thermal treatment at a temperature of 150 °C for ten minutes. Subsequent to the thermal treatment and cooling down to room temperature, the PDMS layers were UV-cured. Note: The scratches were built on purpose.

3.3 Tuning the elastic modulus via UV irradiation

Figure 5(a) shows the increase in the elastic modulus E of the electro-sprayed films as a function of irradiation time. The experimentally derived values are also listed in Table 1. The prolongation of irradiation time from 30 to 120 s results in elastic moduli increasing from 165 to 1'300 kPa.

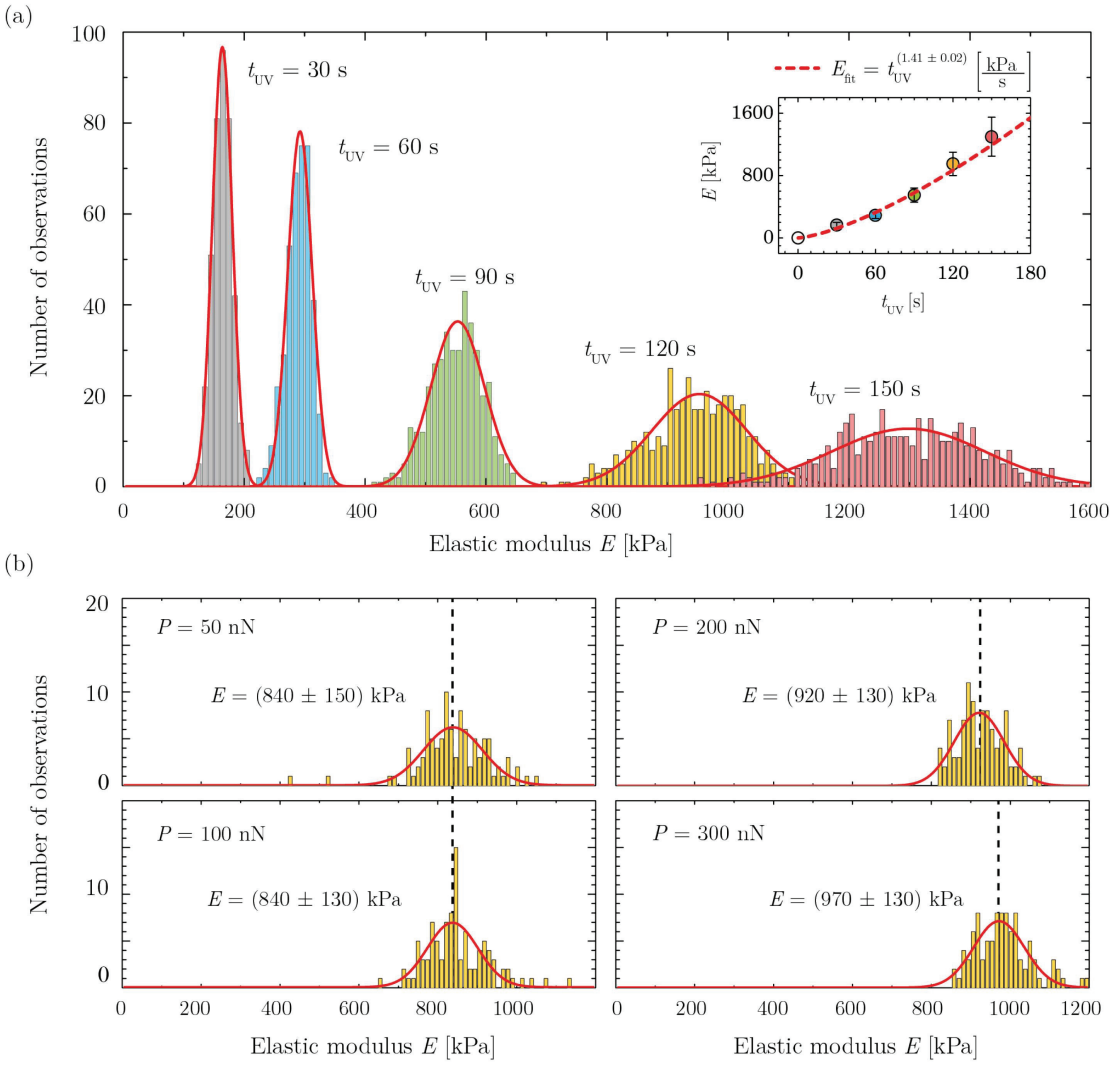

Figure 5. (**a**) UV-curing of GP367 silicone films. The elastic modulus E can be tuned with the irradiation dose using a 200 W Hg-Xe lamp. (**b**) Elastic modulus of a UV-cured silicone film, calculated for selected loads P and related nanoindentation depths δ. A six-fold higher load $P = 300$ nN with an average indentation depth of (420 ± 50) nm reveals that the silicone film is uniformly cured over the whole thickness. The thickness of the investigated sample was (2.1 ± 0.2) m.

Table 1. Elastic moduli and water contact angles of the UV-cured PDMS films for selected irradiation times.

UV irradiation time [s]	**Elastic modulus *E*** [kPa]	**Shear modulus *G*** [kPa]	**Water contact angle** [deg]
30	165 ± 35	55 ± 12	111 ± 1
60	290 ± 40	100 ± 14	107 ± 1
90	550 ± 90	180 ± 30	106 ± 1
120	950 ± 150	950 ± 50	105 ± 1
150	1300 ± 250	430 ± 84	103 ± 1

The crosslinking mechanism responsible for the stiffness increase, however, was not completely identified [22]. It is assumed that thiol radicals, which are formed by UV irradiation, play a crucial role in the photo-polymerization of thiol-ene polymers. These radical species are also probably responsible for the crosslinking of the polymer chains into a three-dimensional network. It has been reported that under ambient conditions, oxygen is incorporated into the polymer network [23] and reacts with carbon radicals to form peroxyl radicals. Indeed, we observed smaller water contact angles for the longer irradiation times shown in Table 1. The longer the sample has been irradiated, the more peroxyl radicals may form and the polymer membrane becomes more and more hydrophilic.

The data shown in Figure 5(b) indicate that the PDMS films are uniformly cured. The calculated elastic modulus does not change significantly for the selected loads and resulting indentation depths, though one recognizes a slight increase in the highest selected load. Presumably, this marginal increase relates to substrate effects. Here, the average indentation depths were already (420 ± 50) nm. A possible gradient in crosslinking, with a stiff, skin-like layer on top and a soft/liquid bulk, as reported for a UV-cured, vinyl-terminated PDMS using a deuterium UV lamp, can be excluded [24].

3.4 Increased interaction of the Au electrode with the PDMS membrane

The limited adhesion of Au to commercially available Sylgard® 184-PDMS is well known [25]. A peel-off test, as displayed in Figure 6, clearly demonstrates that the Au electrode interacts only with the SH-functionalized PDMS network, whereas the Au electrode on Sylgard® 184 peeled off easily. The increased adhesion of Au results from the thiol groups and formed disulfide bonds. Thiols and disulfide bonds interact strongly with Au [22].

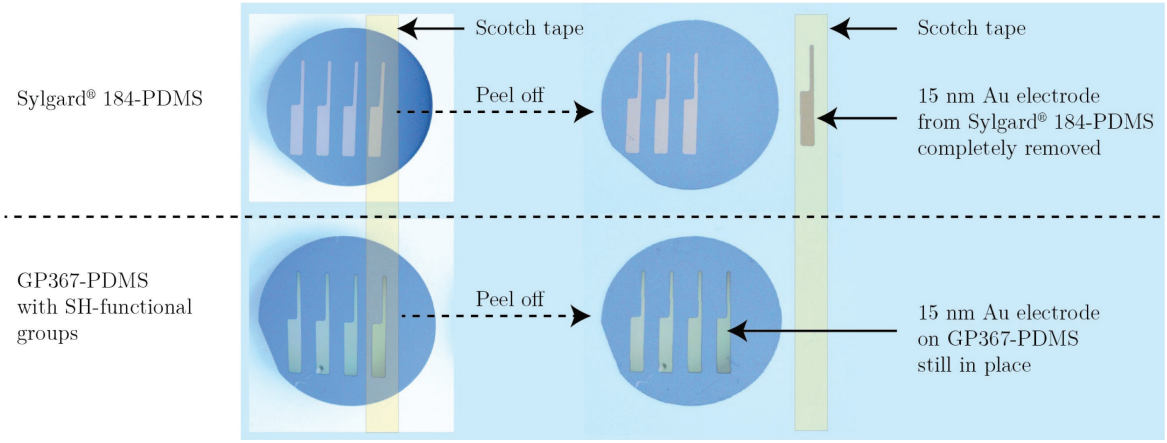

Figure 6. Adhesion of an Au electrode to thermally-cured Sylgard® 184-PDMS and UV-cured GP367-PDMS. A peel-off test with Scotch tape reveals the limited adhesion of Au on PDMS to be fixed using SH-functional groups.

Au films on pure PDMS most likely follow the Volmer-Weber growth mode, leading to a cluster-like Au electrode [25]. Au clusters with a nominal size of (40 ± 20) nm were observed on both PDMS films, as shown in Figure 7. However, the root-mean-square roughness (RMS) of Au on GP367 was significantly smaller than for Au on Sylgard® 184, showing values of (3.8 ± 0.5) and (5.3 ± 0.5) nm, respectively. The initial RMS value of the sprayed and UV-cured PDMS film was determined at only (0.3 ± 0.1) nm.

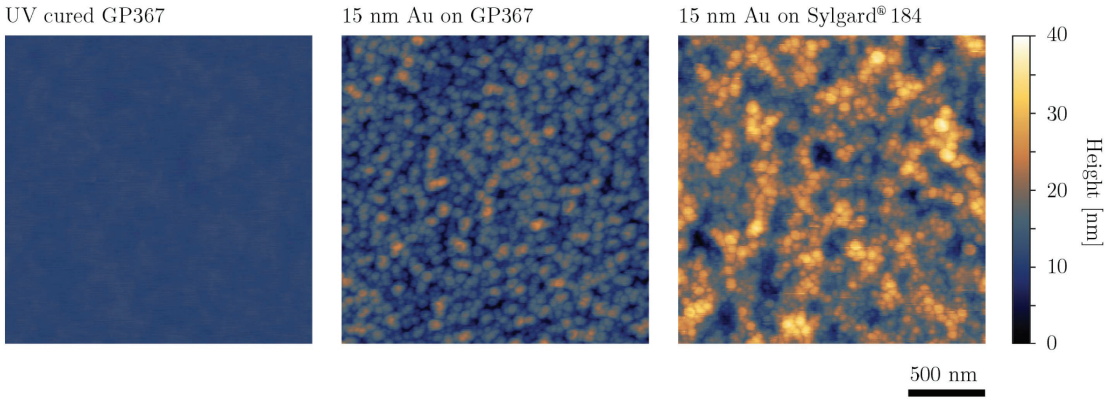

Figure 7. The three AFM scans show 2 × 2 m^2 areas of a (left) UV-cured GP367 PDMS film, (middle) a 15 nm-thin Au electrode on GP367, and (right) a 15 nm Au electrode on Sylgard® 184 PDMS film. The initial root-mean-roughness (RMS) value of (0.3 ± 0.1) nm for the UV-cured GP367 increased to (3.8 ± 0.5) nm after the evaporation of 15 nm Au at a distance of 40 cm. The RMS value for Au on Sylgard® 184, at (5.3 ± 0.5) nm, was even higher.

4. CONCLUSIONS

Using SH-functionalized PDMS, soft and smooth elastomer films with thicknesses of only 1 m can be fabricated. The elastic modulus of these layers can be tuned between 165 and 1'300 kPa. Compared to previous studies, the stable single-cone jet enabled us to produce a film that fully covered the substrate in less than one minute [13]. Subsequent UV-polymerization, without applying any photoinitiators, allowed us to form a homogenously crosslinked thin film. In addition, the adhesive layer between the electrode and elastomer was not required, as the Au nanoclusters form covalent bonds to the SH groups on the elastomeric network. Confluent PDMS layers were obtained even at a thickness as thin as (220 ± 70) nm using 1 vol% solutions. Films thicker than 1 m are required to obtain smooth films suitable for the fabrication of low-voltage DETs. Selecting the experimentally proven values for the dielectric layer with $E = 290$ kPa, $\varepsilon = 2.7$, $h_p = 1$ m and a voltage of $U = 42$ V, the calculated compressive strain s_z corresponded to about 15 %. In the next step, a multiple nozzle arrangement and a rolling endless sheet substrate should be employed to increase film homogeneity further. With thermal treatment and *in situ* UV-curing, this process will enable the fabrication of low-voltage, multilayer DETs.

ACKNOWLEDGMENTS

The financial support of the nano-tera.ch initiative, project SmartSphincter, as well as the Swiss Nanoscience Institute (SNI) for the financial contribution to the AFM are gratefully acknowledged. The authors wish to thank Irene Piskoti, from Genesee Polymers Corporation, Burton MI, USA, for kindly providing one pint of GP-367 at no charge. The authors also wish to thank to Monica Schönenberger, from the Nanotech Service Lab at the University of Basel, for her assistance with the 3D laser microscope.

REFERENCES

[1] Anderson, I. A., Gisby, T. A., McKay, T. G. et al., "Multi-functional dielectric elastomer artificial muscles for soft and smart machines," *J. Appl. Phys.* **112**(4), 041101 (2012).

[2] Brochu, P., and Pei, Q., "Advances in dielectric elastomers for actuators and artificial muscles," *Macromol. Rapid. Commun.* **31**(1), 10-36 (2010).

[3] O'Halloran, A., O'Malley, F., and McHugh, P., "A review on dielectric elastomer actuators, technology, applications, and challenges," *J. Appl. Phys.* **104**(7), 071101 (2008).

[4] Rosset, S., and Shea, H. R., "Small, fast, and tough: Shrinking down integrated elastomer transducers," *Appl. Phys. Rev.* **3**(3), 031105 (2016).

[5] Sia, S. K., and Whitesides, G. M., "Microfluidic devices fabricated in poly(dimethylsiloxane) for biological studies," *Electrophoresis* **24**(21), 3563-3576 (2003).

[6] Molberg, M., Crespy, D., Rupper, P. et al., "High breakdown field dielectric elastomer actuators using encapsulated polyaniline as high dielectric constant filler," *Adv. Funct. Mater.* **20**(19), 3280-3291 (2010).

[7] Poulin, A., Rosset, S., and Shea, H. R., "Printing low-voltage dielectric elastomer actuators," *Appl. Phys. Lett.* **107**(24), 244104 (2015).

[8] Töpper, T., Weiss, F. M., Osmani, B. et al., "Siloxane-based thin films for biomimetic low-voltage dielectric actuators," *Sens. Actuators A* **233**, 32-41 (2015).

[9] Weiss, F. M., Madsen, F. B., Töpper, T. et al., "Molecular beam deposition of high-permittivity polydimethylsiloxane for nanometer-thin elastomer films in dielectric actuators," *Mater. Des.* **105**, 106-113 (2016).

[10] Duduta, M., Wood, R. J., and Clarke, D. R., "Multilayer dielectric elastomers for fast, programmable actuation without prestretch," *Adv. Mater.* **28**(36), 8058-8063 (2016).

[11] Pelrine, R., Kornbluh, R., Joseph, J. et al., "High-field deformation of elastomeric dielectrics for actuators," *Mater. Sci. Eng. C* **11**(2), 89-100 (2000).

[12] Töpper, T., Lörcher, S., Weiss, F. et al., "Tailoring the mass distribution and functional group density of dimethylsiloxane-based films by thermal evaporation," *APL Mater.* **4**(5), 56101 (2016).

[13] Weiss, F. M., Töpper, T., Osmani, B. et al., "Thin film formation and morphology of electrosprayed polydimethylsiloxane," *Langmuir* **32**, 3276-3283 (2016).

[14] Loo, Y. L., Willett, R. L., Baldwin, K. W. et al., "Additive, nanoscale patterning of metal films with a stamp and a surface chemistry mediated transfer process: Applications in plastic electronics," *Appl. Phys. Lett.* **81**(3), 562-564 (2002).

[15] Osmani, B., Deyhle, H., Weiss, F. M. et al., "Morphology and conductivity of Au electrodes on polydimethylsiloxane using (3-mercaptopropyl) trimethoxysilane (MPTMS) as an adhesion promoter," *Proc. SPIE* **9798**, 979822 (2016).

[16] Byun, I., Coleman, A. W., and Kim, B., "Transfer of thin Au films to polydimethylsiloxane (PDMS) with reliable bonding using (3-mercaptopropyl) trimethoxysilane (MPTMS) as a molecular adhesive," *J. Micromech. Microeng.* **23**(8), 085016 (2013).

[17] John, E. S., James, W. M. C., and Paul, M., "Calibration of rectangular atomic force microscope cantilevers," *Rev. Sci. Instrum.* **70**(10), 3967-3969 (1999).

[18] Gupta, S., Carrillo, F., Li, C. et al., "Adhesive forces significantly affect elastic modulus determination of soft polymeric materials in nanoindentation," *Mater. Lett.* **61**(2), 448-451 (2007).

[19] Carrillo, F., Gupta, S., Balooch, M. et al., "Nanoindentation of olydimethylsiloxane elastomers: Effect of crosslinking, work of adhesion, and fluid environment on elastic modulus," *J. Mater. Res.* **20**(10), 2820-2830 (2005).

[20] Weiss, F. M., Töpper, T., Osmani, B. et al., "Electrospraying nanometer-thin elastomer films for low-voltage dielectric actuators," *Adv. Electron. Mater.* **1500476**, (2016).

[21] Tang, K., and Gomez, A., "Monodisperse electrosprays of low electric conductivity liquids in the cone-jet mode," *J. Colloid Interface Sci.* **184**(2), 500-511 (1996).

[22] Grönbeck, H., Curioni, A., and Andreoni, W., "Thiols and disulfides on the Au (111) surface: the headgroup−gold interaction," *J. Am. Chem. Soc.* **122**(16), 3839-3842 (2000).

[23] Cramer, N. B., Scott, J. P., and Bowman, C. N., "Photopolymerizations of thiol−ene polymers without photoinitiators," *Macromolecules* **35**(14), 5361-5365 (2002).

[24] Töpper, T., Wohlfender, F., Weiss, F. M. et al., "Characterization of ultraviolet light cured polydimethylsiloxane films for low-voltage, dielectric elastomer actuators," *Proc. SPIE* **9798**, 979821 (2016).

[25] Graudejus, O., Gorrn, P., and Wagner, S., "Controlling the morphology of gold films on poly(dimethylsiloxane)," *ACS Appl. Mater. Interfaces* **2**(7), 1927-1933 (2010).

*Further author information: (send correspondence to B.O.)

3 Conclusions and Outlook

The fabrication of confluent and flat nanometer-thin PDMS films with compliant and soft electrodes is an important step towards the fabrication of low-voltage multi-stack actuators for biomedical devices. We have shown that thin-film DETs exert the expected forces and can be easily measured using an in-house built apparatus. The detected actuation values correspond reasonably well to the predictions. Actuation forces F of single-layer DETs calculated from Eq. (1.2) are below 1 mN. The apparatus is well suited also for the characterization of multi-layer actuators. It allows the detection of electrical breakdowns as well as self-clearance effects of DETs.

For the fabrication of PDMS films, OMBD is the method of choice. Confluent and homogeneous PDMS films were obtained at thicknesses of a few hundreds of nanometers. The main drawbacks of this method are the limitation to short-chain polymers, low deposition rates, and the expensive equipment. In contrary, ESD is by two orders of magnitude faster and is being considered as the method of choice for the fabrication of multi-layer DETs. However, the still micrometer-sized droplets landing on the substrate form a rough surface. As shown in this work, thermal treatments can flatten the surface of viscous PDMS films, heal defects and contribute to confluent layers at this scale. Using other solvents, such as acetone, could be an alternative to generate finer droplets and fabricate smoother films. For both methods, ultraviolet light (UV) induced cross-linking of the PDMS network is of great importance.

Moreover, we show that SH-functionalized PDMS can be electro-sprayed and cross-linked using a high power Hg-Xe-UV lamp with its peak intensity at 365 nm. This allows to cure the PDMS films even in atmospheric conditions. The elastic modulus can be easily set with the irradiation dose between 165 and 1'300 kPa. Compared to previous studies, the stable single-cone jet enabled us to produce a film that fully covered the substrate in less than one minute. Subsequent UV-polymerization, without applying any photo-initiators, allowed us to form a homogeneously cross-linked thin film. In addition, the adhesive layer between the electrode and elastomer was not required, as the Au nanoclusters form covalent bonds to the SH groups on the elastomer network. Confluent PDMS layers were obtained even at a thickness as thin as (220 ± 70) nm using 1 vol. % solutions. However, using the existing setup, films thicker than 1 µm were smooth and suitable for the fabrication of low-voltage DETs. Selecting the experimentally proven values for the PDMS film with $E = 165$ kPa, $\varepsilon = 2.7$, $d = 1$ µm, and $U = 42\ V$, the calculated compressive strain according to Eq. (1.2) corresponds to ~ 25 %. In the next step, a multiple nozzle arrangement and a rolling endless sheet substrate should be employed to increase film homogeneity further. ESD can be easily scaled for industrial production. Thermal treatments and in situ UV-curing will enable the fabrication of low-voltage, multi-layer DETs.

Furthermore, we have demonstrated an innovative approach to realizing soft and compliant Au electrodes on PDMS films. Compliant electrodes are essential components for DETs, neuroprosthetics and flexible electronics. The two main paths to increase the compliance include the manipulation of intrinsic material properties of the electrode, or its structural features, such as the introduction of wrinkles. Wrinkling is a universal phenomenon exhibited by a compressed stiff film resting on a soft substrate. Here we demonstrate that by tuning oxygen plasma parameters, we are able to fabricate soft and nanostructured Au electrodes on soft PDMS films. Our results, combining topological and mechanical film properties, shed light on the formation and reformation of wrinkles associated with an intrinsic compression of the metal film. The interplay between metal electrode and nanostructured elastomer film allows for tuning local morphology and related mechanics. Especially important is the ability to suppress the stiffness impact of the thin metal electrode on the entire sandwich nanostructure. Thin-film DETs, which can be operated at low voltages, require such intrinsically compressed, soft electrodes. Especially for dielectric elastomer actuators with thousands of nanometer-thin layers, it is essential to suppress any rise in stiffness.

Our results show that using vinyl-terminated PDMS prepolymers with a low molecular weight, one can bypass the need of any solvent or curing agent to fabricate nanometer-thin PDMS films with tunable nanostructures. By varying the oxygen plasma parameters, we were able to tune the amplitude between 30 and 300 nm and periodicities ranging from 500 to 2'800 nm. As plasma treatments do not only change the surface morphology but also influence the chemistry and the related mechanics of the surface layers, cross-linking mechanisms via reactive species generated through photo-ionization and ion bombardments have to be considered. Atomic force microscopy (AFM) was used to measure film thickness, amplitude and wrinkle periodicity of the PDMS films. The average elastic modulus was extracted out of nanoindentation measurements. The mechanical mapping with sub-micrometer resolution reveals an anisotropy of the elastic modulus at the sub-micrometer level of the wrinkled films. Nanoindentation measurements show that nano-hills are stiffer than nano-valleys. One can speculate on the reasons for this anisotropy. Geometrical phenomena could lead to an enhanced structural stiffness for hills. As wrinkle formation is related to material transport, a thickness modulation of the silica-like layer might be another explanation for this effect.

Finally, we have shown that probing a DC-powered thin-film DET with an AFM spherical tip leads to increased indentation depths by several ten percent, as verified by dynamic FE models. Furthermore, AFM scans revealed increased roughness of the Au electrode when the voltage is applied to the DET. Charge accumulation is found to be responsible for the softening effect of the DET structure. In conclusion, electrodes with a controlled wrinkle topology can be prepared to trigger a preferred direction of the actuation.

Bibliography

[1] Becker, H., Stenzl, A., Wallwiener, D., and Zittel, T., [*Urinary and fecal incontinence*], Springer, Berlin, Heidelberg (2005).

[2] Fattorini, E., Brusa, T., Gingert, C., Hieber, S., Leung, V., Osmani, B., Dominietto, M., BÃ¼chler, P., Hetzer, F., and MÃ¼ller, B., "Artificial muscle devices: Innovations and prospects for fecal incontinence treatment," *Ann. Biomed. Eng.* **44**, 1–15 (2016).

[3] Madden, J., Vandesteeg, N., Anquetil, P., Madden, P., Takshi, A., Pytel, R., Lafontaine, S., Wieringa, P., and Hunter, I., "Artificial muscle technology: physical principles and naval prospects," *IEEE J. Ocean. Eng.* **29**(3), 706–728 (2004).

[4] Madsen, F., Daugaard, A., Hvilsted, S., and Skov, A., "The current state of silicone-based dielectric elastomer transducers," *Macromol. Rapid Commun.* **37**(5), 378–413 (2016).

[5] Rosset, S. and Shea, H., "Small, fast, and tough: Shrinking down integrated elastomer transducers," *Appl. Phys. Rev.* **3**(3), 031105 (2016).

[6] Pelrine, R., Kornbluh, R., Pei, Q., and Joseph, J., "High-speed electrically actuated elastomers with strain greater than 100%," *Science* **287**(5454), 836–839 (2000).

[7] OâHalloran, A., OâMalley, F., and McHugh, P., "A review on dielectric elastomer actuators, technology, applications, and challenges," *J. Appl. Phys.* **104**(7), 071101 (2008).

[8] Carpi, F., De Rossi, D., Kornbluh, R., Pelrine, R., and Sommer-Larsen, P., [*Dielectric elastomers as electromechanical transducers: Fundamentals, materials, devices, models and applications of an emerging electroactive polymer technology*], Elsevier, Amsterdam (2008).

[9] Pelrine, R., Kornbluh, R., Joseph, J., Heydt, R., Pei, Q., and Chiba, S., "High-field deformation of elastomeric dielectrics for actuators," *Mater. Sci. Eng. C* **11**(2), 89–100 (2000).

[10] Osmani, B., TÃ¶pper, T., Deschenaux, C., Nohava, J., Weiss, F., Leung, V., and MÃ¼ller, B., "Micro- and nanostructured electro-active polymer actuators as smart muscles for incontinence treatment," *AIP Conf. Proc.* **1646**(1), 91–100 (2015).

[11] Molberg, M., Crespy, D., Rupper, P., NÃ¼esch, F., MÃ¥nson, J. A. E., LÃ¶we, C., and Opris, D. M., "High breakdown field dielectric elastomer actuators using encapsulated polyaniline as high dielectric constant filler," *Adv. Funct. Mater.* **20**(19), 3280–3291 (2010).

[12] TÃ¶pper, T., Weiss, F. M., Osmani, B., Bippes, C., Leung, V., and MÃ¼ller, B., "Siloxane-based thin films for biomimetic low-voltage dielectric actuators," *Sensor Actuat. A Phys.* **233**, 32–41 (2015).

[13] Osmani, B., Aeby, E., and MÃ¼ller, B., "Stress measurements of planar dielectric elastomer actuators," *Rev. Sci. Instrum.* **87**, 053901 (2016).

[14] Osmani, B., Deyhle, H., TÃ¶pper, T., Pfohl, T., and MÃ¼ller, B., "Soft electrodes on elastomeric substrates near the critical stress regime," *Adv. Mater. Technol.* **revision submitted** (2017).

[15] Osmani, B., Deyhle, H., Weiss, F., TÃ¶pper, T., Karapetkova, M., Leung, V., and MÃ¼ller, B., "Morphology and conductivity of au electrodes on polydimethylsiloxane using (3-mercaptopropyl)trimethoxysilane (mptms) as an adhesion promoter," *Proc. SPIE* **9798**(979822), 979822 (2016).

[16] Osmani, B., TÃ¶pper, T., Siketanc, M., Kovacs, G., and MÃ¼ller, B., "Electrospraying and ultraviolet light curing of nanometer-thin polydimethylsiloxane membranes for low-voltage dielectric elastomer transducers," *Proc. SPIE* **10163**, 101631E (2017).

[17] Weiss, F., TÃ¶pper, T., Osmani, B., Peters, S., Kovacs, G., and MÃ¼ller, B., "Electrospraying nanometerâthin elastomer films for lowâvoltage dielectric actuators," *Adv. Electron. Mater.* **2**, 1500476 (2016).

[18] Weiss, F., TÃ¶pper, T., Osmani, B., Deyhle, H., Kovacs, G., and MÃ¼ller, B., "Thin film formation and morphology of electrosprayed polydimethylsiloxane," *Langmuir* **32**, 3276–3283 (2016).

[19] TÃ¶pper, T., LÃ¶rcher, S., Weiss, F., and MÃ¼ller, B., "Tailoring the mass distribution and functional group density of dimethylsiloxane-based films by thermal evaporation," *APL Mater.* **4**(5), 056101 (2016).

[20] McCoul, D., Hu, W., Gao, M., Mehta, V., and Pei, Q., "Recent advances in stretchable and transparent electronic materials," *Adv. Electron. Mater.* **2**(5), 1500407 (2016).

[21] Rosset, S. and Shea, H., "Flexible and stretchable electrodes for dielectric elastomer actuators," *Appl. Phys. A* **110**(2), 281–307 (2013).

[22] Li, T., Huang, Z., Suo, Z., Lacour, S., and Wagner, S., "Stretchability of thin metal films on elastomer substrates," *Appl. Phys. Lett.* **85**(16), 3435–3437 (2004).

[23] Osmani, B., Gerganova, G., and MÃ¼ller, B., "Biomimetic nanostructures for the silicone-biosystem interface: tuning oxygen-plasma treatments of polydimethylsiloxane," *Eur. J. Nanomed.* **9**(2), 69 (2017).

Acknowledgments

First and foremost, I would like to thank my thesis advisor Prof. Bert Müller for guiding me through the excited last 4 years. He gave me the opportunity to conduct this thesis in a interdisciplinary environment. Within the SmartSphincter project we were in close collaboration with surgeons, engineers and physicists. He gave me the freedom to explore novel approaches to push forward the research of artificial muscles for medical applications. Under his supervision, we managed to install two novel process technologies for the fabrication of ultra-thin polymer films such as organic molecular beam deposition system and the vacuum-enabled electro-spray deposition system.

At this point I would like to thank my co-referee Prof. Roderick Lim for taking the time to evaluate my thesis.

I would like to thank the Swiss Nanoscience Institute for the financial contribution to the atomic force microscope which turned out to be my main characterization tool for the fabricated DET structures.

Not to forget the valuable support from Sascha Martin for helping me with the fabrication of the EAP Box and letting me use his workshop at the Physics Department of the University of Basel as well as the support from Volker Brunner from the workshop at the University Hospital Basel and Andreas Tonin from the electric workshop at the Physics Department in Basel.

Moreover I thank Monica Schönenberger for her support with the AFM and 3D-Laser Microscope at the Nanotech Service Lab.

I really enjoyed the time at the Biomaterials Science Center and would like to thank current and past group members for the great time and support, especially Tino Töpper, Florian Weiss, Vanessa Leung, Thomas Pfohl and Hans Deyhle for their input, helpful discussions and data analysis.

Last but not least I would like to thank all my friends and family who were an amazing support throughout all these years. Special thanks go to my wife Arjeta for her tremendous support during the last months of my thesis. And to my daughter Jona for the interesting experiments on soft electrodes during her Future Day in 2016 and Leona for checking with me the quality of AFM scans on Au electrodes or how she used to call them, the "goldy" thing.